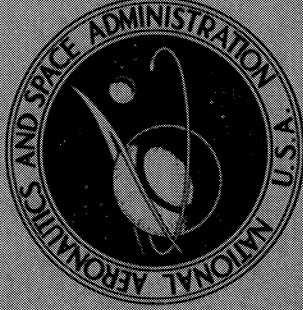


N74-10020

**NASA CONTRACTOR  
REPORT**



NASA CR-2323

NASA CR-2323

**CASE FILE  
COPY**

**NOISE AND WAKE STRUCTURE MEASUREMENTS  
IN A SUBSONIC TIP SPEED FAN**

*by B. Magliozzi, D. B. Hanson, B. V. Johnson,  
and F. B. Metzger*

*Prepared by*

HAMILTON STANDARD

DIVISION OF UNITED AIRCRAFT CORPORATION

Windsor Locks, Conn. 06096

*for Langley Research Center*

NATIONAL AERONAUTICS AND SPACE ADMINISTRATION • WASHINGTON, D. C. • NOVEMBER 1973

1. Report No. NASA CR-2323	2. Government Accession No.	3. Recipient's Catalog No.	
4. Title and Subtitle Noise and Wake Structure Measurements in a Subsonic Tip Speed Fan		5. Report Date November 1973	6. Performing Organization Code
		8. Performing Organization Report No.	
7. Author(s) B. Magliozzi, D. B. Hanson, B. V. Johnson and F. B. Metzger		10. Work Unit No.	
9. Performing Organization Name and Address Hamilton Standard, Division of United Aircraft Windsor Locks, Connecticut 06096		11. Contract or Grant No. NAS 1-11670	
		13. Type of Report and Period Covered Contractor Report	
12. Sponsoring Agency Name and Address National Aeronautics and Space Administration Washington, D. C. 20546		14. Sponsoring Agency Code	
15. Supplementary Notes This is a final report.			
16. Abstract <p>The results of an experimental program are reported which show the effect of blade angle, tip speed, fan pressure ratio, and thrust on noise of a model fan of 0.457m (18 inches) diameter operating at subsonic tip speeds at pressure ratios between 1.06 and 1.15. The fan used in this study had 12 blades, 7 stator vanes, and a spacing between the rotor and stator of 1.85 blade chords. This fan was originally designed for aerodynamic testing and was considered a good performer. It was used in the noise test program as it incorporated features found to reduce noise in an earlier analytical parametric study. For a given pressure ratio the fan was shown to exhibit minimum noise at the blade angle and tip speed near that of maximum aerodynamic efficiency. Also, the noise level and spectrum character of this fan showed excellent correlation with scaled data of a similar larger diameter fan. Results of the program confirm the trends shown in the earlier analytical parametric study which showed that fan noise could be reduced for a given thrust and pressure ratio by increasing fan solidity, improving fan aerodynamic design and operating the fan at an optimum subsonic tip speed.</p> <p>In addition to noise, the blade wake characteristics at the leading edge of the stator were measured in this program. At root and tip sections some difference between predicted and measured wakes was found. However comparisons between predicted and measured wakes at mid span locations was found to be good.</p>			
17. Key Words (Suggested by Author(s)) Q-Fan                      Low Pressure Ratio Acoustic Noise          Fan Noise Blade Wakes              Propulsion Noise Noise Theory		18. Distribution Statement  Unclassified - unlimited	
19. Security Classif. (of this report) Unclassified	20. Security Classif. (of this page) Unclassified	21. No. of Pages 94	22. Price* Domestic, \$3.75 Foreign, \$6.25

## CONTENTS

	Page
SUMMARY .....	1
INTRODUCTION .....	3
TEST DESCRIPTION .....	5
Fan Configuration .....	5
Test Facility Description .....	5
Instrumentation .....	6
Aerodynamic and acoustic instrumentation .....	6
Blade Wake Instrumentation .....	6
Test Procedure .....	7
Fan Operating Conditions .....	8
Data Reduction Procedure .....	9
Aerodynamic data reduction .....	9
Acoustic data reduction .....	9
Blade wake data reduction .....	10
DISCUSSION .....	13
Introduction .....	13
Acoustic Data .....	13
Trends in acoustic data as measured .....	13
Influence of wind and blockage on noise .....	16
Comparison of fan noise at 1.402 m (4.6 ft) diameter .....	17
Comparison of fan noise at 66720 N (15000 pound) static thrust .....	17
Comparison of measured and predicted fan noise .....	19
Blade Wake Evaluation .....	20
Introduction .....	20
Wake data at Flow Condition I .....	21
Wake data at Flow Condition II .....	22
Wake data at Flow Condition III .....	22
Periodic wake characteristics .....	22
Wake modulation characteristics .....	23
Relation of wake characteristics to noise .....	23
Evaluation of stator harmonic noise using measured wakes .....	24
CONCLUSIONS .....	27
REFERENCES .....	29

## LIST OF ILLUSTRATIONS

Figure		Page
1	0.457 Meter (18 inch) Fan Definition	33
2	View Looking Into Fan Inlet	34
3	Test Area Plan View	35
4	Fan, PTR, Anechoic Platform, and Microphone System	36
5	High Response Aerodynamic Probes	37
6	Equipment Employed in High Response Data Acquisition	38
7	0.457 M (18 in) Diameter Fan Test Map	39
8	0.457 M (18 in) Diameter Fan Noise Variation with Net Thrust	40
9	Sound Pressure Level Variation with Blade Angle and Tip Speed at Constant Thrust	41
10	Comparison of Narrow Band Spectra	42
11	PNL Variation with Tip Speed at Constant Thrust	43
12	0.457 M (18 in) Diameter Fan Noise Variation with Pressure Ratio	44
13	0.457 M (18 in) Diameter Fan Noise Variation with Tip Speed	45
14	Fan Noise Variation with Tip Speed at Constant Blade Angle	46
15	Comparison of Narrow Band Spectra at Constant Blade Angle	47
16	Fan Noise Variation with Tip Speed at 1.094 Pressure Ratio	48
17	Comparison of Narrow Band Spectra at Constant Pressure Ratio	49
18	Sideline Perceived Noise Level Variation with Pressure Ratio at Constant Tip Speed	50
19	Sideline Perceived Noise Level Variation with Tip Speed at Constant Pressure Ratio	51
20	Effect of Wind and Inlet Disturbance on Tone Noise	52
21	Effect of Wind and Inlet Disturbance on Noise Directivity	53
22	0.457 M (18 in) Diameter Fan Scaled to 1.402 M (4.6 ft) Diameter	54
23	1.402 M (4.6 ft) Diameter Fan Data	55
24	Comparison of Scaled 0.457 M (18 in) Diameter Fan Noise and 1.402 M (4.6 ft) Diameter Fan Noise	56
25	Comparison of Spectra from Two Fans - Condition #1	57
26	Comparison of Spectra from Two Fans - Condition #2	58
27	Comparison of Spectra from Two Fans - Condition #3	59
28	Comparison of Spectra from Two Fans - Condition #4	60
29	PNL Variation with Tip Speed at Constant Thrust Scaled to 1.402 M (4.6 ft) Diameter	61
30	0.457 M (18 in) Diameter Fan Noise Scaled to 66720 N (15000 lb) Thrust	62
31	0.533 (21 in) Diameter Fan Noise Scaled to 66720 N (15000 lb) Thrust	63

## LIST OF ILLUSTRATIONS (CONT)

Figure		Page
32	1.402 M (4.6 ft) Diameter Fan Noise Scaled to 66720N (15000 lb) Thrust	64
33	Comparison of PNL Versus Pressure Ratio Variation for the Three Fans	65
34	Comparison of Noise Spectra at 1.08 Pressure Ratio Scaled to 66720 N (15000 lb) Thrust	66
35	Comparison of Measurements and Predictions - Condition #1	67
36	Comparison of Measurements and Predictions - Condition #2	68
37	Comparison of Measurements and Predictions - Condition #3	69
38	Comparison of Measurements and Predictions - Condition #4	70
39	Comparison of Measured and Calculated Noise Levels Scaled to a Diameter of 1.402 M (4.6 ft) at 38.0, 43.0, and 47.1 Deg Blade Angle	71
40	Comparison of Measured and Calculated Noise Levels Scaled to a Diameter of 1.402 M (4.6 ft) at 52.6, 57.4 and 62.5 Deg Blade Angle	72
41	Comparison of Measured and Calculated PNL Variation with Pressure Ratio for a 45360 KG (100,000 lb) Aircraft	73
42	Sketch of Velocity Vectors	74
43	Comparison of Resultant Velocity Profiles for Flow Condition I	75
44	Comparison of Air Angles for Flow Condition I	76
45	Comparison of Resultant Velocity Profiles for Flow Condition II	77
46	Comparison of Air Angles for Flow Condition II	78
47	Comparison of Resultant Velocity Profiles for Flow Condition III	79
48	Comparison of Air Angles for Flow Condition III	80
49	Hot Wire Anemometer Data Showing Wake Modulation	81
50	Fractional Velocity Defect Comparisons for Test Condition I	82
51	Fractional Wake Width Comparisons for Test Condition I	83
52	Fractional Velocity Defect Comparisons for Test Condition II	84
53	Fractional Wake Width Comparisons for Test Condition II	85
54	Fractional Velocity Defect Comparisons for Test Condition III	86
55	Fractional Wake Width Comparisons for Test Condition III	87
56	Contribution of Stator to Harmonic Noise at Flow Condition I	88
57	Contribution of Stator to Harmonic Noise at Flow Condition II	89
58	Contribution of Stator to Harmonic Noise at Flow Condition III	90



# NOISE AND WAKE STRUCTURE MEASUREMENTS

IN A

## SUBSONIC TIP SPEED FAN

By B. Magliozzi, D. B. Hanson, and F. B. Metzger  
of Hamilton Standard, Division of United Aircraft Corporation  
And  
B. V. Johnson of United Aircraft Research Laboratories

### SUMMARY

An experimental program has been conducted where noise characteristics of a subsonic tip speed fan were established and rotor wake details were measured at the leading edge of the stator assembly. The primary objective of this program was to verify the trends shown in an earlier analytical parametric study (ref 1). In that study, it was shown that increased fan solidity and optimized aerodynamics at the optimum operating tip speed were very powerful tools in the design of quiet fans.

The present program made use of an existing fan designed for wind tunnel aerodynamic tests. It was considered a good aerodynamic performer and did incorporate configuration variables found in reference 1 to minimize noise, such as few blades and few stators and a gap between rotor and stators of approximately two blade chords. The key features of this fan, relative to earlier tested fans, are higher solidity and the operation of the fan "on design". Earlier noise tests reported in reference 2 made use of a low solidity design which, due to power restrictions, could not be operated at its design tip speed and blade angle.

Tests in this program were conducted under ideal conditions with very low wind on a drive system with the axis of rotation high enough from the ground to eliminate inlet distortion due to ground vortex ingestion. The cantilever mount of the fan on the test facility also prevented the generation of inlet distortion due to facility support structures under the fan shroud. This cantilever mount also permitted measurement of inlet and aft quadrant noise in a single test run. The fan was tested with a generous inlet lip installed over the flight lip of the shroud to prevent separation under static test conditions. Measurements were made in the acoustic far field. Noise from ground reflection was eliminated by use of an anechoic platform on the ground between the fan and the microphone.

In addition to a complete set of data showing the effects of blade angle, thrust, tip speed and fan pressure ratio on noise, measurements of wakes generated by the fan rotor were obtained using special hot wire anemometry techniques. Mea-

surements were made at three operating conditions with the hot wire anemometer probe mounted at the leading edge of the stator at several radial stations.

Results of the noise measurements show that, for a given pressure ratio, minimum fan noise occurs at the blade angle and tip speed near that of maximum aerodynamic efficiency. Also, comparison of the noise data from this fan with that of a larger, similar fan shows excellent correlation, indicating that model scale tests can be utilized in developing full scale quiet fans. The fan noise data also confirm that the fan tested produces less noise than a lower solidity fan tested earlier (see reference 2). The data in this report confirms the trends of reference 1, which indicated that higher solidity and an optimum aerodynamic design would lead to reduced noise. Wake measurements indicate that differences between predicted and measured wakes exist at the root and tip of the blades. However, the mathematical model for rotor wakes used in noise predictions of reference 1 appears good at mid span. From the results presented in this report it appears that further reductions in fan noise can be achieved by refinement in fan aerodynamics.

## INTRODUCTION

Work over the past several years at NASA and in industry has shown that significant fan noise reduction can be achieved by reducing pressure ratio and tip speed. Most significant reductions appeared to occur as tip speed was reduced from the current turbofan tip speeds in the supersonic region to a speed just below sonic. This change in operating speed eliminated the multiple tones at harmonics of rotational speed (buzz saw noise). The remaining noise consisted of tones at blade passage frequency and its harmonics superimposed on a broadband noise floor. In 1970, an experimental program was conducted using an existing model of a subsonic tip speed fan (ref. 2). While this fan was operated off design due to test facility limitations, the high quality noise data obtained permitted development of a noise prediction methodology (ref. 1) which was used to conduct a parametric study to show the optimum configuration for a quiet subsonic tip speed fan. Results of this study (ref. 1) showed that a fan with an optimum aerodynamic design having a high solidity and operating at low tip speed offered significant noise reduction potential. The experimented program described in this report summarizes results of tests on a fan which is higher in solidity than the one tested in reference 1 and is on design aerodynamically at the test conditions.

The report includes a discussion of the measurement procedures, data reduction procedures, and test results from both the noise and wake measurement portions of this program. Also, comparisons between wake predictions and measurements are discussed. Finally, comparisons between predicted and measured noise levels are shown and the reduction in noise for a given pressure ratio and thrust, for the fan tested, relative to the fan tested in reference 2 is shown. The reader interested in the tabulated 1/3 octave band levels, narrow band spectrum plots, and blade wake data from this program will find them published under separate cover as NASA CR-132259.



## TEST DESCRIPTION

### Fan Configuration

A sectional view of the model fan tested in this program is shown in figure 1. This fan was originally designed for wind tunnel aerodynamic performance studies and was adapted to the requirements of this program by the design and construction of a new bellmouth inlet duct for operation under static conditions. The new duct inlet, which may be seen in figure 1, includes a generous lip designed to prevent flow separation during the static ground testing.

The fan rotor is 0.457 m (18 inches) in diameter, has a hub-to-tip ratio of 0.5, 12 blades, and an integrated solidity (total blade area/flow duct annular area) of 0.78. Its design point is 236 m/sec (775 ft/sec) tip speed with a fan stage pressure ratio of 1.18. The rotor blades incorporate modified NACA series 65 airfoil section with a maximum thickness approximately equal to 2.5 percent of the chord at the tip and 15.5 percent at the root. The blades have approximately 30 degrees of twist. Figure 2 shows a view looking into the bellmouth inlet at the rotor.

The stator assembly consists of 7 swirl recovery vanes which have a constant chord of 9.44 cm (3.72 in.), a maximum thickness of 9 percent of the chord, and incorporate NACA series 400 airfoil sections. The vanes are located downstream of the rotor so the distance between the trailing edges of the rotor blades and the leading edges of the stator vanes at a blade angle of 58 degrees is equal to 1.85 mean rotor blade chords.

The exhaust nozzle has an exit area of 0.1138 m<sup>2</sup> (1.225 sq ft) for an area ratio of 0.924.

### Test Facility Description

The tests were conducted on a level, asphalt-covered open area. The fan was driven by a variable frequency drive, electrically powered Propeller Test Rig (PTR). The center of the fan was located approximately 3.35 m (11 ft) above the ground plane. The area was free of obstructions within more than 100 m (328 ft) except for the PTR and instrumentation control building of dimensions 2.74 m high by 2.74 m wide by 6.71 m long (9X9X22 ft) located behind and to the side of the PTR, as shown in figure 3.

Noise measurements were made along a 7.62 m (25 ft) radius by means of a microphone which was indexed in 10-degree increments from 0 degrees (i.e., directly in front of the fan, on axis) to 150 degrees. Also, two stationary microphones were

located at 3.05 m (10 ft) at 60 and 120 degrees. All microphones were located at fan centerline height. Figure 4 is a photograph of the fan, test facility and microphone support system.

For all of the acoustic tests, an anechoic platform was located on the ground mid-way between the fan and the microphones. This platform minimized the influence of ground reflection on the noise data permitting measurements which are equivalent to those that would be measured if the fan had been operated in free space. A detailed description of this platform is given in NASA CR 132259 along with results of tests to evaluate its performance.

### Instrumentation

Aerodynamic and acoustic instrumentation. - The fan drive system was equipped with a torque meter and thrust meter for measurement of rotor torque and rotor thrust. Also, a 60-tooth wheel was used with a magnetic pickup for rpm measurement; and a once-per-revolution (1P) pickup was included for synchronization purposes during later analysis.

A total pressure rake was located at the fan duct exit. This array consisted of 10 area-averaged Kiel probes. Also, the static pressures on the inner and outer walls of the exit annulus were measured. This instrumentation allowed the calculation of the fan exit pressure ratio and the total fan thrust. Other instrumentation was included for measuring wind speed and direction, ambient temperature, and relative humidity.

Noise was measured with Bruel and Kjaer (B&K) 1.27 cm (1/2-inch) diameter condenser microphones type 4133 having an essentially flat frequency response to 40,000 Hz. B&K type 2614 cathode followers were used with the microphone cartridges, and B&K type A0 0029 30 m (100 ft) extension cables were used to link the microphones to the recording system located in the control room. The data was recorded on magnetic tape using a Hamilton Standard/Ampex AR200 14-track system operating at 1.524 m/sec (60 inches/sec) tape speed with wide-band FM record amplifiers having flat frequency response from dc to 40,000 Hz. The microphones were calibrated using a B&K type 4230 calibrator.

Blade Wake Instrumentation - Two types of fast response probes were used in the program: a two-sensor Datametrix hot-wire probe and a dynamic total-pressure probe, both shown in figure 5. These probes were located in the plane defined by the vane leading edges, mid-way between two vanes, as indicated in figure 1. The hot-wire probe was designed so one sensor (AA) is always approximately perpendicular to the resultant mean velocity and is thus independent of flow angle fluctuations in the rotor blade wakes. The second sensor (BB) is in a plane perpendicular to sensor AA and is sensitive to flow angle variations. The probes were custom-built

for the United Aircraft Research Laboratories by Datametrix utilizing sensors with tungsten wire of 0.0127 mm (0.00050 in.) diameter and 2.54 mm (0.100 in.) length. Both sensors were mounted in a catenary configuration to minimize strain-gage effects and to increase the durability of the probe. The hot-wire sensors were operated in the constant-current mode using a Datametrix Model 1900 Constant-Current Anemometer. Sensor AA was operated as a resistance thermometer with a current sufficient to measure the wire resistance with a good signal-to-noise ratio, but with a temperature less than 0.22°K (0.5° F) above the ambient temperature. Both Sensors AA and BB were operated at elevated temperatures where both sensors responded to mass flow variations as well as temperature fluctuations and Sensor BB responded to air angle fluctuations. A flat frequency response in excess of 50 kHz was obtained for both the heated and unheated sensors with a compensating amplifier.

The dynamic total pressure probe had a diameter of 1.65 mm (0.065 in.) to minimize probe blockage effects and a sensor location selected to coincide with the center of the hot-wire sensor AA when the probe centerlines are matched. The miniature pressure sensor in the probe was manufactured by Kulite Semiconductor Products. The sensor is a silicon diaphragm with a wheatstone bridge incorporated in it. The sensor had an active diameter of 0.711 mm (0.028 in.) excited by 5.0 volts dc. The natural frequency of the sensor was 250 kHz; and, since the diaphragm was known to have a second-order response, the sensor response was calculated to be within 4 percent of the true value for frequencies from dc to 50 kHz.

The block diagram for the system, which used the probes described above, is shown in figure 6.

#### Test Procedure

For the aerodynamic and acoustic noise measurements, the following parameters were recorded on magnetic tape:

- Acoustic signals
- Wind speed
- Rotor rpm
- 1P pipper
- Rotor torque
- Rotor thrust
- Voice (for identification of runs, etc.)
- Time and run codes

Prior to testing, the system was allowed to warm up to ensure stability. Prior to each day's running, a calibration tape was prepared. This recording included the microphone calibration signals using the B&K microphone calibrator, as well as rotor thrust and torque and wind speed calibrations. Subsequent reels of data were normalized by means of a full scale standardization signal injected into each channel with the recording system gains normalized.

In addition to the recording of the above parameters, the following was hand logged: test condition, date and time of day, blade angle, rpm, thrust, torque, wind speed and direction, ambient temperature, relative humidity, barometric pressure, total and static pressures at the fan duct exit, and all preamplifier gain settings. Much of this information was also voiced on the tape recording for redundancy.

Two proximity pickups, located in the rotor plane 90 degrees apart, were used to monitor the clearance between the rotor tip and the shroud. This data was not recorded or logged, but used only to ensure positive clearance during the testing.

The test procedure adopted resulted in the following sequence. The test condition (i.e., rotor rpm and blade angle) was set and allowed to stabilize. The tape system was then activated with the indexing microphones (two microphones were used - one for redundancy) located at 150 degrees. Approximately 30 seconds of data were recorded. The indexing microphones were then moved to 140 degrees, without interrupting the recording process. Again, approximately 30 seconds of data were recorded for that microphone location. This process was repeated until a continuous recording of at least 5 minutes had been obtained. This procedure allowed recording of long bursts of data for later correlation of the signals from the two stationary microphones to wind condition and to observe temporal variations of the various fan noise components. Subsequent to the 5-minute continuous recording, the tape transport was stopped while the indexing microphones were being moved. Contiguous with the magnetic recordings, the previously mentioned parameters were hand logged.

For blade wake measurements, the test procedure was as follows. The signals were recorded sequentially to allow the data to be taken at the same point in the fan model. The "clock" used to ensure averaging of data from wakes of the same rotor blades was a once-per-revolution pimper signal. The probes were aligned at the mean flow angle calculated by the Hamilton Standard fan aerodynamic performance procedure. Mean sensor and flow properties were recorded by hand and the sensor fluctuating voltages and pimper signal were recorded on magnetic tape simultaneously.

#### Fan Operating Conditions

The fan operating conditions for this program are summarized in Table I. The tip speed, blade angle, input power, and pressure ratio were measured quantities, while the net thrust was calculated from the blade angle, input power, and tip speed based on previous performance data from earlier aerodynamic tests on this fan.

The ranges covered include blade angle from 38 to 62.5 degrees, tip speed from 147 to 273 m/sec (483 to 895 ft/sec), input power from 89 to 298 Kw (119 to 400 shp), and fan pressure ratio from 1.060 to 1.151.

Figure 7 shows the input power plotted versus tip speed at constant blade angle. The test conditions were initially selected on the basis of constant pressure ratio lines. Approximately constant pressure ratio lines are seen in the vicinity of 1.07, 1.10, 1.12, and 1.14. The advantage of testing a variable pitch fan in an acoustic research program can be seen in figure 7 where a wide range of tip speeds can be seen to produce essentially constant pressure ratio and, therefore, essentially constant thrust. Tests of fixed pitch fan models allow only tests along one blade angle line so the added dimension of pitch change influence cannot be investigated.

#### Data Reduction Procedure

Aerodynamic data reduction. - The aerodynamic data was acquired to define the exit pressure ratio and the power transmitted to the rotor. Since the radial locations of the total pressure probes were area weighted, the exit pressure ratio was computed by summing the pressures and dividing by 10. This number was then divided by the barometric pressure. The power was calculated from the rpm and rotor torque. Net thrust was calculated based on the power input to the rotor, the blade angle, and the rpm plus performance data measured under static conditions during the wind tunnel tests of this fan conducted in an earlier test program.

Acoustic data reduction. - All data was analyzed by 1/3-octave bands. The data from the indexing microphone was processed by a General Radio Model 1921 real time analyzer interfaced with a Hewlett-Packard high-speed paper-tape punch. Since the analyzer covers the range 25 to 20,000 Hz, the data was played back at half speed. With an integration time of 32 seconds, the resulting spectra were equivalent to those of the actual data from 50 to 40,000 Hz with 16 seconds integration time. The data were analyzed for each operating condition and for each of the 16 microphone locations. The punched tape data were then transferred to computer cards and used as input for a computer program which tabulates the data, corrects the data to remove excess atmospheric attenuation, calculates the sound power levels (PWL) for each 1/3-octave band, scales the data to another thrust level if required (assuming constant tip speed and constant thrust-per-diameter-squared), extrapolates the data to a specified radius and sideline, and calculates the Perceived Noise Level (PNL) and Tone Corrected Perceived Noise Level (PNLT).

Narrow band analyses were performed using a Spectral Dynamics SD301B real time spectrum analyzer with an SD302B ensemble averager. The analyzer was set to an effective, 3-dB down-point, bandwidth of 60 Hz and used over the range 0 to

20,000 Hz. For most of the data, 512 ensembles were averaged, although some shorter runs allowed only 256 averages. These represent analyses of 1024 and 512 degrees of freedom or 25.6 and 12.8 seconds of data, respectively.

The harmonic and 1/2-harmonic (i. e., the broadband noise midway between harmonics) levels obtained from the narrow band plots were tabulated and used to compute the harmonic and 1/2-harmonic PWL for each fan operating condition. These were used to establish the fan noise signature and to compare with theoretical calculations of fan noise.

Blade wake data reduction. - The time-dependent hot wire and fast response total pressure data were reduced to obtain the temporal periodic variation of flow velocities at each test point. The first step in the data reduction procedure was to obtain a temporal variation of each data signal by playing the taped signal into SAICOR Correlation and Probability Analyzer Model 42 used as a signal enhancer. The signal enhancer integrates the signal over 100 selected time steps after a trigger signal pulse for  $512 \times 2^N$  periods where N is an integer from 1 to 9. The time step was selected such that the time for one blade gap to pass the sensor was 25 to 35 percent of the time steps. This provided a sufficient number of data points for good blade wake definition. The 100 integration time steps could also be delayed up to 200 time steps; this feature allowed a total of 300 time steps to be examined (approximately 10 out of the 12 blade gaps). A once per revolution pulse was used to trigger the signal enhancer. For these tests, data from 1024 revolutions of the fan rotor were used to obtain the periodic data. The enhanced data were digitized on a magnetic tape for computer processing. Additional information provided for data reduction include probe calibration data, mean flow properties, mean sensor properties, and amplifier-attenuation settings.

The data reduction was accomplished using the Data Reduction Procedure for Periodically Unsteady Compressible Flow developed by United Aircraft Research Laboratories. The first operation in this procedure is to calculate the fluctuating thermodynamic properties and the absolute velocity from the heated and unheated vertical wire hot-wire data and the high response total pressure probe data. The calculation procedure is similar to that described by Morkovin in reference 3. The second operation in the Data Reduction Procedure is to calculate the fluctuating flow angle from the hot-wire data obtained from the heated and unheated vertical hot wire and the heated horizontal hot wires. In the final operations, the fluctuating velocities are combined with the time-averaged velocity measurements to obtain the temporal periodic variation of flow velocities in the stationary coordinate system at the measurement location. These velocities in the stationary coordinate system are translated to the rotor coordinate systems by subtracting the rotor tangential velocity from the temporally varying velocity. This Data Reduction Procedure has several advantages over other procedures (e. g., references 4 and 5) used to calculate the periodically unsteady flow behind rotor or fan blades. One advantage is that using the data obtained with a Constant Current Anemometer rather than a constant resistance wire allows the fluctuating temperature to be measured and to be accounted for in the flow

angle fluctuation calculation. The wire recovery temperature or flow total temperature fluctuations increases with rotor tip speed and is very important in high speed high pressure-ratio fans. A second advantage is that the local thermodynamic properties of the compressible flow (i. e., pressure, temperature, and velocity) are determined in a coupled manner rather than assuming one thermodynamic property value as is required when only pressure fluctuation data and heated hot wire data are available. Again, this advantage is greater when the fluid pressure and temperature fluctuate large amounts as in the case for high tip speed fans. For the present tests, it is believed that good approximate velocity and air angle fluctuations could be obtained using constant fluid property assumptions in evaluating the hot wire data from the horizontal and vertical sensors.

All of the analyzed data described above are published under separate cover as NASA CR-132259.



## DISCUSSION

### Introduction

Both acoustic and blade wake information was obtained in the program described in this report. In the following discussion, the acoustic data is described first, followed by a detailed discussion of the wake data. In this acoustic discussion, the trends of noise with thrust, pressure ratio, and tip speed, as well as spectrum character, are described first in model scale as measured. Then, data are scaled to a 1.402m (4.6 ft) diameter and compared with test data measured on a 1.402m (4.6 ft) diameter fan similar in design. Also, the 0.457 in. (18 in.) fan data are compared with test data from the lower solidity 0.533m (21 in.) diameter fan, both scaled to 66720 newtons (15000 lbs) thrust. Finally the noise data are compared with predicted levels. In the wake data discussion, the measured results are first discussed and then the qualitative and quantitative implications of the wake characteristics on stator noise generation are discussed.

### Acoustic Data

In the following discussion, the data contained in NASA CR-132259 were utilized to establish noise trends for source noise evaluation. Processed 1/3 octave band sound pressure level data were used to establish the variation of the fan noise with such parameters as tip speed, net thrust, and pressure ratio. Narrow band sound pressure level data were used in evaluation of tone and broadband noise components. Narrow band sound power level data were used in evaluating the relationship of wake characteristics to noise and in comparisons between measured and predicted sound spectra. Also, a discussion of limited tests showing the influence on noise of wind and inflow distortion due to small disturbances is included. The scaled data were used to compare the noise of the 0.457m (18 in.) fan tested in this program with that from an earlier design of 0.533 m (21 in.) diameter which was tested in 1970 (see ref. 2) and with a very similar, full scale fan of 1.402 m (4.6 ft) diameter which is now being tested at Hamilton Standard in a NASA Lewis contract.

Trends in acoustic data as measured. - Figure 8 shows the fan noise data as a function of the corrected fan net thrust. The noise levels plotted are the maximum PNL on a 7.62 m (25 ft) sideline with attenuation due to atmospheric absorption corrected to standard conditions. As this figure shows, the curves of PNL vs thrust for the six test blade angles can be included in a band approximately 6 PNdB wide. The average slope of these curves is 8 PNdB per doubling of thrust. This slope may at first appear inconsistent with 6 dB per doubling of thrust expected from classical fan noise scaling laws. However, figure 8 is based on test data which was obtained at constant blade angle, so the thrust increase is the result of a tip speed increase. It is therefore suggested that the 2 dB increase in the slope is due to a tip speed effect.

For this fan, the variation of noise with tip speed cannot be considered a simple function, since truly optimum aerodynamic operating conditions exist in only part of the fan operating envelope. In general, the noise generated by a fan will be lowest at some operating condition associated with high aerodynamic performance. Both the 62.5 and 57.4 degree blade angle curves show minima near 2300 and 2400 newtons (520 and 540 pounds) of thrust, respectively. These two operating conditions represent tip speeds of 206 and 210 m/sec (675 and 688 ft/sec), respectively. A similar inflection point is seen in the 52.6 degree blade angle curve at the thrust value corresponding to approximately 200 m/sec (656 ft/sec) tip speed. The minimum noise occurs for the 43 and 47.1 degree blade angle conditions, while the highest noise levels are for the 57.4 degree blade angle conditions. Figure 9 was prepared to illustrate the variation in noise level with blade angle and tip speed at constant thrust. This figure shows the 1/3-octave band spectra at 7.62 m (25 feet) and 120 degrees azimuth for the four operating conditions at or near 2300 newtons (520 pounds) thrust. The low and high frequency components are seen to be very similar for the four blade angles, whereas the mid frequency bands, particularly those containing the harmonics of blade passing frequency, show the greatest difference and also have the most effect on the PNL. The 43 degree blade angle condition is the quietest, although it also has the highest tip speed. The noise levels then increase with increasing blade angle and decreasing tip speed until 57.4 degrees at 210 m/sec (688 ft/sec) which is the condition of highest noise level. The level drops again at 62.5 degrees and 206 m/sec (675 ft/sec). Figure 10 shows a comparison of the narrow band noise spectra at 120 degrees azimuth for the noisiest and the quietest conditions in figure 9. It can be seen that again there appears little difference in the broadband noise levels, but the tone levels show a large difference.

Figure 11 shows a cross plot of the noise against tip speed at constant thrust levels of 1500, 2000, and 2600 newtons (337, 450, and 585 pounds), respectively. The tip speeds used in this figure were interpolated from the test points plotted in figure 8 and the tip speeds in Table I assuming that the thrust is proportional to the tip speed squared. A family of curves is, thus, obtained which shows that, for a given thrust, there is a blade angle/tip speed combination which produces a minimum noise. For the above thrust levels, the minima are seen to be at 200, 228, and 235 m/sec (656, 748, and 771 ft/sec) tip speed for 1500, 2000, and 2600 newtons (337, 450, and 585 pounds), respectively. Also, it can be seen that blade angle for minimum noise does not remain fixed as thrust is varied. At 1500 and 2000 newtons (337 and 450 pounds) the minimum occurs at 43 degrees, while the minimum noise occurs at 50 degrees for the 2600 newton (585 pound) case.

Figure 12 shows the fan noise variation with pressure ratio for constant blade angles. This plot shows similar trends to those described above; viz, the noise levels are higher for the 38 degree blade angle, decrease to a minimum near the 47.1 degree blade angle, then increase again with increasing blade angle. The heavy line in the figure joins the probable minimum noise level achievable in this fan over the range

of blade angles and tip speeds tested. This line appears to have fairly constant slope from a pressure ratio of 1.09 to a pressure ratio of 1.13. Since no data exists at 52.6 degree blade angle beyond a pressure ratio of 1.142 and at 57.4 degree blade angle beyond a pressure ratio of 1.151, the curve has been extrapolated on the basis of the characteristics of the fan at the test conditions plotted. This extrapolation is shown as a dashed line in figure 12.

Figure 13 shows the noise data plotted against corrected tip speed with constant pressure ratio lines (based on information in figure 12). Again, minimum noise points are seen to occur at a particular tip speed for a given pressure ratio.

The effects of tip speed on the 1/3-octave band sound pressure levels are illustrated in figure 14 for the 47.1 degree blade angle (i. e., the blade angle showing the lowest noise for a given pressure ratio). The levels shown in figure 14 are those measured at 120 degrees azimuth and 7.62 m (25 ft) distance and include standard day excess atmospheric attenuation. The spectra show that in model scale the perceived noise level is dominated by the 1/3-octave bands containing blade passage tone and, to a lesser extent, its harmonics. The narrow band plots equivalent to the 1/3-octave band plots in figure 14 are shown in figure 15. The broadband noise in figure 15 may be shown to vary approximately as the tip speed to the seventh power, although one would expect (based on data from the literature) that the broadband noise in this fan should be due to dipole sources such as vortex noise and, thus, vary as the tip speed to the sixth power. Also the tone levels for the three conditions are shown to vary in a similar manner as those of the broadband noise levels.

Figure 16 shows the 1/3-octave band levels for the fan plotted as a function of tip speed and blade angle at a constant pressure ratio of 1.094. The spectra in these curves are seen to be dominated by the 1/3-octave bands containing blade passage frequency and its harmonics while the high frequency 1/3-octave bands remain relatively constant. Figure 17 shows the equivalent narrow-band spectra. The broadband noise in figure 17 can be seen to be constant and independent of the tip speed and appears to be a function of the pressure rise, or energy input, only. The tones, however, do show a strong variation with the tip speed as was found in figure 16.

Figure 18 shows the 7.62 m (25 ft) sideline noise levels plotted with varying fan pressure ratio at constant tip speed (approximately 210 m/sec (688 ft/sec)). This curve shows that, generally, the fan noise exhibits a peak in the noise in the aft quadrant at 110 to 120 degrees azimuth. The directivity pattern does not change appreciably with pressure ratio as the PNL at all locations increase fairly uniformly.

Figure 19 shows the 7.62 m (25 ft) sideline noise levels plotted with varying tip speed at a constant pressure ratio of about 1.094. Although the same general directivity pattern is seen in this figure as was shown in figure 18, there appears to be a stronger dependence on tip speed than was seen for pressure ratio. The noisiest

point is seen to be at 100 to 110 degrees for a tip speed of 189 m/sec (620 ft/sec). The quietest tip speed, 212 m/sec (697 ft/sec), is seen to also have the smoothest directivity function.

Influence of wind and blockage on noise. - At the completion of the acoustic test portion of the program two tests were conducted to study the influence of wind speed and fan inlet blockage on the noise generated by the fan. To evaluate the effect of wind speed on noise, the fan was operated at one condition; viz, 57.4 degrees blade angle at 187 m/sec (613 ft/sec) tip speed, with nearly zero and approximately 2.7 m/sec (6 mph) wind speed. Since air is drawn into a statically operating fan around the inlet lip, the influence on noise of the small instrumentation cable support post between the fan shroud and the ground was evaluated. This support, 4.43 cm (1.75 in.) in diameter, which can be seen in figure 4, was located approximately 25 cm (10 in.) below the duct and 36 cm (14 in.) back of the inlet lip.

During these tests, long data samples recorded by the stationary microphones located at 60 and 120 degrees azimuth on a 3.05 m (10 ft) radius were analyzed by means of a tracking filter centered on the blade passing frequency and then on its second harmonic. The results of this analysis are summarized in figure 20, which shows the correlation between the noise levels and the wind speed and inflow distortion.

In the front quadrant, typified by the data from the 60-degree azimuth microphone, the average level of the blade passage frequency is practically unaffected by either wind or flow disturbance, although the fluctuations in level are significantly greater during low wind conditions. The second harmonic is seen to be affected by both wind and flow disturbance.

In the aft quadrant, i. e., the data from the 120 degree microphone, the level of the blade passage frequency is affected by wind speed only, whereas the second harmonic is affected by the combination of low wind and the flow disturbance.

Note that under low wind condition the tone levels fluctuate approximately  $\pm 7$ dB over a time span of 15 to 20 seconds. From this it can be concluded that long data samples are needed for good statistical averaging.

Figure 21 shows the effect of the wind and inlet flow disturbance on the sideline PNL. Although the difference in the levels for the three configurations tested is small, it is seen that the lowest sideline PNL values occur for the case with the post removed. Also, in the cases with the post in place, the levels are essentially independent of the wind speed.

From this limited study it is concluded that even small inlet disturbances in an ideal test facility can have a measurable effect on noise produced by a fan (2 PNdB in figure 21). In the case of the low tip speed fan tested, this effect is most pronounced at the point of maximum sideline noise, which occurred aft of the plane of rotation at 100 degrees.

Comparison of fan noise at 1.402 m (4.6 ft) diameter. - In the previous discussion, the noise trends in model scale were summarized. This information is of interest for small fans with low thrust requirements. However, trends at larger diameters are of more interest in typical large-vehicle installations. The discussion below summarizes the PNL and spectral characteristics for the model fan scaled to 1.402 m (4.6 ft) in diameter. Levels are also compared with test data from a 1.402 m (4.6 ft) diameter fan of similar design.

Figure 22 shows the maximum 152 m (500 ft) sideline PNL plotted versus pressure ratio for the 0.457 m (18 in.) diameter fan scaled to an equivalent 1.402 m (4.6 ft) diameter fan, while figure 23 shows the 1.402 m (4.6 ft) diameter fan test data. The similarity in basic configuration of these two fans is shown in Table II. The heavy line in figures 22 and 23 indicate the minimum noise level at a given pressure ratio. These two minimum noise lines are compared in figure 24. The smaller fan shows slightly higher noise levels below about 1.15 pressure ratio, the point where the two fans produce equal noise. The similarities of the noise from these two fans is illustrated in figures 25 through 28, which show 1/3-octave band plots for four representative operating conditions. Here the data from the 0.457 m (18 in.) diameter fan has been scaled to the equivalent of a 1.402 m (4.6 ft) diameter fan. The data from these figures show that the portion of the noise spectrum dominated by broadband noise, i. e., the 1/3-octave band levels at 1600 Hz and above, is very similar to that from the smaller fan, being generally 1 to 3 dB higher. This slightly higher level of broadband noise is the reason for the PNL of the smaller fan being slightly higher than that of the other fan. The slightly higher level of noise of the 1.402 m (4.6 feet) fan at 400 Hz and lower is due to engine noise contribution which does not exist in the 0.457 m (18 in.) fan. This difference, however, does not contribute to differences in PNL because it occurs at low frequencies.

Figure 29 shows the noise trend of the 0.457 m (18 in.) diameter fan scaled to 1.402 m (4.6 ft) in diameter as a function of tip speed for three constant thrust levels. Trends are seen to be similar to those in figure 11 where data in model scale are plotted. It is interesting to note in figure 29 that the minimum noise occurs at blade angles from 40 to 47 degrees so operation at a fixed pitch would produce noise slightly higher than the minimums.

Comparison of fan noise at 66720 N (15000 pound) static thrust. - The test data from the 0.533 m (21 inch) diameter fan tested in 1970 (ref. 2), and data from the 1.402 m (4.6 ft) diameter fan tested in 1972 were scaled to a common thrust level of 66720 N (15000 pounds) for comparison. Table II presents a comparison of the fan characteristics. It can be seen that the 0.457 m (18 in.) and 1.402 m (4.6 ft) fan are

similar while the 0.533 m (21 in.) fan is different. The maximum PNL referred to in the following discussion is the peak PNL on a 152.4 m (500 ft) sideline based on measured fan noise adjusted in level and frequency to an equivalent fan producing 66720 N (15000 pounds) thrust extrapolated to 152.4 (500 ft) sideline distance assuming spherical spreading of sound and standard atmospheric attenuation.

Figure 30 shows the scaled PNL for the 0.457 m (18 in.) diameter fan plotted against pressure ratio. The heavy line passes through the minimum noise points and represents the best (i.e., lowest noise) blade angle and tip speed combination that gives the required thrust at the given pressure ratio for this fan. Figures 31 and 32 show similar plots for the 0.533 m (21 in.) and 1.402 m (4.6 ft) diameter fans, respectively.

The 0.457 m (18 in.) and 1.402 m (4.6 ft) diameter fans, which are similar in design, show essentially the same slope of PNL variation with pressure ratio, there being an increase of about 5 PNdB for a pressure ratio range of 1.04 to 1.09, whereas the 0.533 m (21 inch) diameter fan, which was lower in solidity and operating off design, shows a PNL increase of 9 PNdB over the same pressure ratio range. This conclusion is illustrated in figure 33 which shows the minimum PNL lines superimposed on the same figure. As this figure shows, the 0.457 m (18 in.) and 1.402 m (4.6 ft) diameter fans have very nearly equal PNL's over the range of pressure ratios tested while the 0.533 m (21 in.) diameter fan is generally significantly noisier. This important result confirms the trend shown in reference 1, where it was predicted that a higher solidity fan operating close to its design point would produce lower noise than a lower solidity fan operating off design.

Figure 34 shows a comparison of the scaled 1/3-octave band levels measured for the 1.402 m (4.6 ft) and 0.533 m (21 in.) diameter fans and interpolated data for the 0.497 m (18 in.) diameter fan at the pressure ratio of 1.08 where the difference in PNL between the noisiest fan and the quietest fan is 4.5 PNdB. As this figure shows, the spectra from the 0.457 m (18 in.) and 1.402 m (4.6 ft) diameter fans are similar and both contain less mid frequency noise than does the 0.533 m (21 in.) diameter fan. It should be noted that the spectrum of the 0.457 m (18 in.) fan shown in this figure differs from spectra for other microphone locations in that the fundamental of blade passing frequency (in the 250 Hz band) is lower than that of the second harmonic (in the 500 Hz band). Examination of the sound power level (PWL) data shows a more conventional relationship in which the fundamental slightly exceeds the second harmonic. The spectrum in figure 34 was chosen because it occurred at the location of the maximum sideline PNL. Although the low frequency noise of the 0.533 m (21 in.) diameter fan falls further below the constant noy contour than that of the other two fans, its mid frequency noise is considerably above the constant noy contour. Thus, on a subjective basis, as reflected by the PNL values, the 0.533 m (21 in.) diameter fan is noisier than the 0.457 m (18 in.) or the 1.402 m (4.6 ft) fan because of its significantly higher mid frequency noise. It should also be noted that the peak in the 250 Hz 1/3-octave band for the 1.402 m (4.6 ft) diameter fan is abnormally high at the particular

operating condition shown. At higher pressure ratios, where a lower blade angle produces minimum noise, it is found that this peak is more consistent with the data shown for the 0.457 m (18 in.) fan. It is possible that the inflow disturbances due to atmospheric conditions and test rig support structure have more influence on the blade passage frequency noise of the 1.402 m (4.6 ft) diameter fan than disturbances which existed during the 0.457 m (18 in.) fan tests.

Figure 34 shows another important result which was predicted in reference 1, i. e., increased rotor solidity allows operation at a lower tip speed for a given pressure ratio. Operation under optimum aerodynamic design conditions at the minimum tip speed results in minimum noise. It can be seen that as solidity increases from the 0.72 solidity of the 0.533 m (21 in.) fan to the 0.78 solidity of the 0.457 m (18 in.) fan to the 0.85 solidity 1.402 m (4.6 ft) fan, the tip speed for a pressure ratio of 1.08 drops from 238 m/sec (780 ft/sec) to 210 m/sec (688 ft/sec) and then to 167 m/sec (550 ft/sec).

Comparison of measured and predicted fan noise. - Figures 35 through 38 show comparison of measured and predicted 1/3-octave band PWL for the four conditions shown previously in figures 25 through 28. The PWL's shown in these figures are those for an equivalent 1.402 m (4.6 ft) diameter fan. Predictions were made with the fan noise computer program used in reference 1. The 1.402 m (4.6 ft) diameter fan is considered more appropriate for comparisons than a smaller size model when discussing PNL, since most applications require fans as large or larger than 1.402 m (4.6 feet) in diameter. The PNL's indicated in figures 35 through 38 are the maximum for the 1.402 m (4.6 ft) diameter fan on a 152 m (500 ft) sideline.

In general, these four plots show that the prediction procedure tends to overestimate the mid frequency noise and underestimate the high frequency noise. It is interesting to note that this effect tends to be self-compensating in the calculation of PNL so that the agreement in the sideline PNL is quite good. This can be seen in figures 39 and 40 where the 152 m (500 ft) sideline noise levels are plotted as a function of tip speed for blade angles. Note that in this figure the data were again scaled to that of an equivalent 1.402 m (4.6 ft) diameter fan. From figures 39 and 40, an obvious conclusion is that the prediction procedure slightly underestimates noise at high blade angles and overestimates at low blade angles. The trend of noise with tip speed is, however, very well predicted. The agreement between measured and predicted levels is very good for the 52.6 degree blade angle case where it may be seen that the calculated levels are within about 1 PNdB of the measured levels.

Figure 41 was prepared to relate the results of the program reported here to results obtained in earlier studies using a fan noise computer program (see ref. 1). This figure shows the variation of the maximum 152 m (500 ft) sideline PNL of a 45,360 kg (100,000 pound) aircraft as a function of fan pressure ratio based on the 0.457 m (18 in.) diameter test data of figure 30 scaled to a thrust of 66720 N (15,000

pounds) with 6 dB added to account for the presence of four nacelles on the aircraft. Also, for comparison, the predicted levels from reference 1 are shown for the 0.79 solidity unsuppressed fan with optimum exit area ratio as they appear in reference 1 plus the same unsuppressed fan levels from reference 1 adjusted (using reference 1 values) to account for an exit area ratio of 0.924 (i. e. , that of the 0.457 m (18 in.) diameter fan tested in this program) rather than the optimum area ratio.

The agreement between the curve based on test data and the other two curves is seen to be quite good, the difference being less than 3 PNdB except at very low pressure ratios where measured levels are 4.5 PNdB less than levels predicted in reference 1.

### Blade Wake Evaluation

Introduction . - One of the overall goals of the wake velocity and noise measurement studies was to develop a better understanding of the interaction between rotor wakes and the stator which produces noise. In order to provide a background for the data to be presented, the velocity vectors for a classical, constant density inviscid wake flow are shown in figure 42. The upper sketch shows the velocity vectors of the flow into the rotor blade in the stationary and rotor coordinates and the flow behind the blade in the rotor coordinate system. The wake vector is shown for the classical flow case where the blade wake is considered to be aligned with the inviscid flow downstream of the rotor, but having a smaller velocity in the rotor coordinate system. The flow velocities in the rotor coordinate system are translated to the stationary system with the addition of the rotor speed, as shown in the lower sketch of figure 42. The flow in the blade wake has a velocity relative to the inviscid flow which is approximately perpendicular to the mean flow direction. The result is that, as the wake flow passes the stator, the instantaneous angle of attack as shown in the sketch is usually increased. Although the flow behind fan and compressor rotors is more complex than shown on these sketches, the principal velocity relationships are as shown. Behind the rotor, the flow is usually turbulent and is often not stationary with respect to a given blade because of incipient stall or turbulent fluctuations in the wakes. Consequently, the flow at the stator inlet is modulated about the periodic flow structure.

Measurements of the fluctuating velocities were obtained at the stator leading edge plane for three flow conditions. Flow Condition I was at a blade angle of 52.6 degrees and a rotor speed of 10,080 rpm and had a total pressure ratio across the fan of approximately 1.14, one of the highest pressure ratio conditions in the test program. Flow Conditions II and III both resulted in a pressure ratio of approximately 1.07. Flow Condition II had a blade angle of 57.4 degrees, a rotor speed of 6620 rpm, and is considered a high blade-work flow condition. Flow Condition III

had a blade angle of 48 degrees, a rotor speed of 7650 rpm, and is considered a low blade-work flow condition. Data were obtained at 10 equally spaced spanwise locations from 5 percent span to 95 percent span from the stator root for Flow Condition I and at five selected span locations for Flow Conditions II and III.

All the blade wake data obtained in this program are presented in NASA CR-132259.

The following three sections summarize the results from the blade wake data from each of the three measurement conditions.

Wake data at Flow Condition I. - A comparison of the resultant velocity profiles and air angles in both the stationary and rotor coordinate system for the ten span locations for Flow Condition I are presented in figures 43 and 44. The velocity vectors which most clearly represent the classical inviscid wake flow model of figure 42 can be seen at the 65 percent span location. For this span location, the velocities and air angle in the stationary coordinate system are approximately constant except in the wake region. In the wake region, the axial velocity is decreased and the tangential velocity is increased. The work input to the wake flow by the rotor is greater than that put into the inviscid flow because the tangential velocity increase is greater in the wake region. When these velocity vectors are translated to the rotor coordinate system, the classical cascade velocity profile is obtained; the air angle as shown in figure 44 is approximately constant, and the rotor wakes of figure 43 show a velocity defect. Similar results were obtained for the 75 percent span location. However, the results at greater or smaller spans than 65 and 75 percent show effects of the rotor tip vortex, or nonuniformities in the inviscid flow region. At 85 percent span, a twice per blade signal occurs in the stationary coordinate system air angle fluctuation. The small-width air angle decrease (e. g., at a dimensionless time,  $T/\tau = 20$ ) is attributed to the blade wake. The large-width air angle decrease (at  $T/\tau = 35$ ) is attributed to the presence of the secondary flow vortex that exists in the corner formed by the blade suction surface and the fan casing. At 95 percent span, the velocity defects are probably due to the secondary flow corner vortex and not associated with the fan blade wakes. The flow near the root of this fan blade has large variations as shown for the 5 and 15 percent span measurements. The velocity profiles for 5 percent span in the stationary coordinate systems show large velocity fluctuation, but rather small flow angle fluctuations. In the rotor coordinate system, the flow angle fluctuations are large and the blade wake velocity defects are small. These results are attributed to the large secondary flows that occur between the blade and stators near the rotor hub due to the presence of a simulated engine inlet downstream of the rotor which was not passing any significant air flow. The velocity profiles in the rotor coordinate system for 15, 25, and 35 percent span have the classical wake characteristic with little or no flow angle change in the wake. However, the blade wake widths are large, indicating the blade may be partially stalled at this particular operating condition. For the 45 and 55 percent span locations, the blade wake width and velocity defect decrease, but do not have a uniform inviscid flow profile. The blade wake

velocity defects in the rotor coordinate system at 95 percent span are aligned with a velocity defect at 85 percent span and are smaller than the secondary flow corner vortex velocity defect.

Wake data at Flow Condition II. - The resultant periodic velocities and air angles at the stator inlet plane for Flow Condition II are presented in figures 45 and 46. The classical wake structure obtained at 65 percent span for Flow Condition I does not occur for any of these span locations, as all of the present results have flow angle variations in the rotor coordinate system. The fact that these velocity profiles are not classical in nature is attributed to the fact that the fan blades were highly loaded for this flow condition. A comparison of the resultant velocity profiles in figure 45 shows that amplitude of the fluctuations is low (i. e., less than 5 percent from the local mean value) for all five span locations. However, the widths of the disturbances vary from 20 percent to 100 percent of the blade gap.

Wake data at Flow Condition III. - The resultant velocity profiles and air angles obtained at the stator leading edge for Flow Condition III are presented in figures 47 and 48. Flow Condition III had a lightly-loaded blade with the result that the velocity profiles show narrow blade wakes and uniform flow between the blade wakes for 35, 55, and 75 percent span locations. The velocity profiles for 85 and 95 percent span in figure 47 show the larger velocity defects characteristic of the tip region secondary flows. A comparison of the profiles for Flow Condition III shows that velocity defects associated with blade wakes are less than half that of the secondary flow vortex which can be seen at 85 percent span and is indistinguishable at 95 percent span. The modulation of the instantaneous hot wire and total pressure signals about the periodic value was much larger in the tip region than in the midspan region for all three flow conditions. The signal modulation about the periodic values were less than half of the local peak-to-peak variation at midspan and were often two to three times the peak-to-peak variations at the root and tip regions.

Periodic wake characteristics. - The periodic velocity profiles, obtained in the stationary coordinate system and translated to the rotor coordinate system, show a large spanwise variation in the amplitudes and widths of the velocity defects associated with the blade wakes. At the lightly and moderately loaded test conditions, the blade wakes in the rotor coordinate system at 65 and 75 percent span are similar to those typically obtained at an equivalent distance downstream from the blade in cascade tests; i. e., the wakes are narrow and the velocity defect is less than 5 percent of the local resultant velocity. At the heavily loaded test condition, the wakes at the 65 and 75 percent span location are wider than those for the lightly loaded and moderately loaded blades. The amplitude and width of the blade wake velocity defect increased as the blade root was approached until a sinusoidal shape and an amplitude of 10 percent of the local velocity was obtained at the 5 percent span location. Flow angle fluctuation at the root was found to be large, probably because of a simulated engine inlet which was not operated for this program. The major flow perturbations near the rotor tip, at 85 and 95 percent span, appear to be due to a secondary flow vortex caused by the interaction of the rotor blade with the outer shroud wall boundary layer.

Wake modulation characteristics. - In reference 7, it has been shown how the modulation of the rotor blade wakes caused by the turbulence within the wakes leads to broadband acoustic radiation from the stator. In this section a qualitative discussion of the modulation of the measured blade wakes is presented.

Figure 49 shows oscilloscope traces from the hot wire probe for the three flow conditions at root, mid-span, and tip locations. The photographs were made by triggering the oscilloscope with a once-per-revolution trigger while leaving the camera shutter open to capture about 6 successive revolutions of the rotor. Thus, the wake from the same blade appears 6 times at approximately the same location on the photograph. The modulation in amplitude and time of arrival are due to wake turbulence. At mid-span (55% station), the wakes are seen to be isolated or distinct. The considerable amplitude modulation and smaller amount of position modulation (variation in arrival time) conforms well with the modulation model for stator noise reported in references 1 and 7. In the root region (15% station), the wakes are nearly merged and highly turbulent. At the tip, the individual blade wakes are nearly indistinguishable in the turbulence. The major repetitive disturbance seen at the tip at 53-degree blade angle is the secondary flow vortex which can be seen better in the signal enhanced traces of figure 43.

The results of this qualitative study of rotor wake modulation indicates that hot wire anemometer measurements of wake characteristics can be used to gain a better understanding of the influence of wakes at various spanwise locations on noise generation.

Relation of wake characteristics to noise. - The characteristics of the rotor wakes, as measured at the entrance to the stator, have been discussed in some detail in the preceding sections. These wakes have been studied to understand their role in the generation of noise at the stator. This process is discussed in qualitative terms in this section while a quantitative study of the harmonic wake and noise components is presented later.

It was shown in reference 7 how the spectrum components of the stator inlet flow are related to the noise spectrum components: the broadband wake component causes broadband noise and the harmonic wake component causes harmonic noise. In addition, each harmonic of the wake signature couples to the same harmonic of the sound.

Discussing the harmonic noise components first with reference to the harmonic wake components shown in figures 43 through 48, it can be seen that the wake characteristics vary dramatically across the span of the stator inlet. The strong sinusoidal signal, at blade passing frequency in the root regions for Flow Conditions I and II, indicate that the merged wakes are the prime source of blade passing frequency noise generated by the stator. The trend toward merging is not seen for Flow Condition III, although test data were not acquired inside the 35 percent span because of

measurement problems. The periodic component of the flow in the tip region also tends to be sinusoidal, but for different reasons. For all flow conditions, a secondary flow vortex is indicated by the double peak at 75 percent or 85 percent span. At 95 percent span, the viscous wake velocity defect disappears and the secondary vortex dominates. For Flow Condition III, where the root flow appears to be improved, this vortex probably controls the noise at blade passing frequency.

In the mid-span regions, the wakes are isolated or distinct, causing a pulsing signal with significant harmonic content. The higher harmonics in the wake pulse are probably the source of the higher harmonics in the stator radiation. Thus, it is concluded from the available data that the root and tip flow control the stator noise at blade passing frequency while, due to its more pulse-like character, the flow in the mid-span regions contributes more to the higher harmonics of blade passing frequency. The secondary flow vortex may also be a significant noise source in Flow Condition III where the flow is otherwise better behaved.

To study the broadband noise, the modulation about the periodic wake flow shown in figure 49 must be considered. With the probe configuration used, the raw signals cannot be interpreted directly in terms of air angle fluctuations. Hence, the traces in figure 49 can be used only as an indication of modulation relative to the periodic levels. The tip flow shows the greatest modulation and, by comparison with the periodic flow in that region shown in figures 43 through 48, is judged to be a significant source of broadband noise. Similar comments hold for the root flow, but to a lesser degree. The mid-span flow is more nearly periodic and, thus, is probably less of a contributor to the stator broadband noise.

The major conclusion of this wake study is that, for generation of stator noise in the fan tested, secondary flow in the root and tip regions may be more important than the classical two-dimensional viscous rotor wakes.

Evaluation of stator harmonic noise using measured wakes. - It has been shown that interaction of the rotor wake with downstream stators is an important source of broadband and harmonic noise in reference 7. The periodic or repetitive portion of the wake causes a periodic lift response on the stator which, in turn, radiates the periodic part of the stator noise at harmonics of blade passing frequency. There is also a random modulation of the blade wakes about their mean velocity profiles which causes broadband radiation from the stator.

The rotor, similarly, radiates broadband noise and harmonics of blade passing frequency. Since tone and broadband noise produced by a rotor does not differ from that produced by a stator, it is not possible to distinguish the stator contribution from that of the rotor by simply studying narrow band noise spectrum plots such as those of figures 10, 15, and 17. However, the stator noise theory of reference 7 can be used as a guide to determine which portion of the total harmonic radiation can be attributed to the stator by use of wake structure measurements of the fan plus its

noise characteristics. This has been done using the wake data presented earlier in this report. The procedure for this evaluation was as follows: the mean flow parameters such as axial and swirl velocity and effective profile drag coefficient were calculated using an axial flow fan performance computer program. These values were used with the fan noise computer program which predicts wake parameters from the Silverstein wake formulas (ref. 8), stator vane lift response from either the Sears (ref. 9) or the Horlock (ref. 10) theories, and resulting stator noise from the stator noise theory (ref. 7). This computer program prints out the predicted normalized wake velocity defect amplitude,  $\mu c/U$  (the ratio of the peak velocity defect to the undisturbed velocity between blades), and normalized wake width,  $Y/b$  (the ratio of the wake width to the distance between wakes), in a 10 radial station strip analysis. Then, measured values for  $\mu c/U$  and  $Y/b$  were loaded into the noise prediction computer program and the harmonic noise calculation was repeated. Finally, the predicted and measured harmonic spectra was compared.

In Figures 50 through 55 values of  $\mu c/U$  and  $Y/b$  are plotted as a function of percent of span for conditions I, II and III discussed earlier. In each case three curves are shown. The test values were obtained from the measured wake data presented previously. The predicted values labeled "calculation excluding endwall" were calculated using the two-dimensional cascade section loss coefficient for the rotor and the Silverstein wake formulas. For the curves labeled "calculation including endwall loss", the total section loss coefficient including an endwall correction was used with the same Silverstein formulas. It can be seen that this endwall correction improves the wake width predictions of figures 51, 53 and 55 in the root and tip regions since it accounts for all the losses rather than just the two-dimensional losses. However, the endwall loss correction does not produce any clear improvement in the wake defect predictions of figures 50, 52, and 54. The results in figures 50 through 55 show good agreement between test data and calculations in the mid-span region of the stators. The lack of agreement for the three test conditions in the tip region is believed to be due to secondary flows associated with the shroud boundary layer and tip clearance effects. The difference between test and calculation in the root region may also be due to boundary layer and root turbulence effects plus the disturbance due to the simulated core engine inlet (see figure 1) which was operating in this program at the reduced weight flow corresponding to a 60:1 bypass ratio rather than the design value of 15:1.

The merging of the wakes implied by  $Y/b = 1$  is clearly inconsistent with the isolated airfoil wake formulas. Therefore, predictions making use of the test values of  $\mu c/U$  and  $Y/b$  and the predicted mean flow parameters are considered instructive in evaluating the acoustic theory. Results of this study are shown in figures 56, 57 and 58. Because of the approximations in the stator noise theory (ref. 7), the predictions shown in figures 56, 57 and 58 tend to be upper limits for the stator harmonic noise because: (1) the assumption that the stator vanes are acoustically compact (i. e., that the stator vane dimensions are smaller than a wave length) is violated

at the higher harmonics, (2) the unsteady stator forces are assumed to be in phase from root to tip, and (3) any reduction in efficiency due to duct acoustic cut-off is ignored. Also, to eliminate the unpredictable influence of duct directivity, comparisons are made on the basis of harmonic sound power.

Lift response is calculated two ways. First, the traditional Sears analysis is used which accounts only for the upwash, or angle of attack, variations in the stator inflow. Second, the Horlock analysis is used which accounts for the upwash plus the streamwise velocity variations. The phasing of the two velocity components is such that substantial lift cancellation is predicted by the Horlock theory (up to 80% in some cases).

Figures 56, 57, and 58 show the test and predicted harmonic levels for the three flow conditions where measured wake data are available. It can be seen that the use of the Horlock function causes reductions of seven or more decibels across the harmonic spectrum. For the lower harmonics the test results fall between predictions using the Sears and Horlock functions, indicating that the full lift cancellation may not be realized. For the upper harmonics, the stator noise predictions using either of the lift response functions are less than the measurements. Because of the reasonable agreement at low frequencies and the theoretical approximations, which should cause overprediction at high frequencies, it is concluded that the higher harmonics are probably direct rotor radiation due to interaction between the rotor and non-uniform inflow. At Condition III it is probable that the lower harmonics are the result of rotor/stator interactions. However, at Conditions I and II some rotor contribution may exist at the lower frequencies which causes the high level of harmonics seen in the test data. It is, therefore, concluded from this study that a significant portion of the noise measured may be generated by the rotor. While conclusive evidence cannot be derived from the tests conducted in this program, it is probable that the theory provides a good representation of stator noise.

## CONCLUSIONS

The program discussed in this report has presented a unique opportunity to acquire both noise and wake data on a variable pitch subsonic tip speed fan under ideal atmospheric conditions on a test facility with good aerodynamic and acoustic characteristics. The following conclusions have been drawn from the extensive data obtained in the program plus comparisons between this data and predictions using the Hamilton Standard fan noise prediction methodology.

1. The trends in an earlier analytical study (ref. 1) which showed that fan noise could be reduced by increasing fan solidity, improving aerodynamic design and operating at some optimum subsonic tip speed have been confirmed in this program. Also, as predicted in reference 1, no significant influence due to use of few rather than many stators could be observed in the perceived noise level of the fan tested.
2. Small inlet disturbances outside the fan can cause noticeable increases in perceived noise level during static testing. An increase of 2 PNdB due to the presence of a small pipe below the fan shroud was observed for the present program.
3. Comparisons between prediction and test show good agreement on a perceived noise level basis near the design blade angle for the fan over the tip speed range tested. At higher blade angles, predictions are lower than test. At lower blade angles, predictions are higher than test. The spectrum character of the 0.457 m (18 in.) diameter fan noise does differ from that of the 0.533 m (21 in.) diameter fan tested earlier in that the 0.475 m (18 in.) diameter fan produces less mid frequency noise.
4. For a given pressure ratio or thrust, the test data in model scale or full scale show that minimum perceived noise occurs at a blade angle and tip speed near those of maximum aerodynamic efficiency.
5. Comparison of noise spectra and levels for a model fan 0.457 m (18 in.) in diameter scaled to a 1.402 m (4.6 ft) diameter show excellent correlation with test data obtained from a 1.402 m (4.6 ft) diameter fan. This good agreement indicates that model scale tests with their lower cost can be utilized in developing full scale quiet fans.
6. Secondary flows in the rotor wake appear to cause a larger portion of the rotor/stator interaction noise than do the classical two dimensional viscous blade wakes. Merged blade wakes in the root and tip region are probably the primary source of fan noise at blade passing frequency while the isolated wakes at mid-span couple to the higher sound harmonics of the stator radiation. At the three conditions where wake data was obtained, the flow in the endwall region is heavily modulated by turbulence which may be a significant broadband noise source.

7. A quantitative study of harmonic noise using the measured wake properties indicates that stator radiation probably dominates the first 3 to 6 harmonics of blade passing frequency while the higher harmonics are due to interaction of the rotor with inflow distortion.

## REFERENCES

1. Metzger, F. B.; Hanson, D. B.; Menthe, R. W.; Towle, G. B.: Analytical Parametric Investigation of Low Pressure Ratio Fan Noise. NASA Contractor Report CR-2188, March 1973
2. Metzger, F. B.; Ganger, T. G.: Results of Initial Prop-Fan Model Acoustic Testing. NASA Contractor Report CR111842, December 4, 1972.
3. Morkovin, M. V.: Fluctuations and Hot-Wire Anemometry in Compressible Flows. AGARD, Memo 24, November 1956.
4. Morkovin, M. V. and R. E. Phinney: Extended Applications of Hot-Wire Anemometry to High-Speed Turbulent Boundary Layers. AFOSR TN-58-469, June 1958.
5. Whitefield, C. E., J. C. Kelly, and B. Barry: A Three-Dimensional Analysis of Rotor Wakes. Aeronautical Quarterly, November 1972.
6. Fessler, T. F. and M. J. Hartmann: Preliminary Survey of Compressor Rotor Blade Wakes and Other Flow Phenomena with a Hot-Wire Anemometer. NACA Research Memo RM E56A13, June 26, 1956.
7. Hanson, D. B.: A Unified Analysis of Fan Stator Noise. Paper accepted for publication in the Journal of the Acoustical Society of America, 1973.
8. Silverstein, A., et. al.: Downwash and Wake Behind Plain and Flapped Airfoils. NACA Report Number 651, 1939.
9. Sears, W. R.: Some Aspects of Nonstationary Airfoil Theory and its Practical Applications. Journal of Aerospace Science Volume 8, 1941.
10. Horlock, J. H.: Fluctuating Lift Forces on Aerofoils Passing Through Transverse and Chordwise Gusts. Transactions of the ASME, Series A, December 1968.
11. Lowson, M. V.: Theoretical Analysis of Compressor Noise. Journal of the Acoustical Society of America, Vol 47, 1970.



TABLE I

SUMMARY of 0.457 m (18-INCH) DIAMETER FAN OPERATING CONDITIONS

Corrected Tip Speed m/s (ft/s)	Blade Angle Deg.	Net Thrust N (lb)	Input Power kw (shp)	Fan Exit Pressure Ratio
219 (719)	38.0	1383 (311)	104 (140)	1.067
251 (824)		1748 (393)	151 (203)	1.083
200 (657)	43.0	1495 (336)	109 (146)	1.073
244 (801)		2277 (512)	209 (281)	1.106
273 (895)		2647 (595)	261 (350)	1.136
183 (599)	47.1	1423 (320)	97 (130)	1.069
212 (697)		1944 (437)	152 (203)	1.092
247 (811)		2584 (581)	238 (319)	1.127
170 (557)	52.6	1450 (326)	96 (129)	1.069
199 (654)		2024 (455)	159 (213)	1.096
213 (698)		2344 (527)	198 (265)	1.113
225 (737)		2607 (586)	234 (314)	1.114
243 (797)		2940 (661)	298 (400)	1.142
158 (519)	57.4	1397 (314)	93 (124)	1.068
159 (521)		1428 (321)	96 (129)	1.069
189 (620)		2042 (459)	161 (217)	1.094
210 (688)		2371 (533)	219 (293)	1.119
231 (757)		2842 (639)	296 (397)	1.151
147 (483)	62.5	1294 (291)	89 (119)	1.060
177 (581)		1841 (414)	159 (213)	1.088
206 (675)		2322 (522)	230 (309)	1.118
214 (703)		2633 (592)	280 (375)	1.136

TABLE II  
COMPARISON OF THREE FAN DESIGNS

Parameter	Model Fan Tested in Current Program	Large Scale Fan Tested Under Lewis Research Center Contract	Model Fan Discussed in Reference 1
Diameter	0.457m (18 in.)	1.402m (4.6 ft)	0.533m (21 in.)
No. Blades	12	13	12
Hub-to-Tip Ratio	0.5	0.46	0.429
Rotor Solidity	0.78	0.85	0.72
No. Vanes	7	7	22
Vane Solidity	0.56	0.55	0.93
Design Blade Angle	58 deg	56 deg	45 deg
BV Gap at Design Blade Angle	1.85	2.00	2.00
Design Tip Speed	236 m/sec (775 ft/sec)	247 m/sec (810 ft/sec)	290 m/sec (950 ft/sec)
Exit Area Ratio	0.924	0.88	1.0
Blade Section Airfoils	NACA 65A	NACA 65A	NACA 16
Vane Section Airfoils	NACA 400	NACA 400	NACA 65

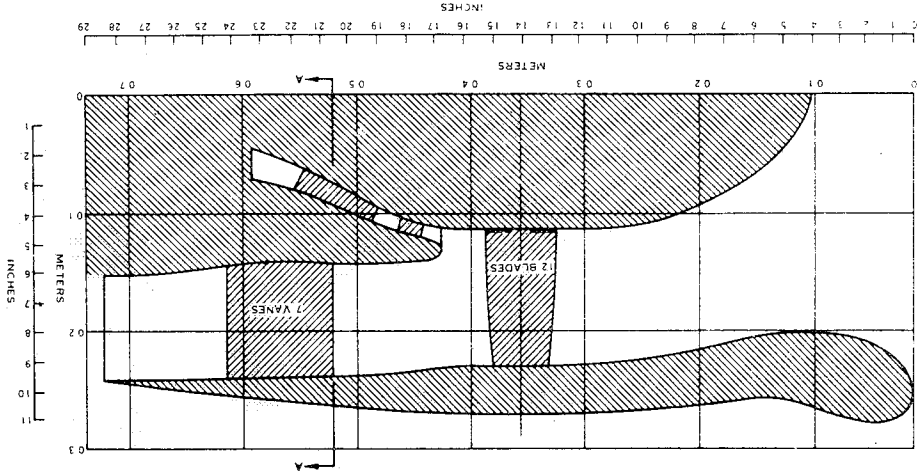
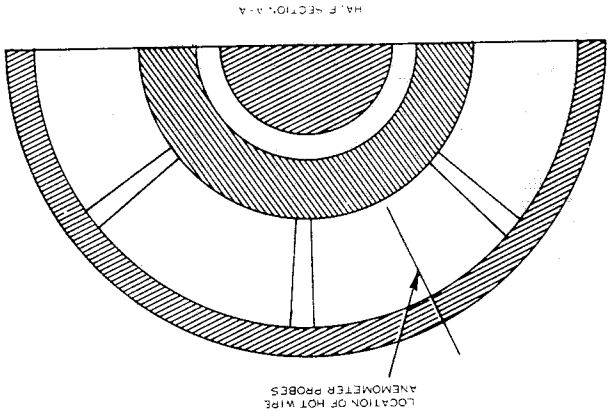
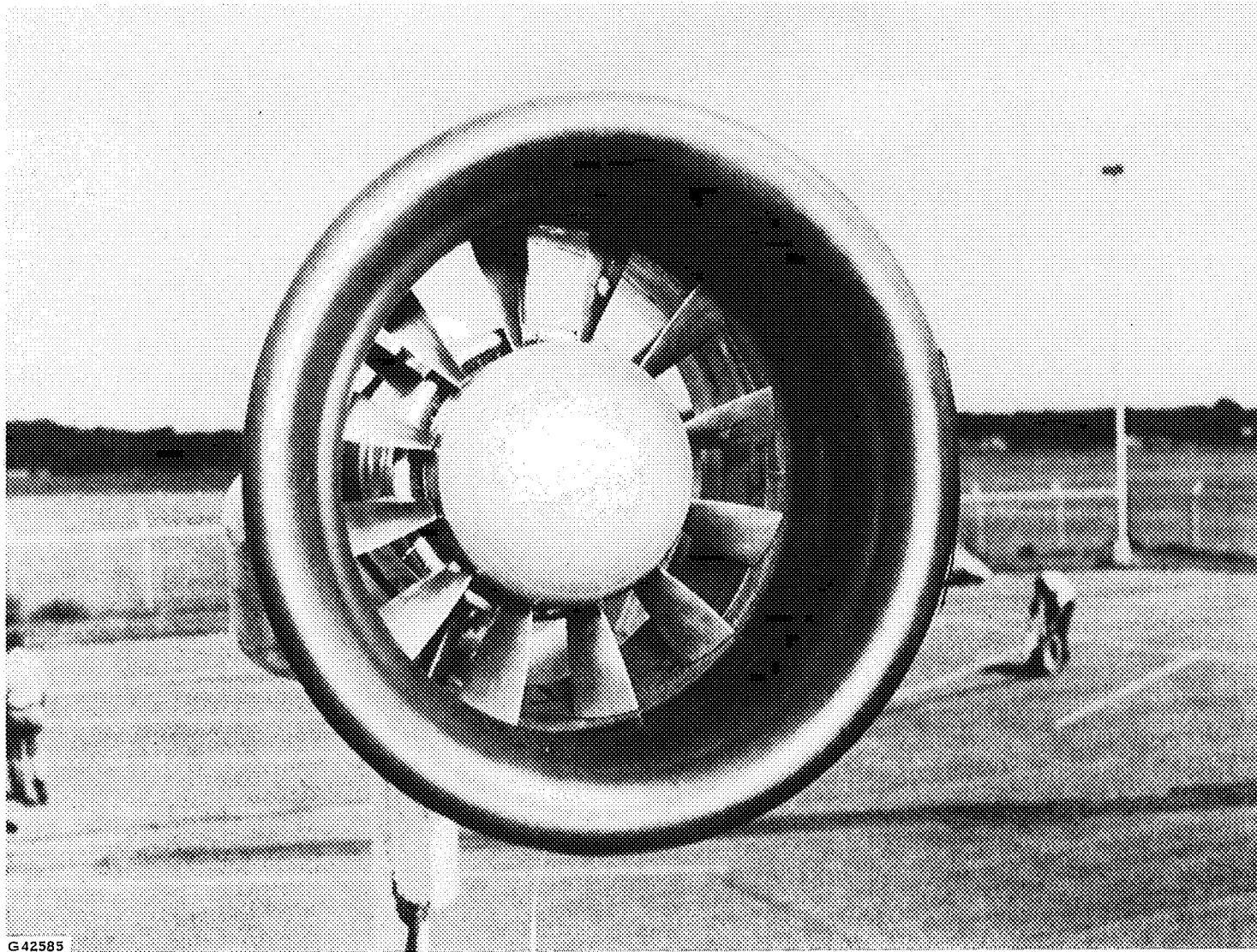


FIGURE 1 0.457 METER (18 INCH) FAN DEFINITION



G42585

FIGURE 2. VIEW LOOKING INTO FAN INLET

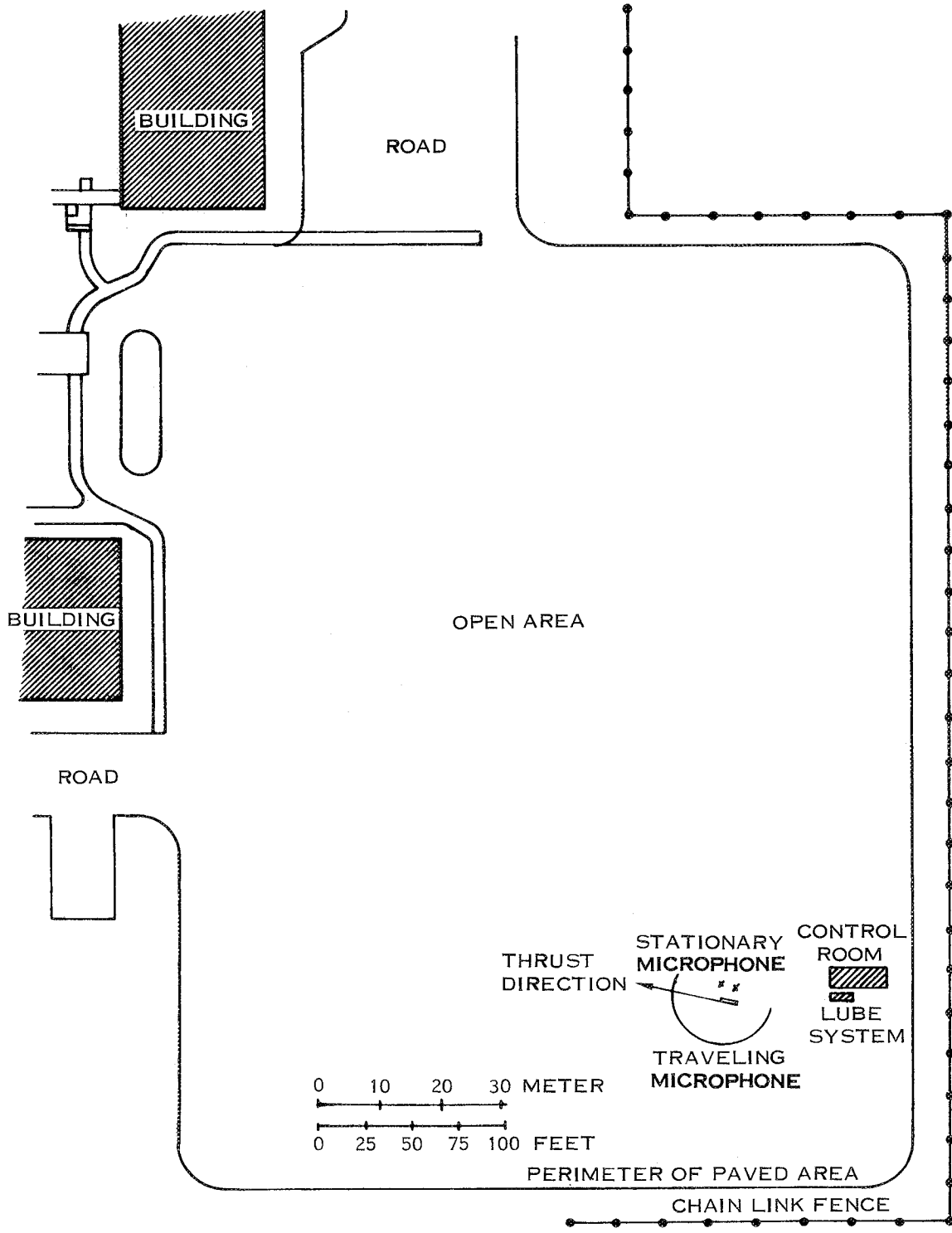
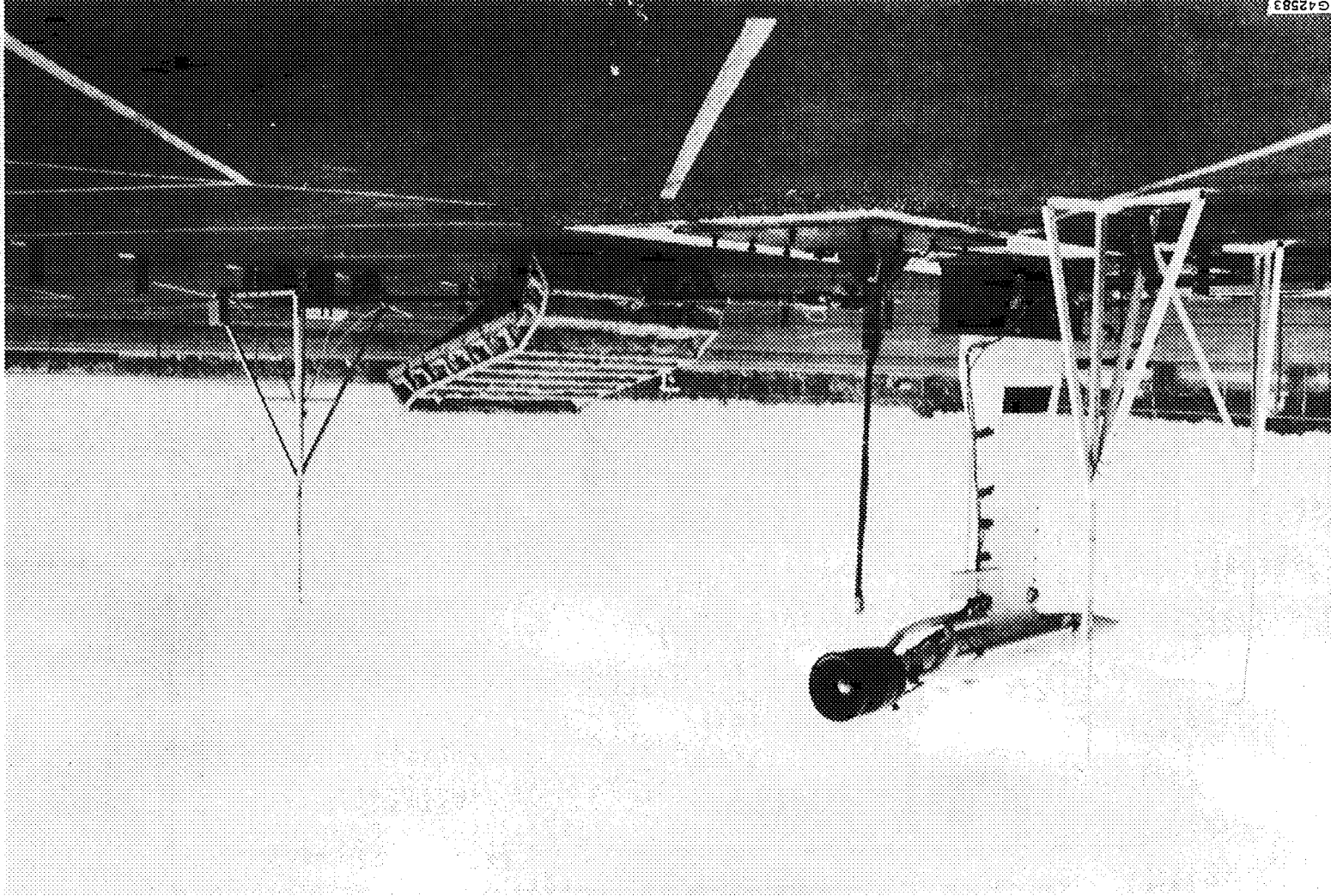


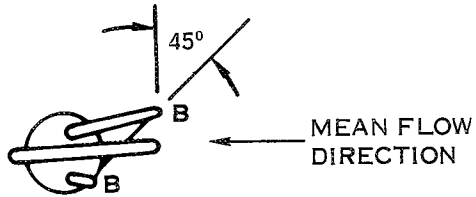
FIGURE 3 TEST AREA PLAN VIEW

FIGURE 4. FAN, PTR, ANECHOIC PLATFORM, AND MICROPHONE SYSTEM



HOT WIRE PROBE

SENSOR AA AND BB  
MATL. TUNGSTEN  
0.0127 MM (0.00050 IN.) DIA.  
2.54 MM (0.100 IN.) LONG



TOTAL PRESSURE PROBE

KULITE SENSOR  
SILICON DIAPHRAM  
0.711 MM (0.028 IN.) ACTIVE DIA.

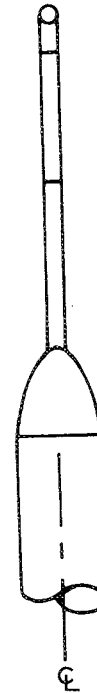
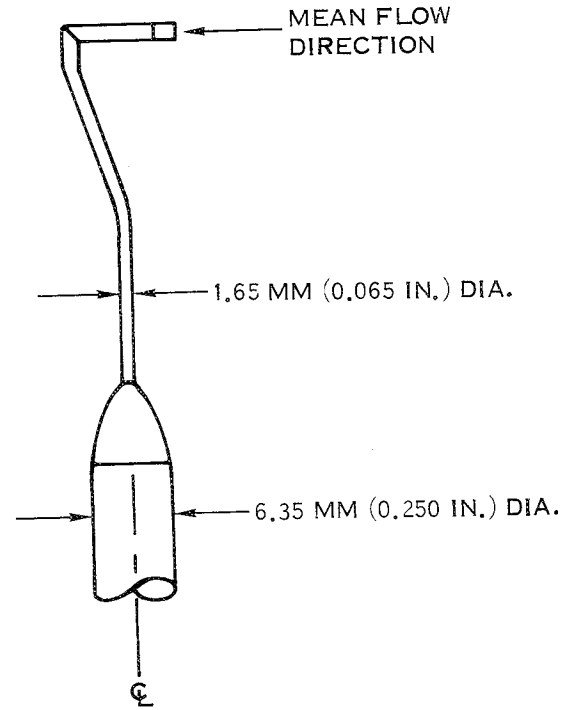
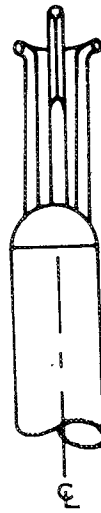
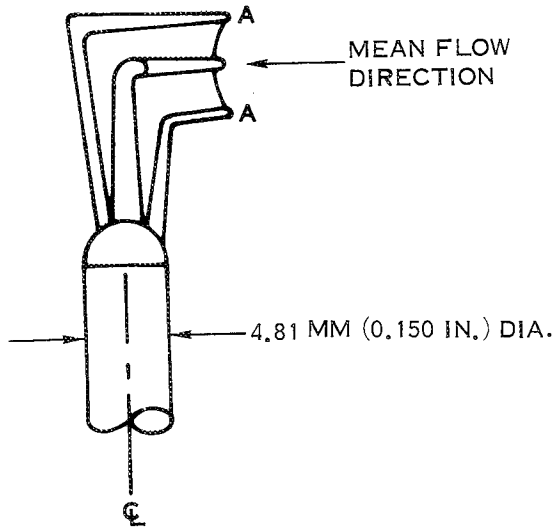
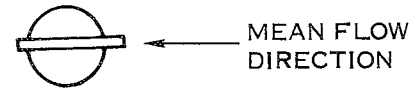
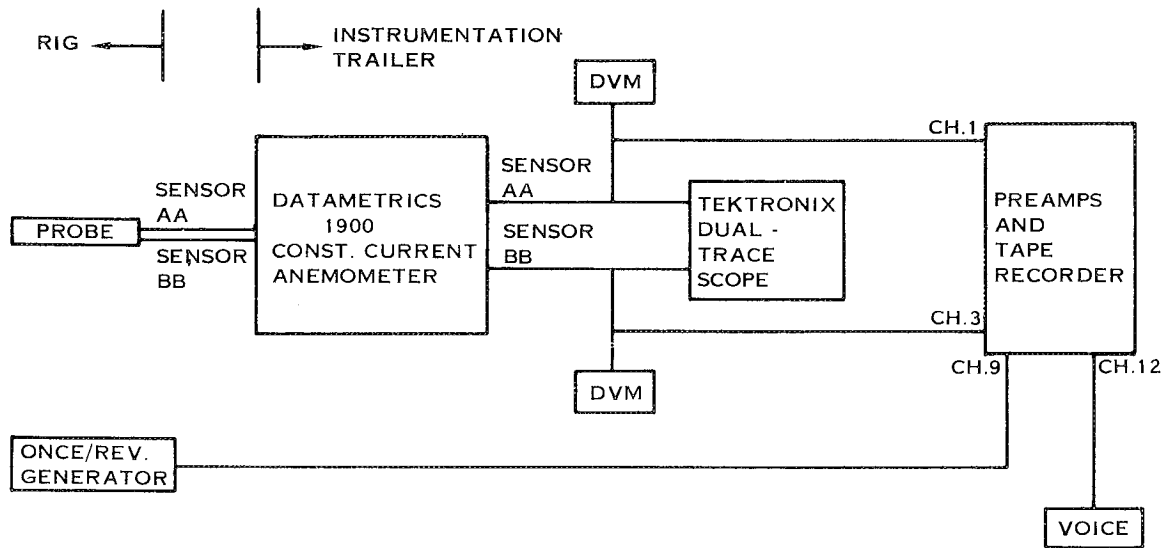


FIGURE 5. HIGH RESPONSE AERODYNAMIC PROBES

### HOT WIRE DATA



### TOTAL PRESSURE DATA

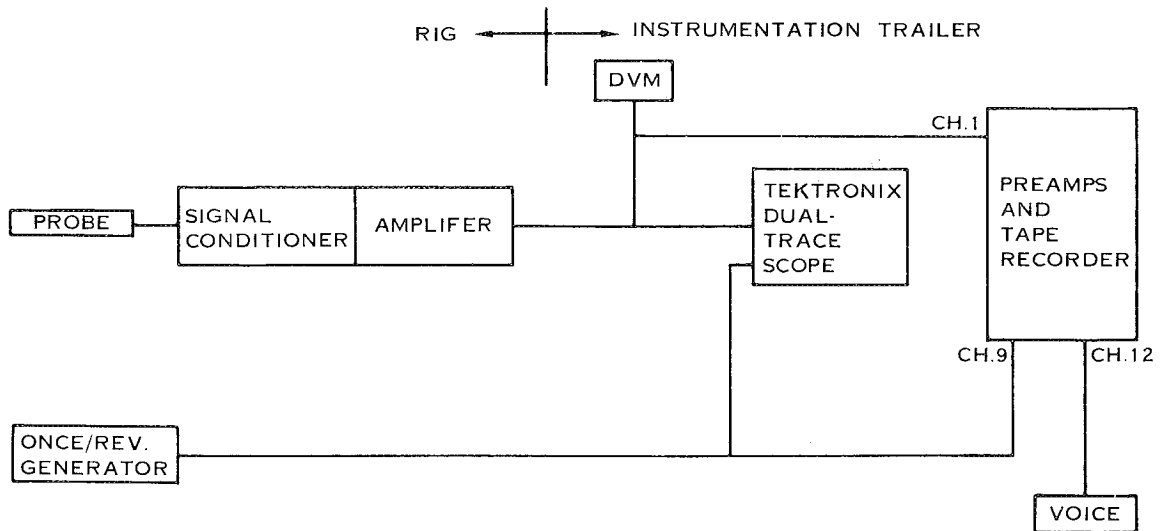


FIGURE 6 EQUIPMENT EMPLOYED IN HIGH RESPONSE DATA ACQUISITION

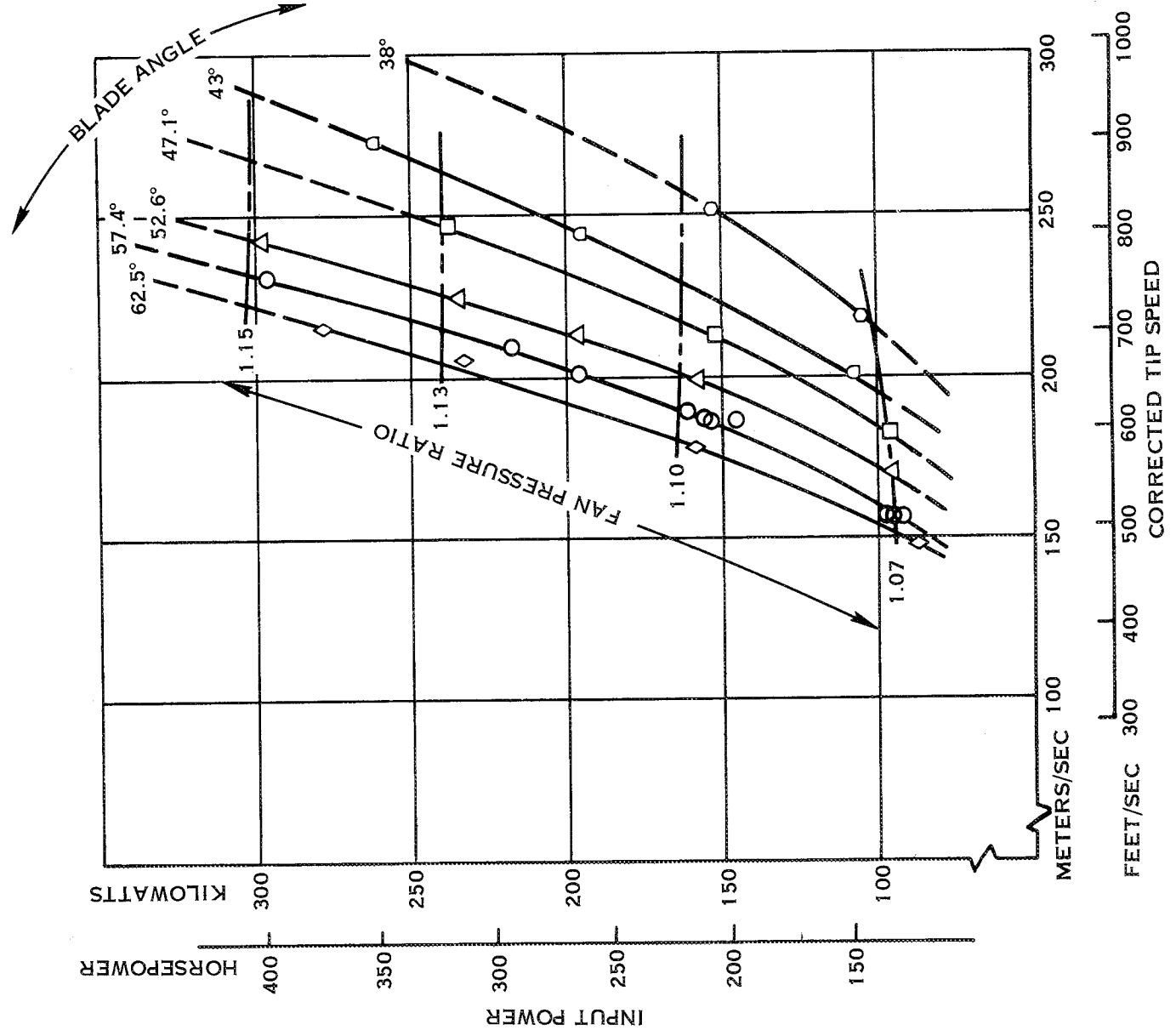


FIGURE 7. 0.457 M (18 IN) DIAMETER FAN TEST MAP

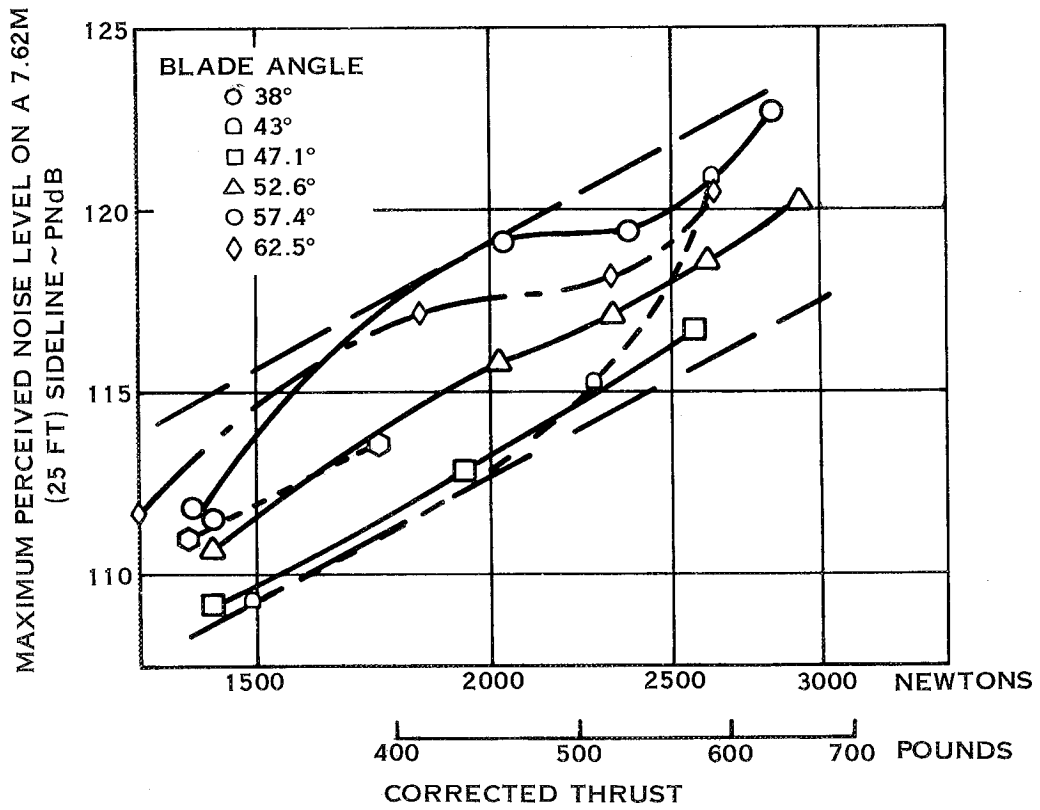


FIGURE 8. 0.457M (18 IN) DIAMETER FAN NOISE VARIATION WITH NET THRUST

SYMBOL	BLADE ANGLE	THRUST		TIP SPEED		PNL PNDB
		N	LB	M/SEC	FT/SEC	
—————	43°	2277	512	244	801	115.3
- - - - -	52.6°	2344	527	213	698	117.1
— · — · —	57.4°	2371	533	210	688	119.4
+ + + + +	62.5°	2322	522	206	675	117.1

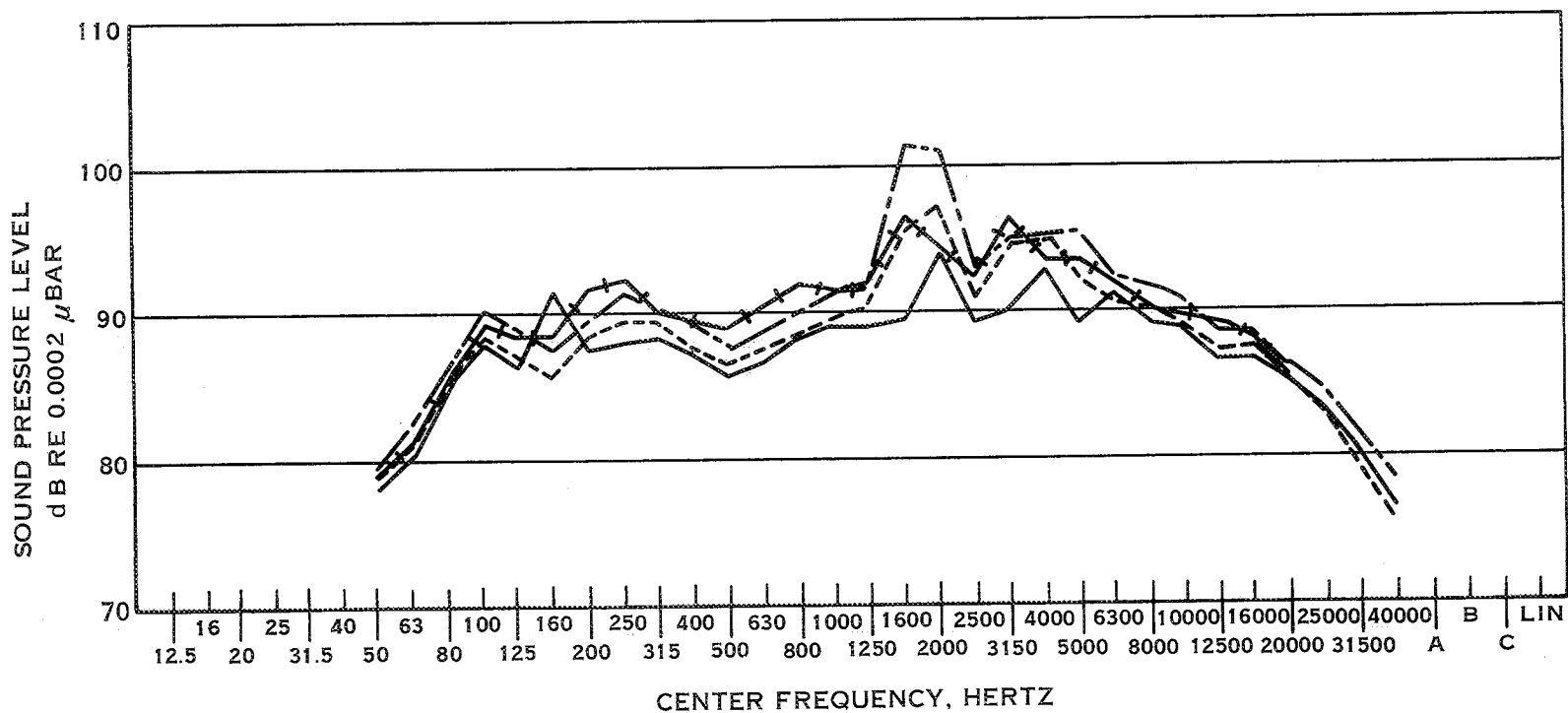


FIGURE 9. SOUND PRESSURE LEVEL VARIATION WITH BLADE ANGLE AND TIP SPEED AT CONSTANT THRUST

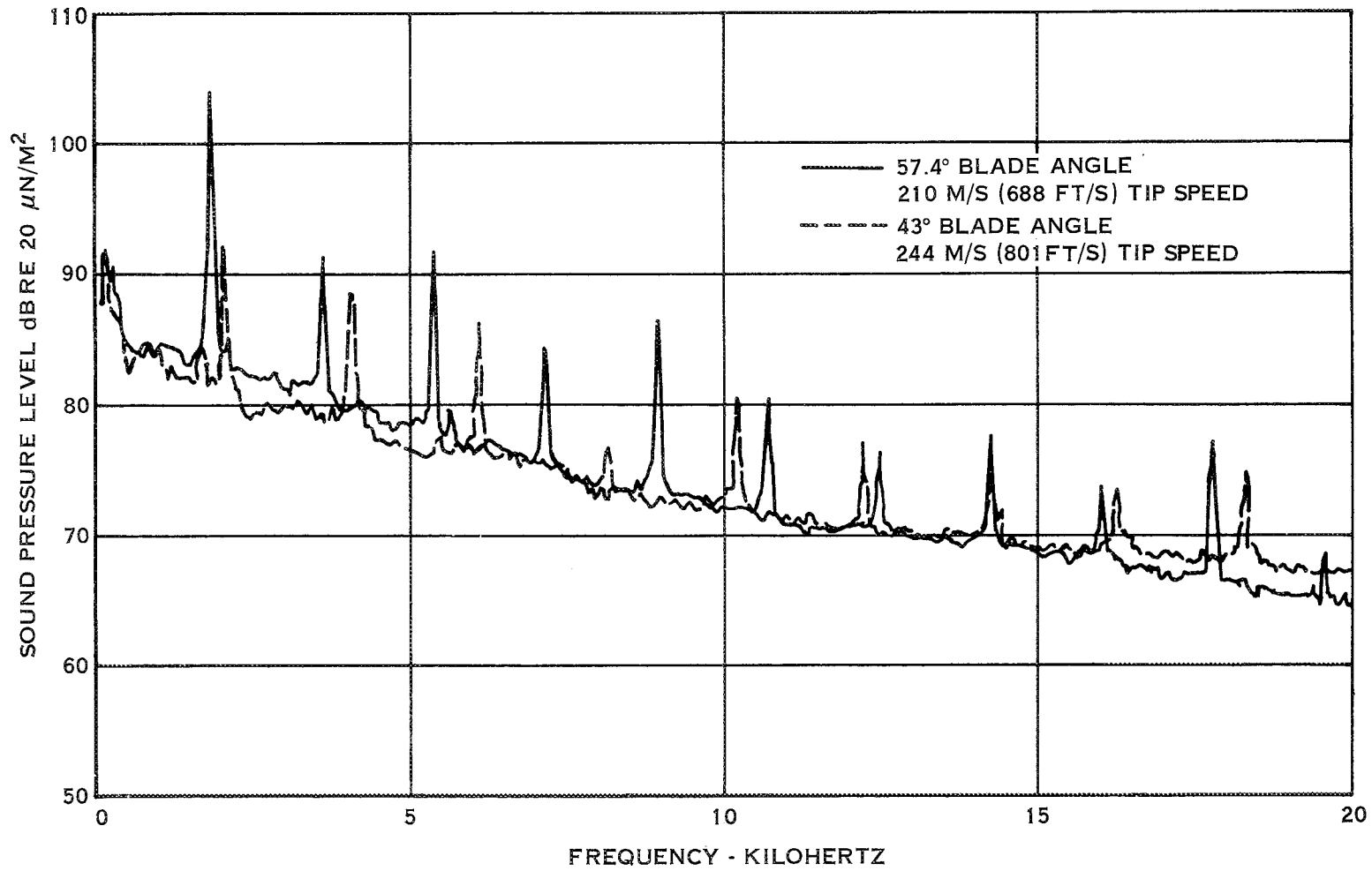


FIGURE 10. COMPARISON OF NARROW BAND SPECTRA

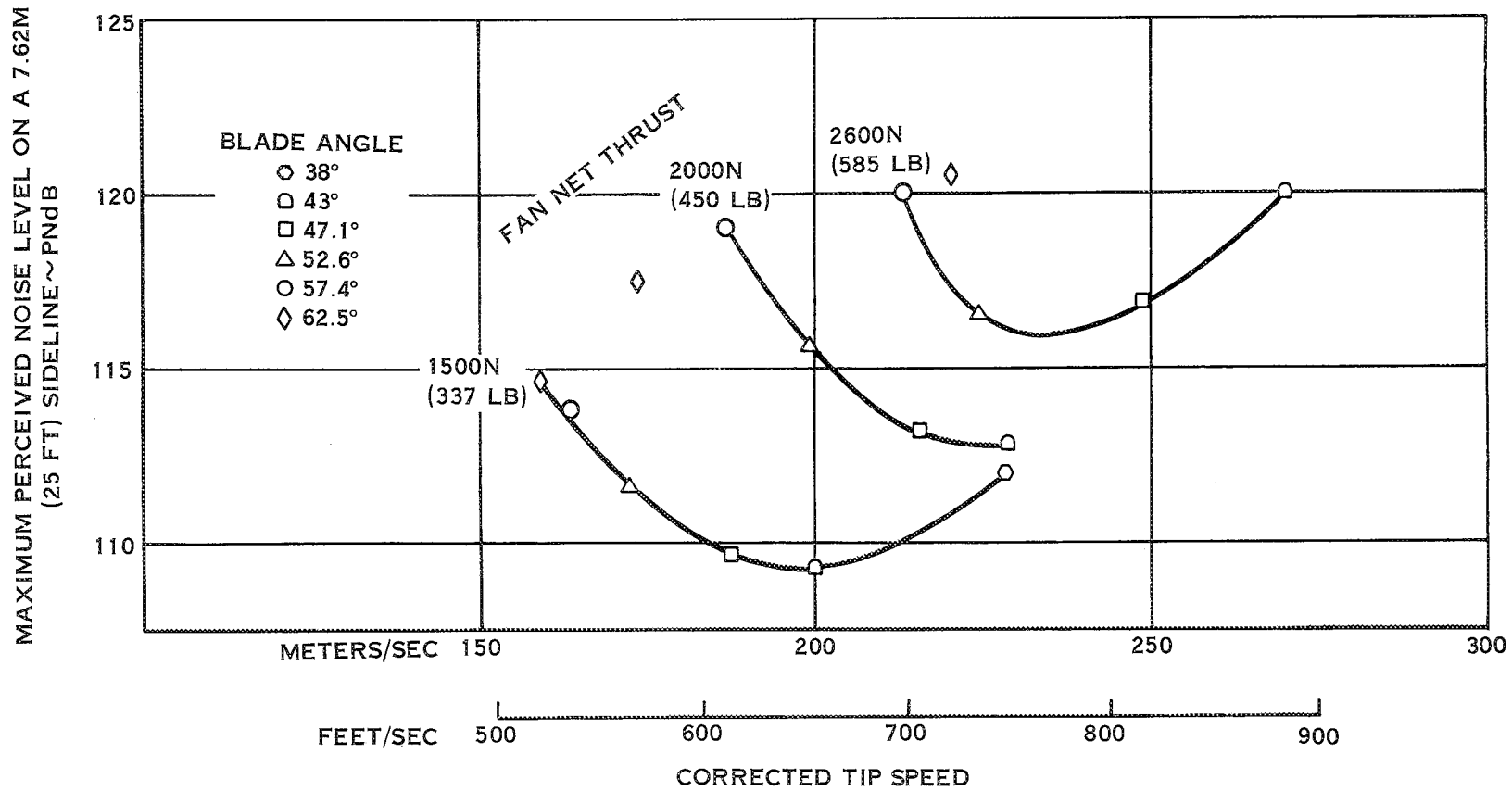


FIGURE 11. PNL VARIATION WITH TIP SPEED AT CONSTANT THRUST

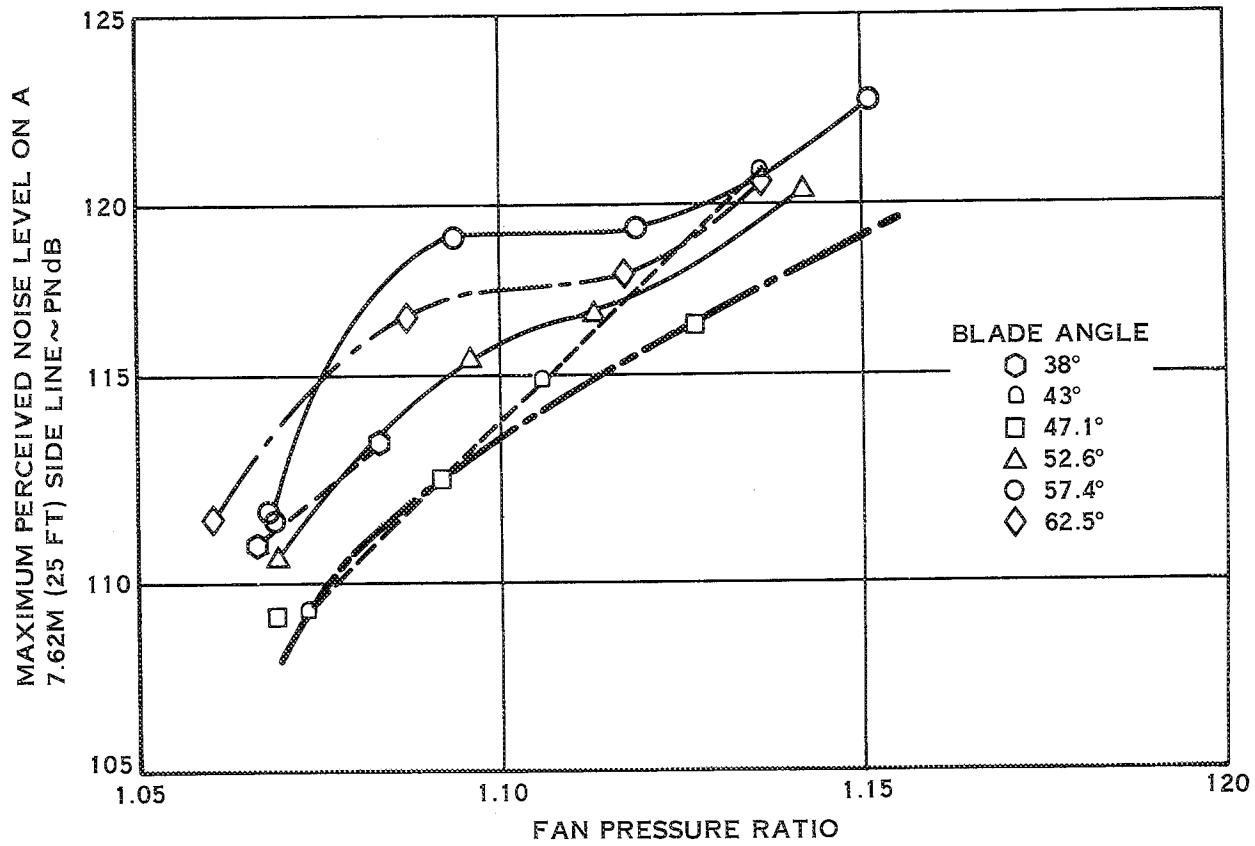


FIGURE 12. 0.457 M (18 IN) DIAMETER FAN NOISE VARIATION WITH PRESSURE RATIO

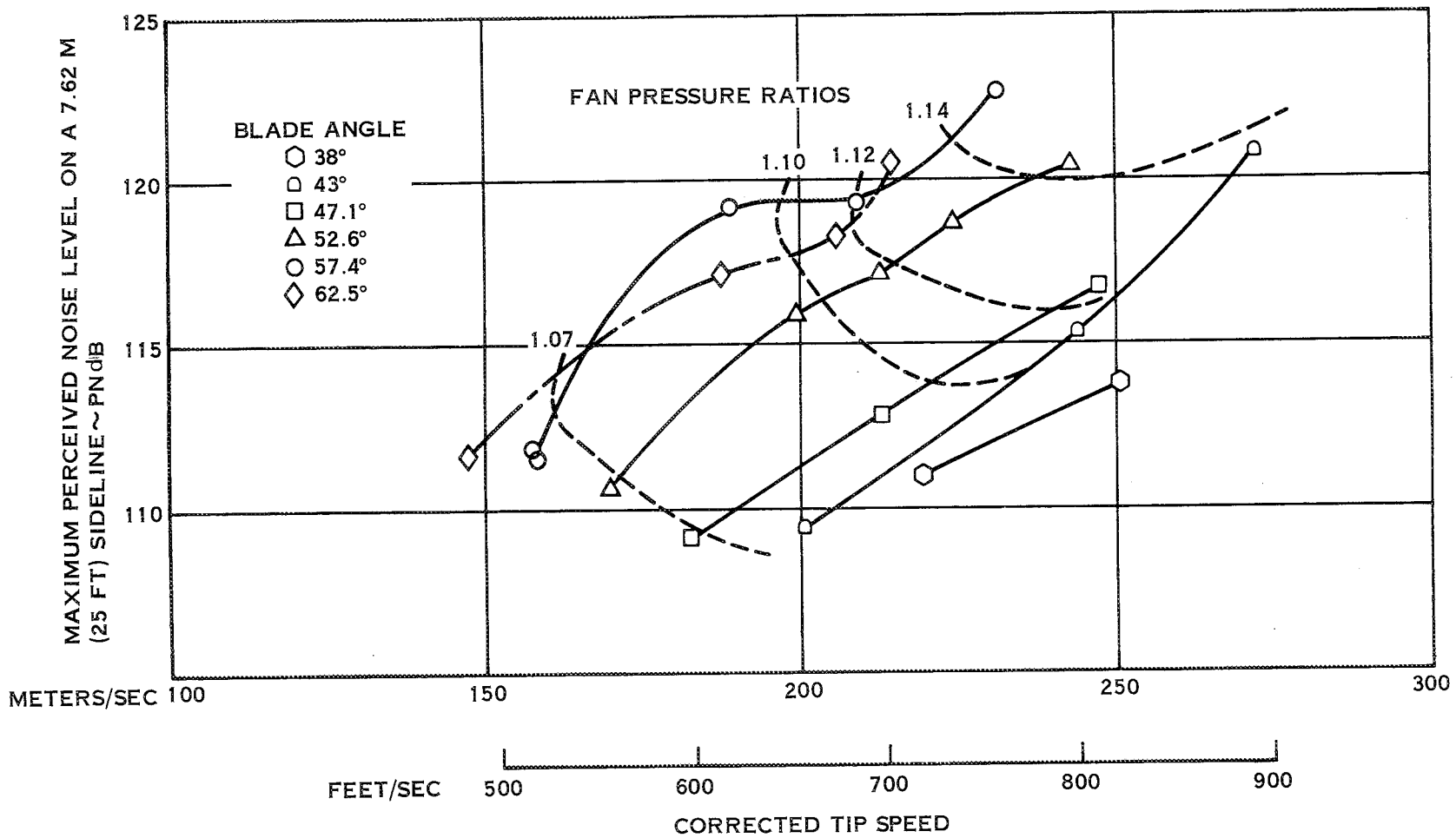


FIGURE 13. 0.457 M (18 IN) DIAMETER FAN NOISE VARIATION WITH TIP SPEED

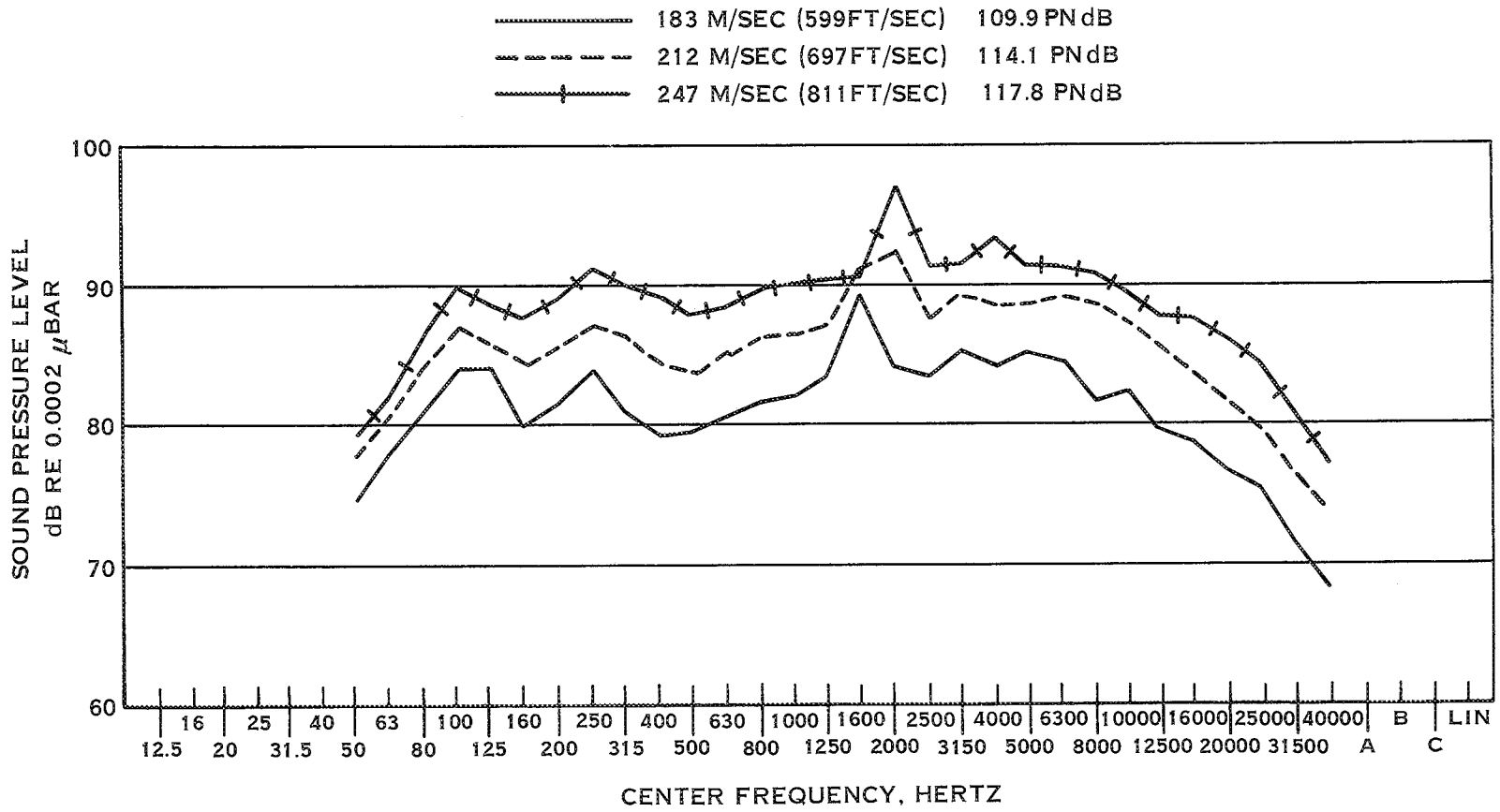


FIGURE 14. FAN NOISE VARIATION WITH TIP SPEED AT CONSTANT BLADE ANGLE

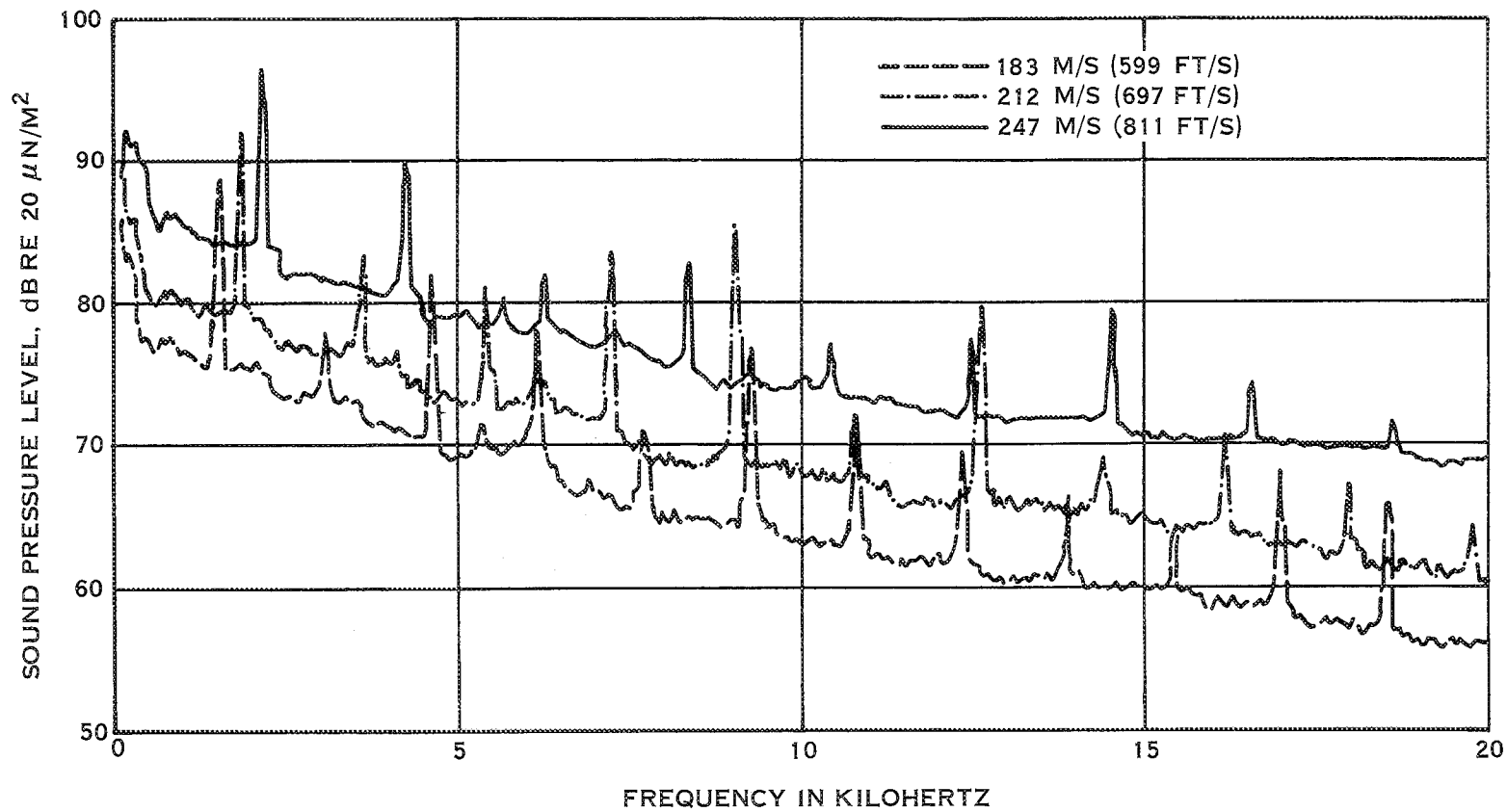


FIGURE 15. COMPARISON OF NARROW BAND SPECTRA AT CONSTANT BLADE ANGLE

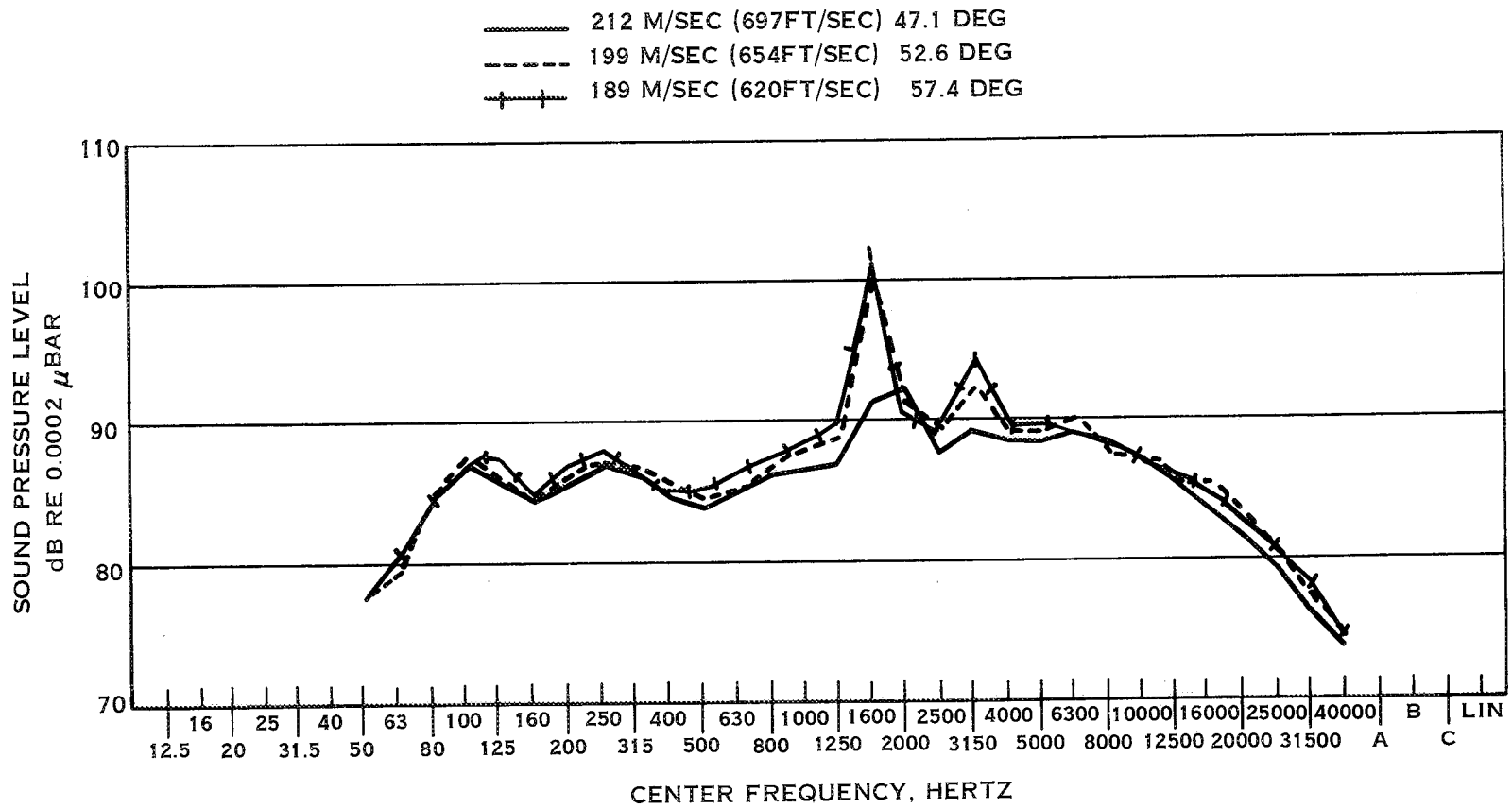


FIGURE 16. FAN NOISE VARIATION WITH TIP SPEED AT 1.094 PRESSURE RATIO

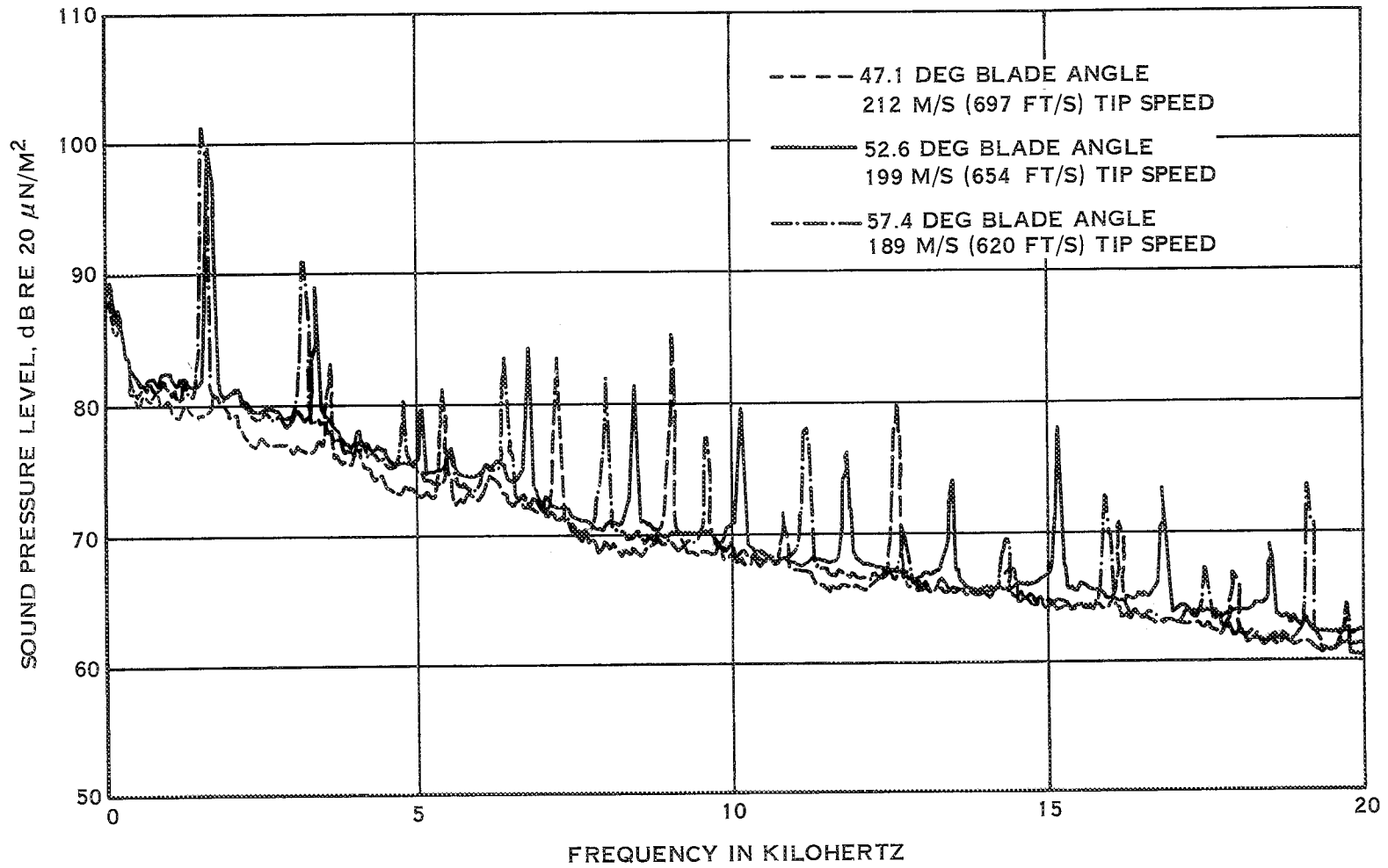


FIGURE 17. COMPARISON OF NARROW BAND SPECTRA AT CONSTANT PRESSURE RATIO

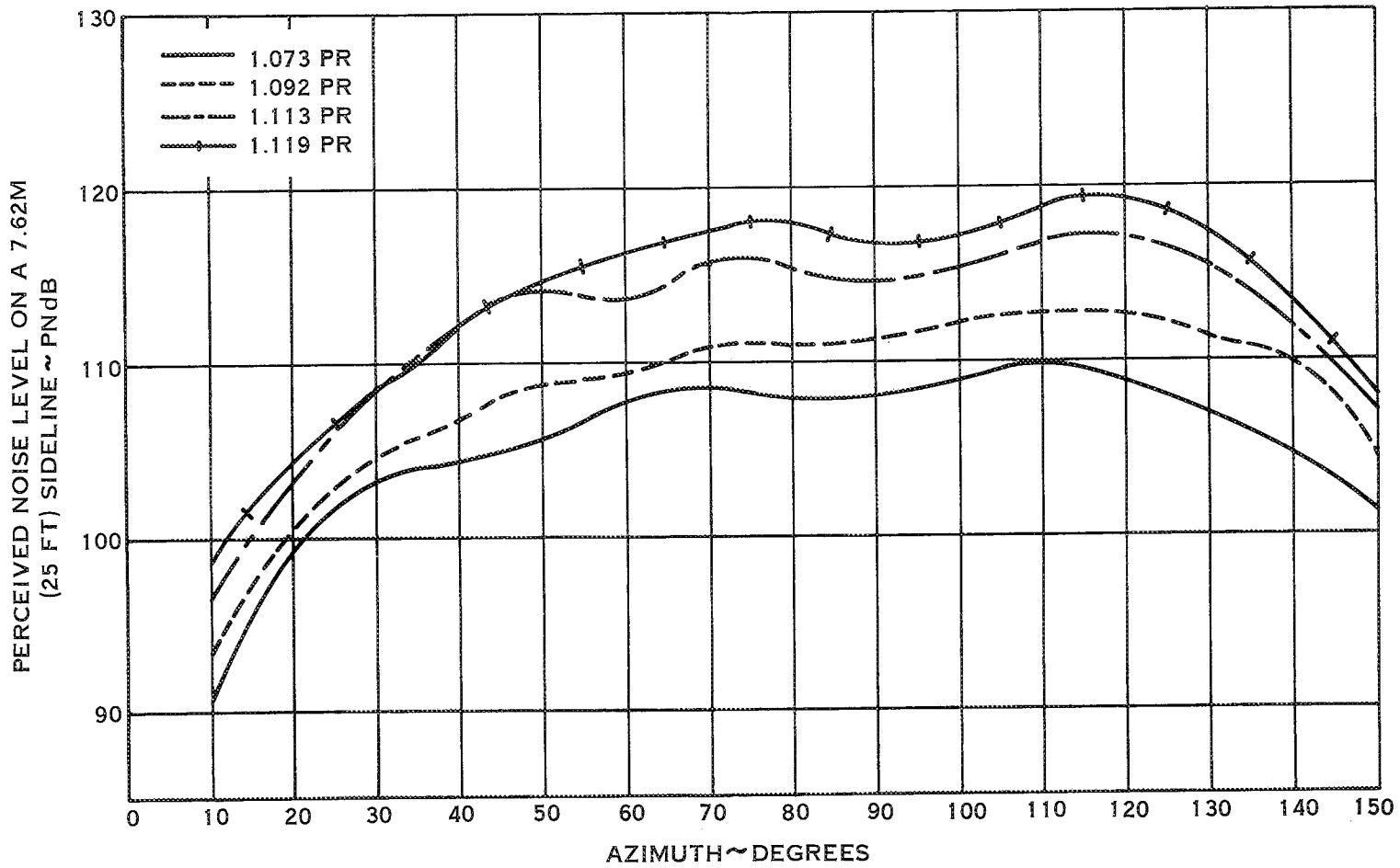


FIGURE 18. SIDELINE PERCEIVED NOISE LEVEL VARIATION WITH PRESSURE RATIO AT CONSTANT TIP SPEED

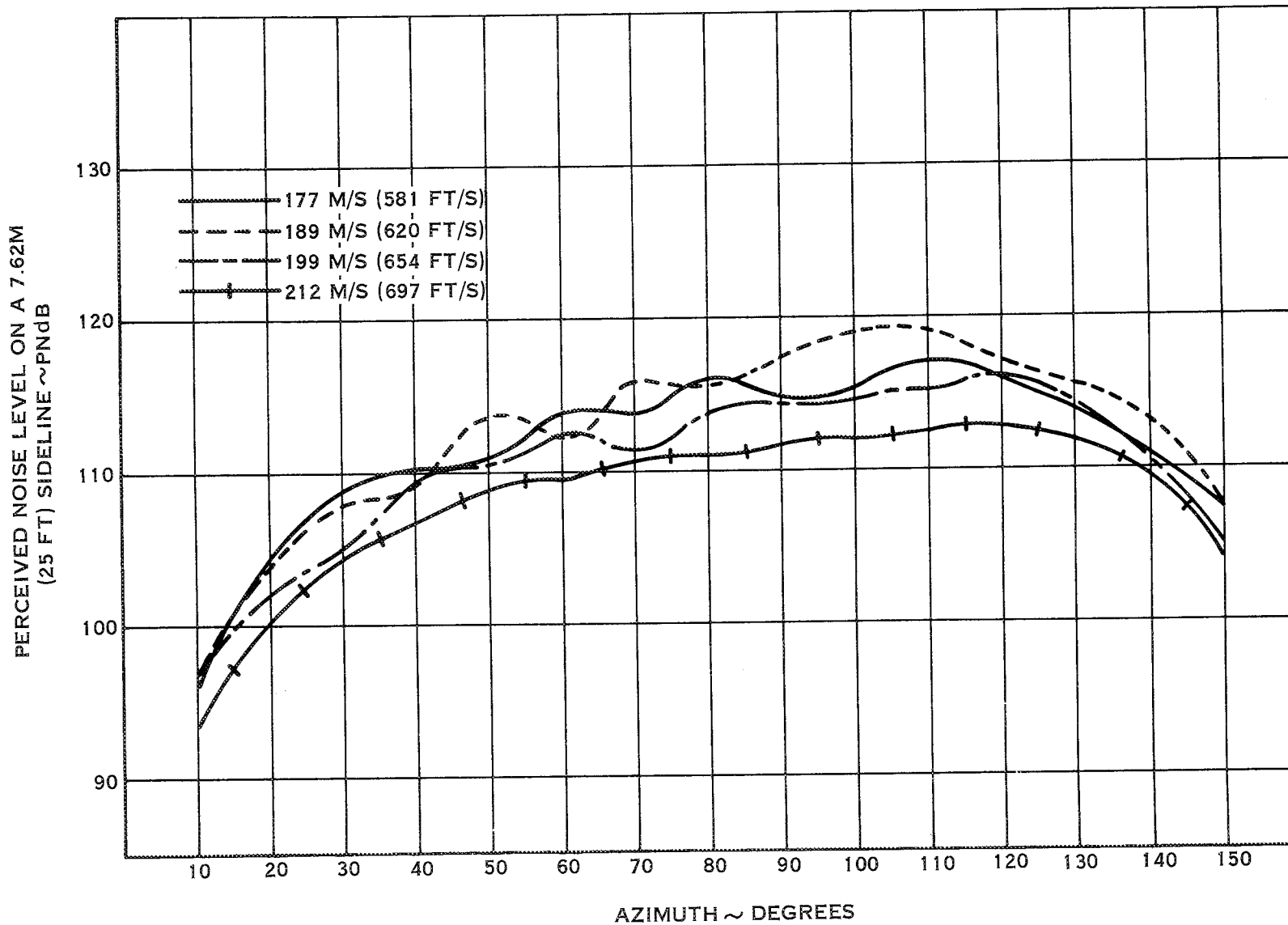


FIGURE 19. SIDELINE PERCEIVED NOISE LEVEL VARIATION WITH TIP SPEED AT CONSTANT PRESSURE RATIO

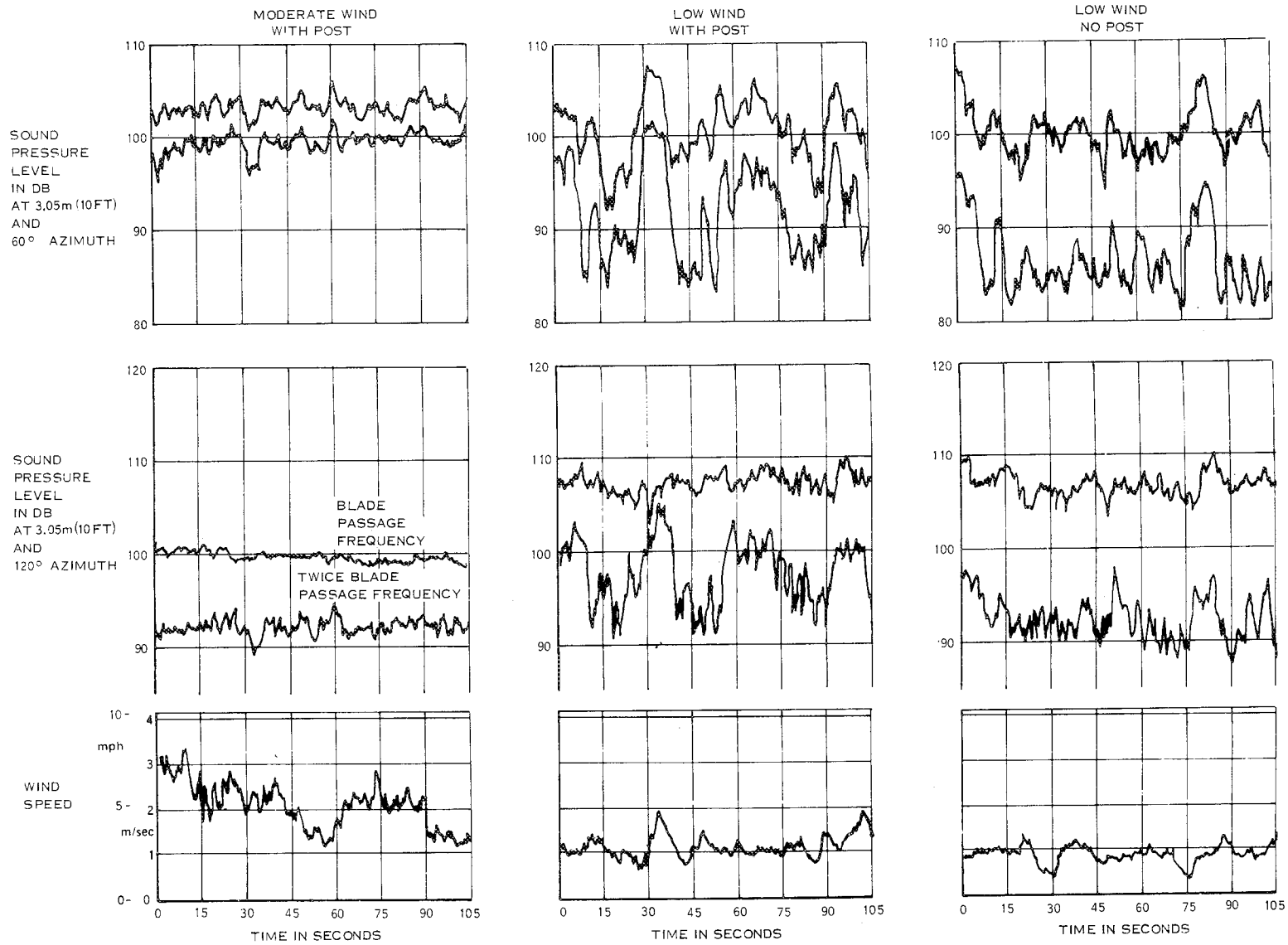


FIGURE 20. EFFECT OF WIND AND INLET DISTURBANCE ON TONE NOISE

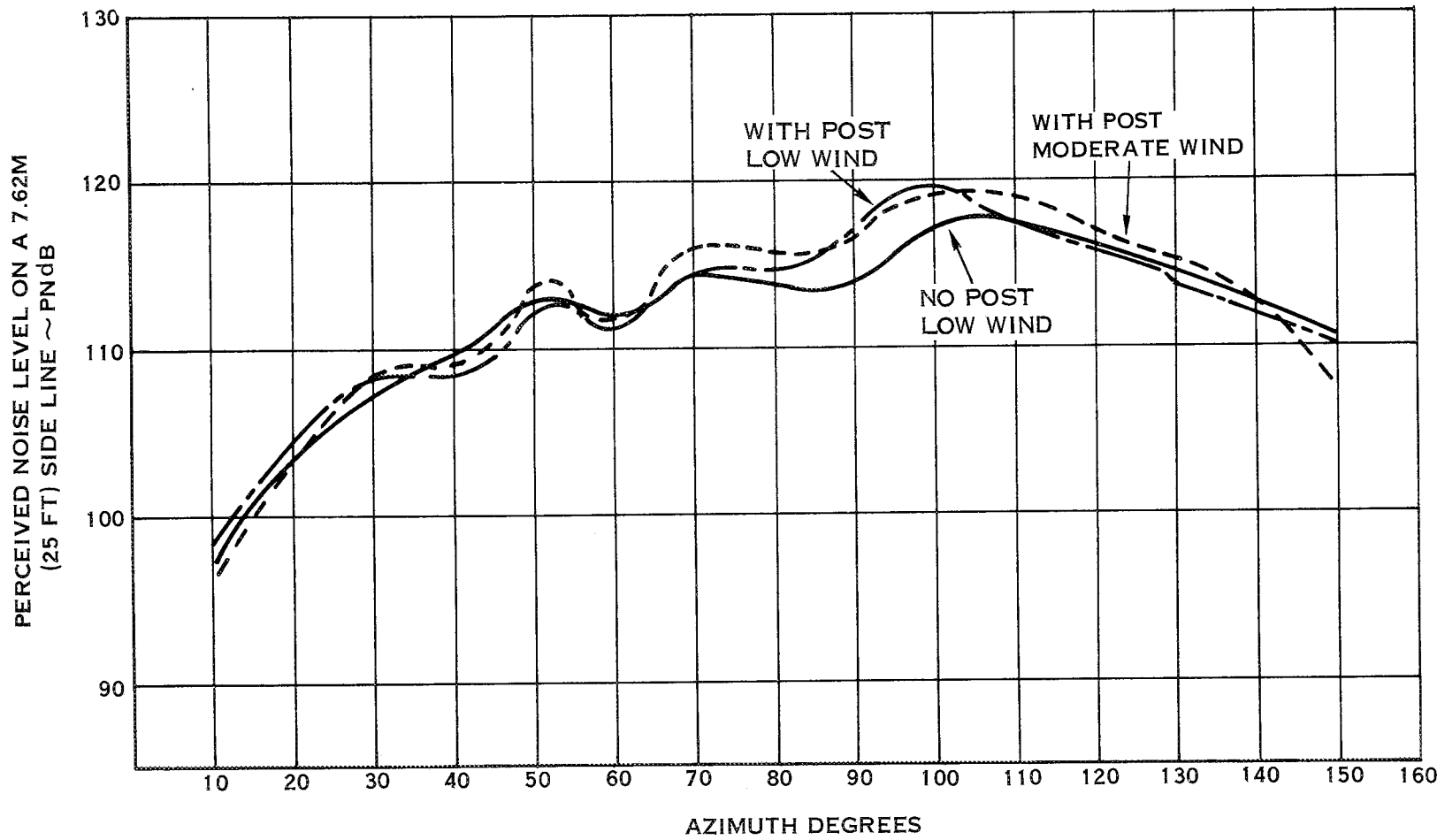


FIGURE 21. EFFECT OF WIND AND INLET DISTURBANCE ON NOISE DIRECTIVITY

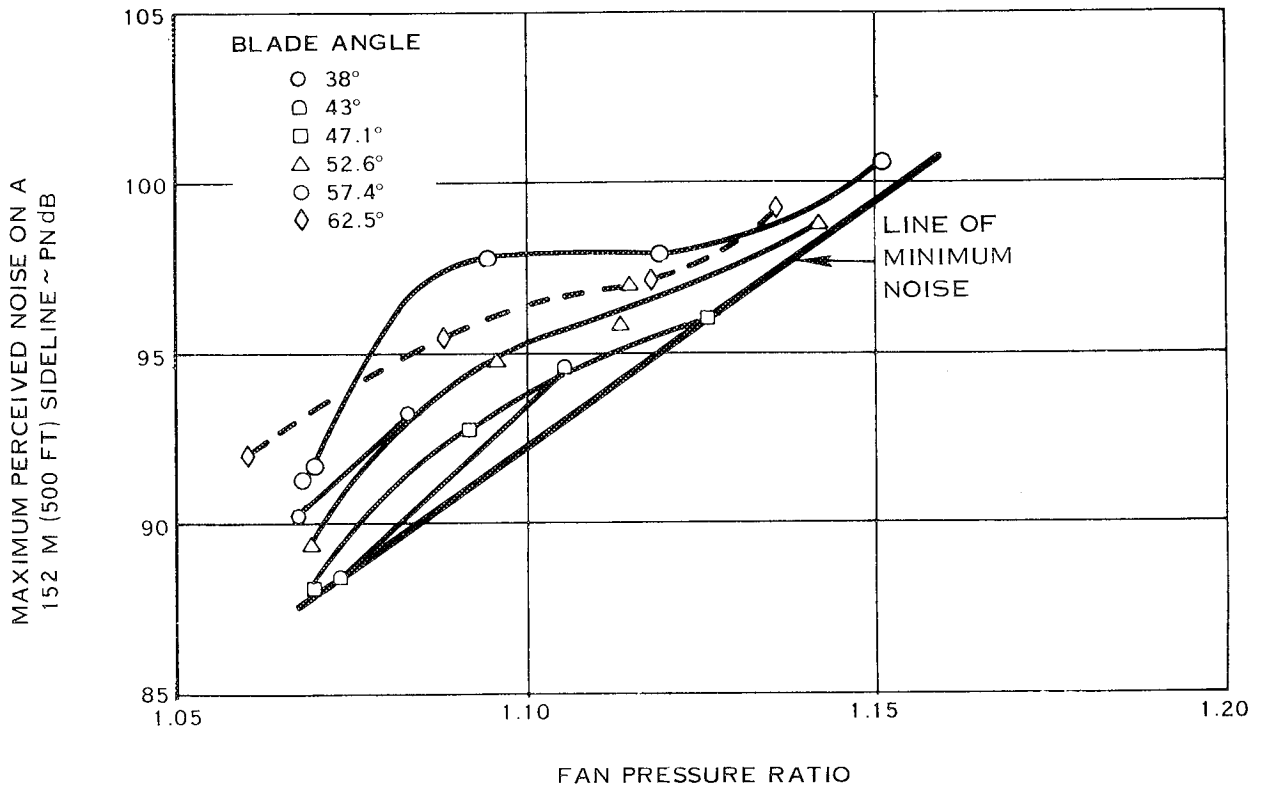


FIGURE 22. 0.457 M (18 IN) DIAMETER FAN SCALED TO 1.402 M (4.6 FT) DIAMETER

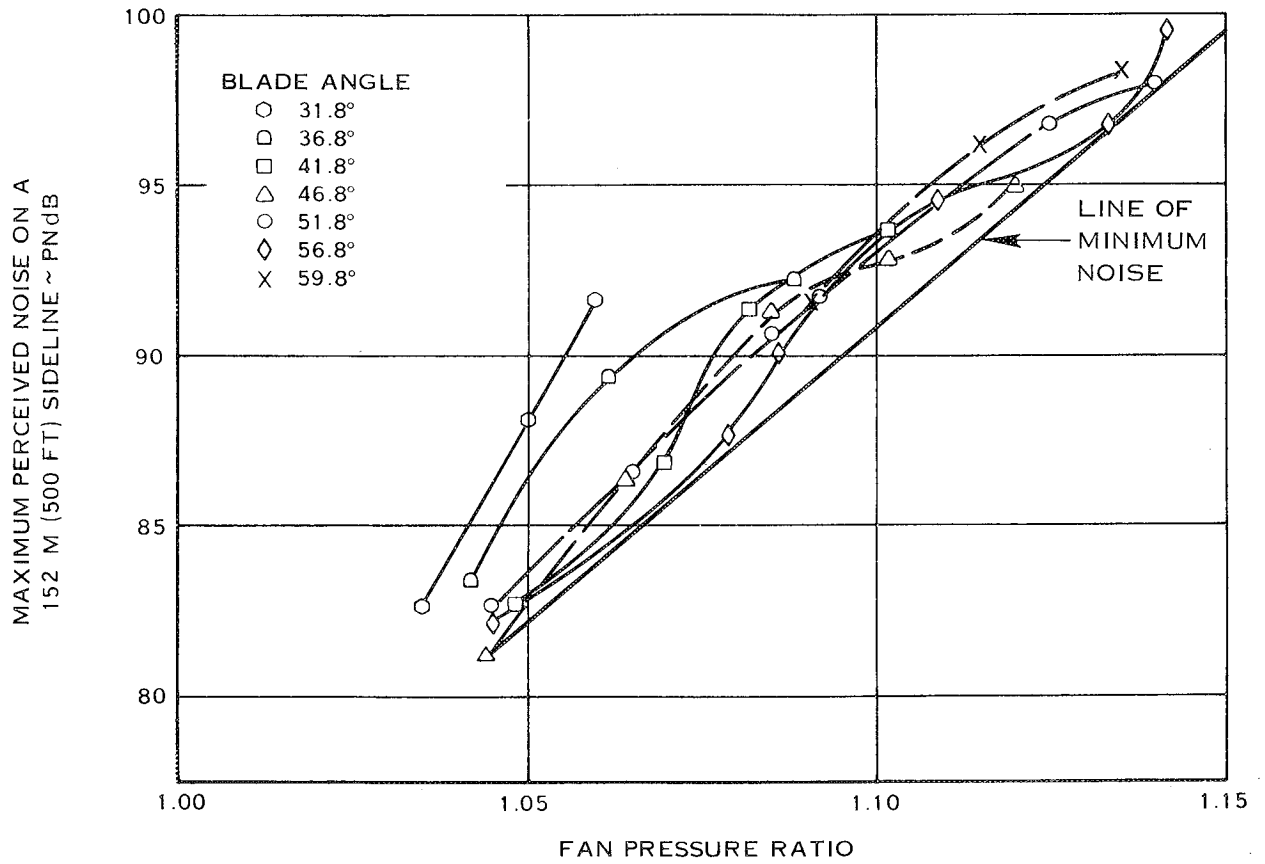


FIGURE 23. 1.402 M (4.6 FT) DIAMETER FAN DATA

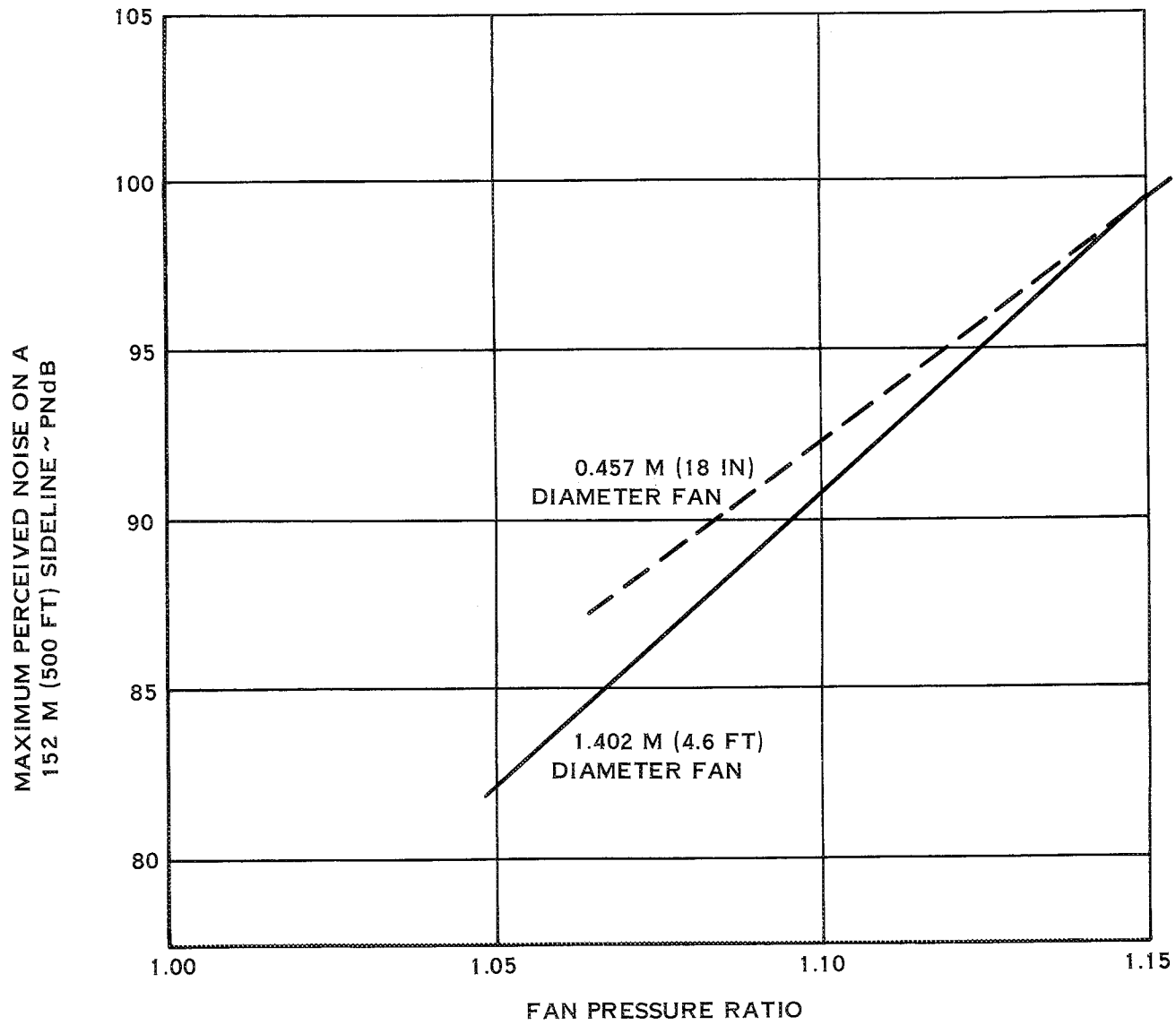


FIGURE 24 COMPARISON OF SCALED 0.457 M (18 IN) DIAMETER FAN NOISE AND 1.402 M (4.6 FT) DIAMETER FAN NOISE

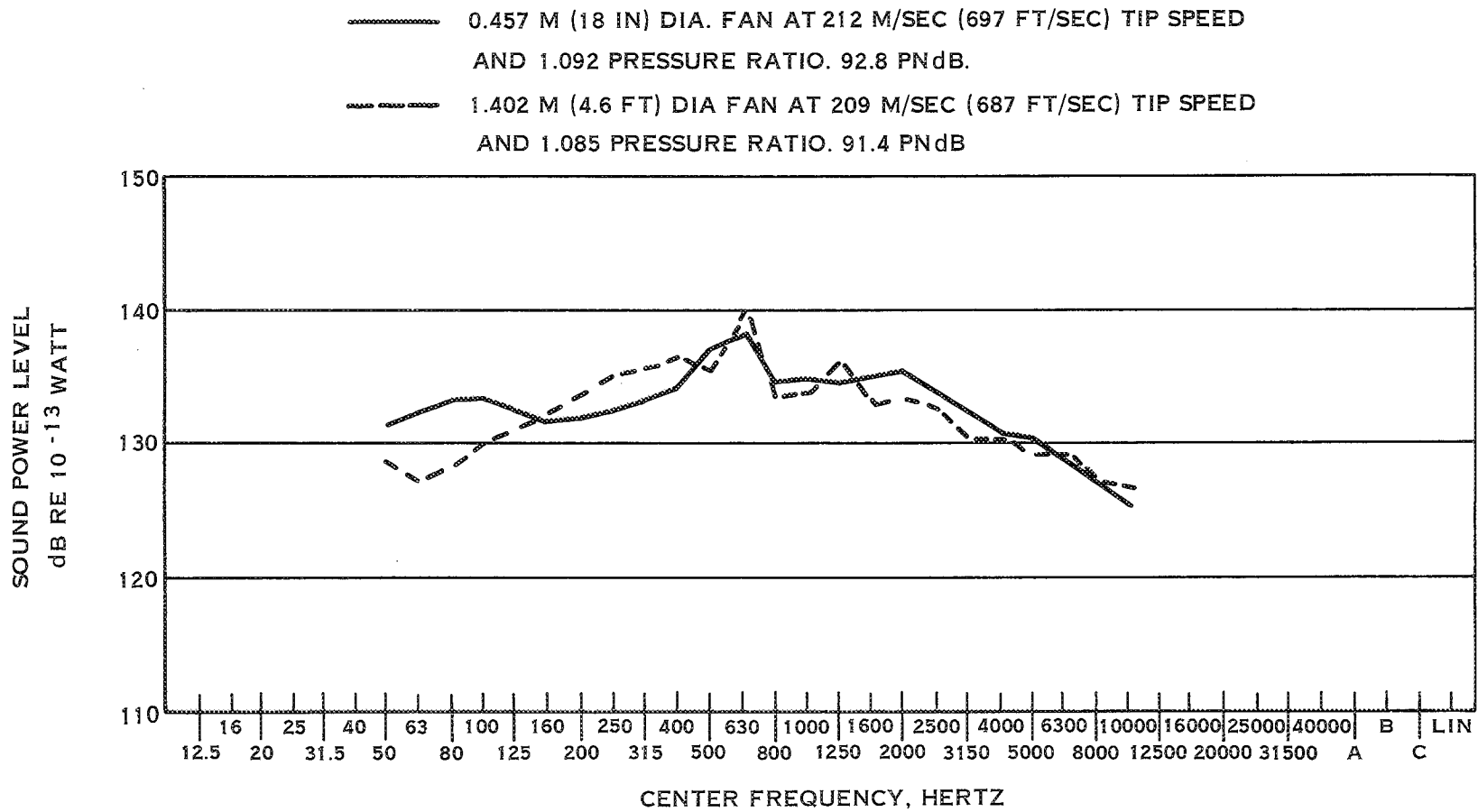


FIGURE 25. COMPARISON OF SPECTRA FROM TWO FANS - CONDITION #1

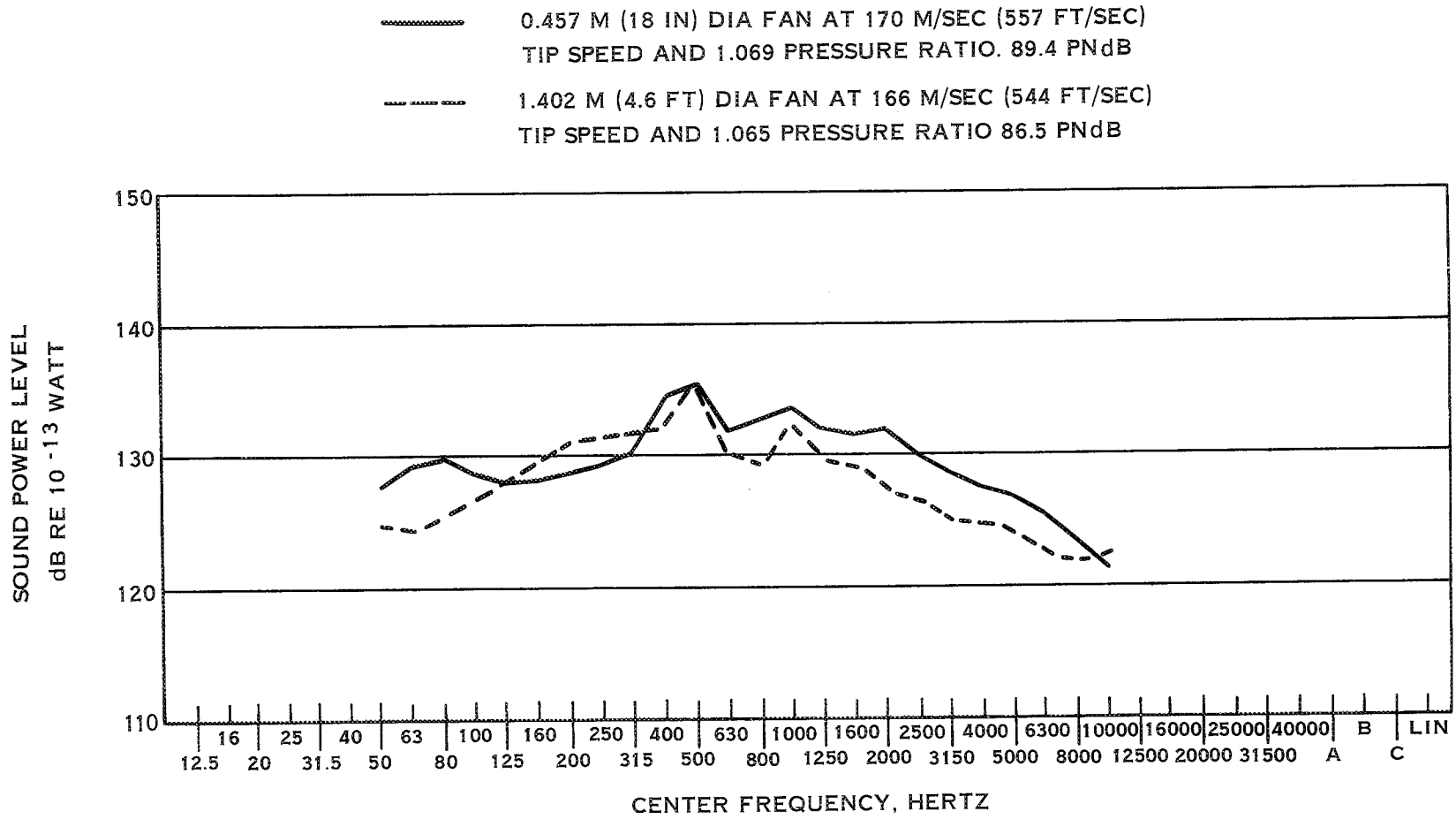


FIGURE 26. COMPARISON OF SPECTRA FROM TWO FANS - CONDITION #2

SOUND POWER LEVEL  
dB RE 10<sup>-13</sup> WATT

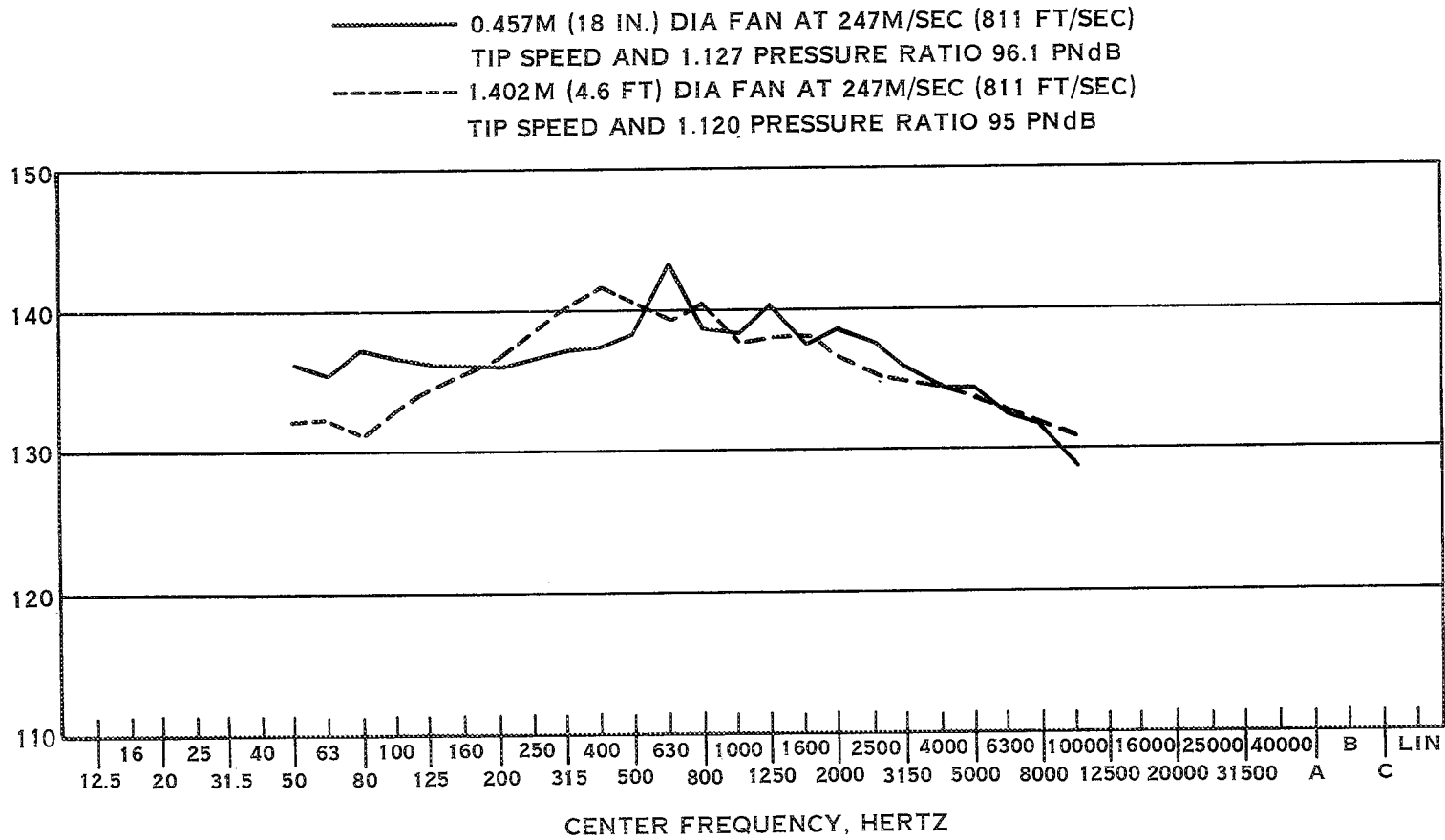


FIGURE 27. COMPARISON OF SPECTRA FROM TWO FANS - CONDITION #3

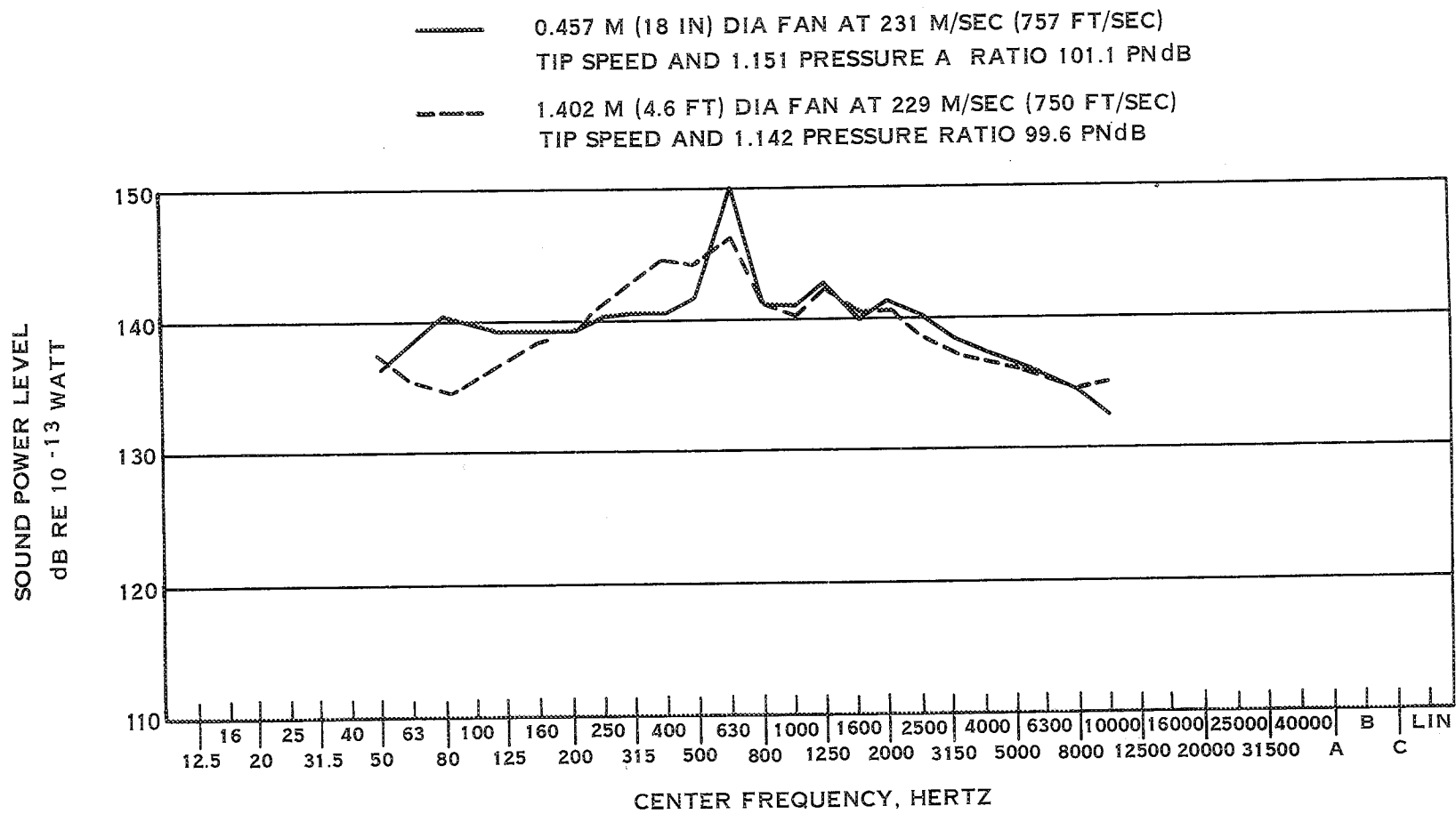


FIGURE 28. COMPARISON OF SPECTRA FROM TWO FANS - CONDITION #4

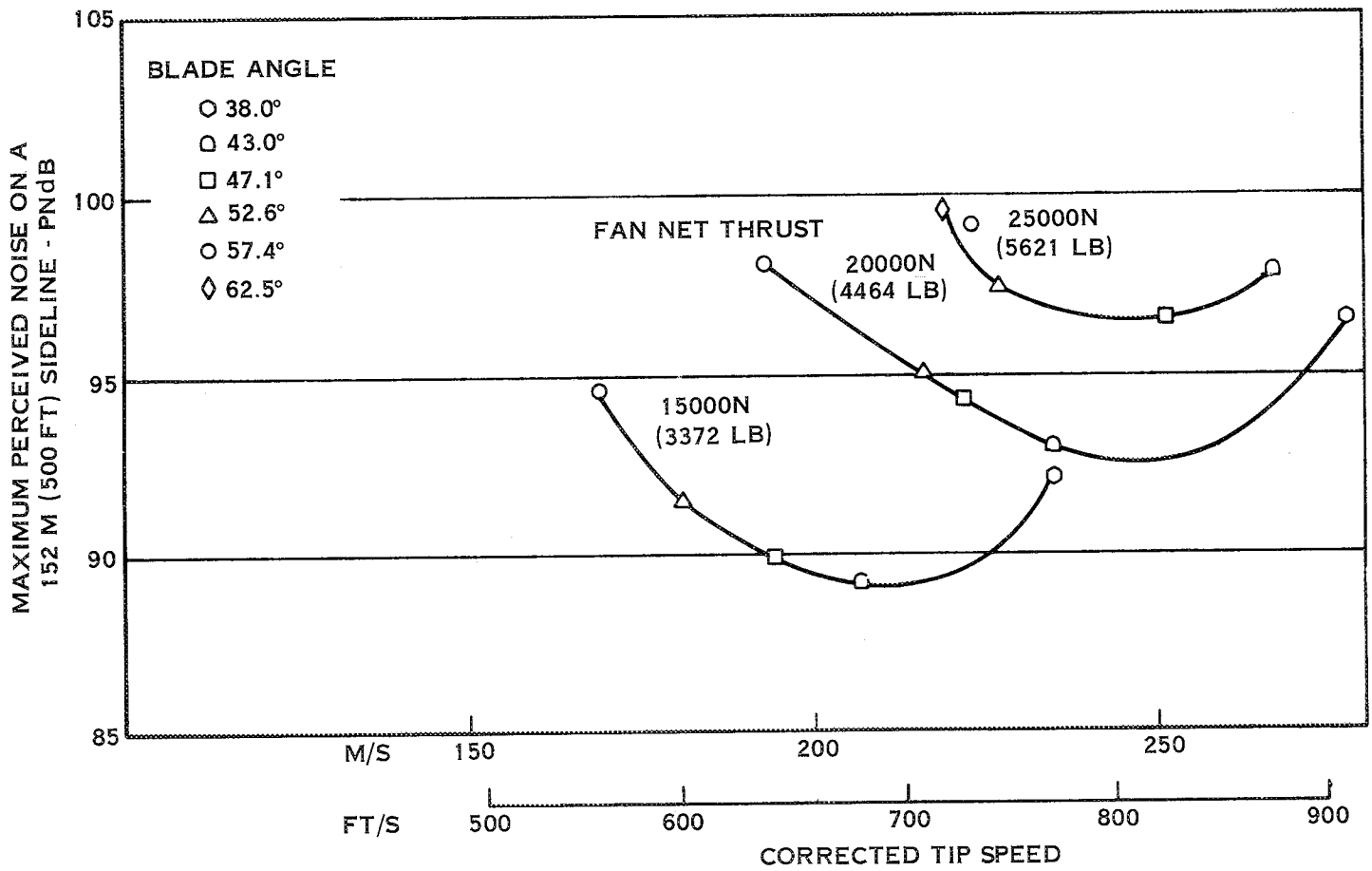


FIGURE 29 PNL VARIATION WITH TIP SPEED AT CONSTANT THRUST SCALED TO 1.402M (4.6 FT) DIAMETER

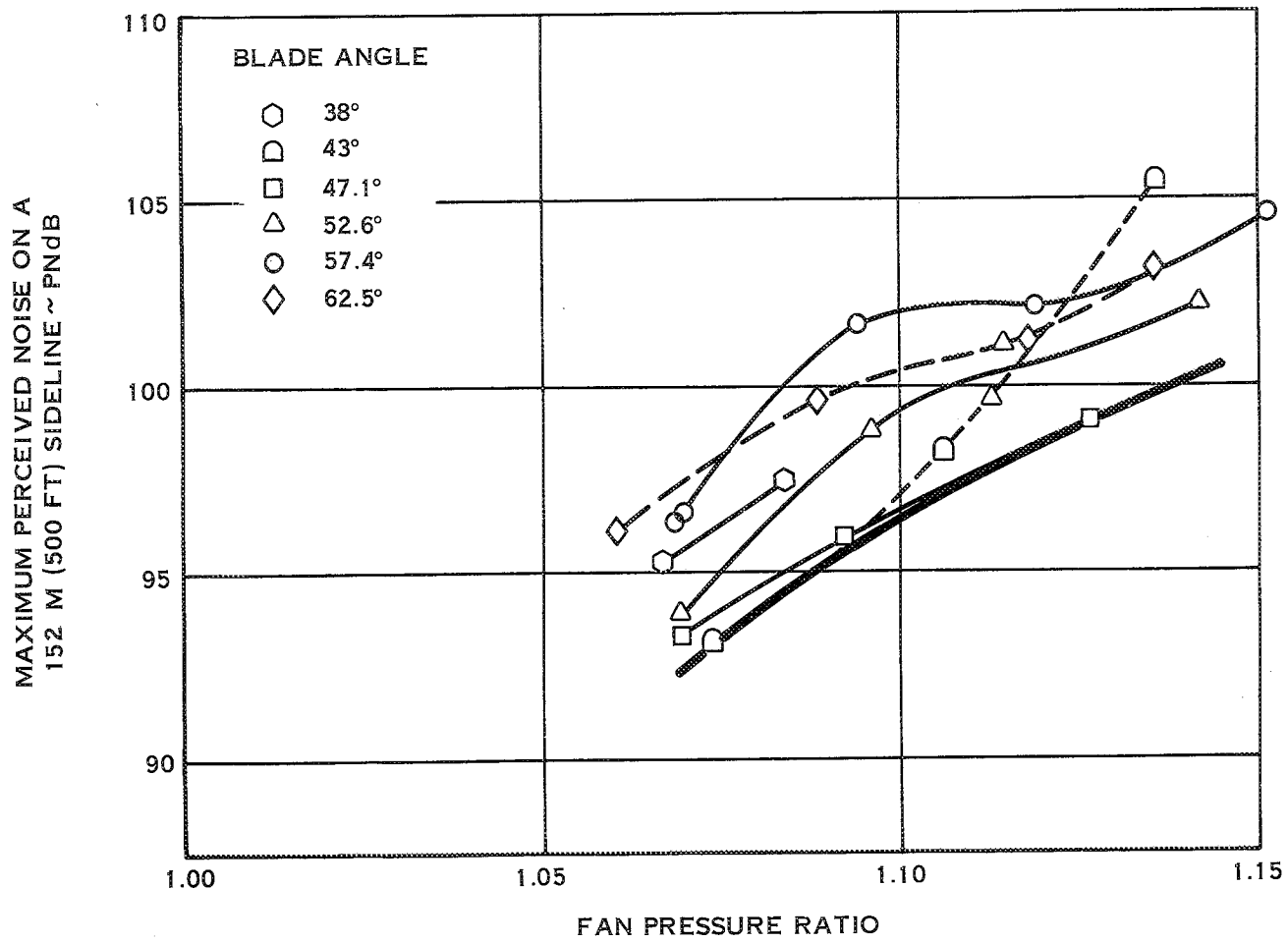


FIGURE 30. 0.457M (18 IN) DIAMETER FAN NOISE SCALED TO 66720 N (15000 LB) THRUST

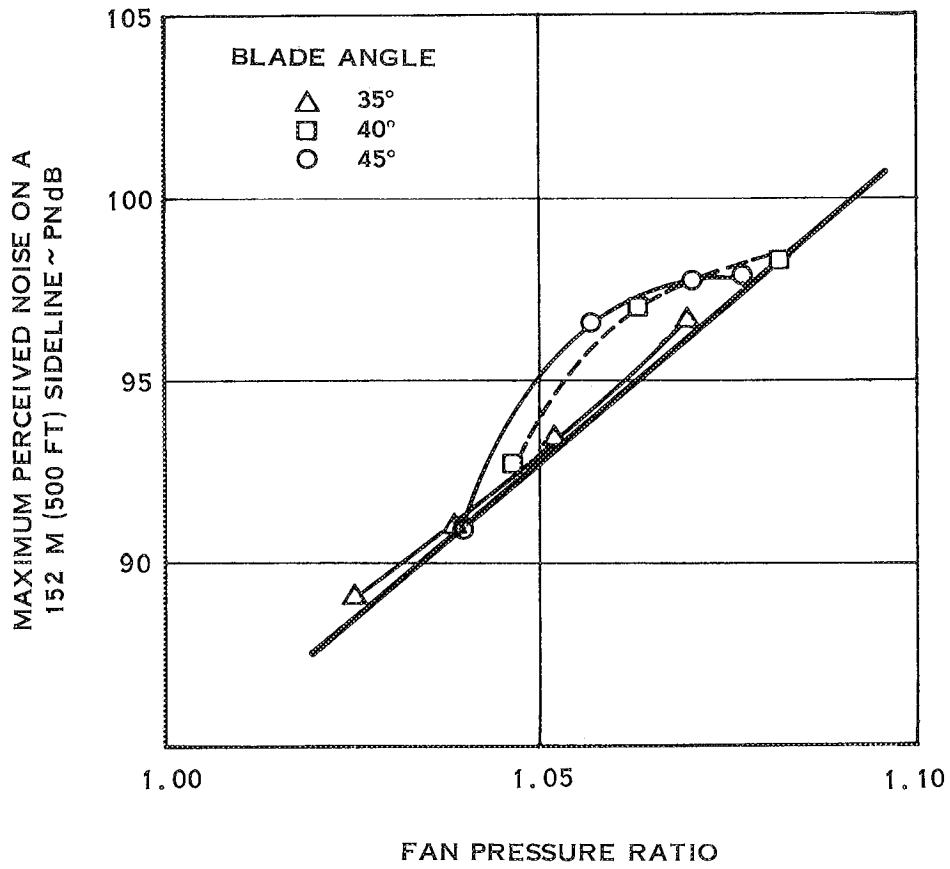


FIGURE 31. 0.533 (21 IN) DIAMETER FAN NOISE SCALED TO 66720 N (15000 LB) THRUST

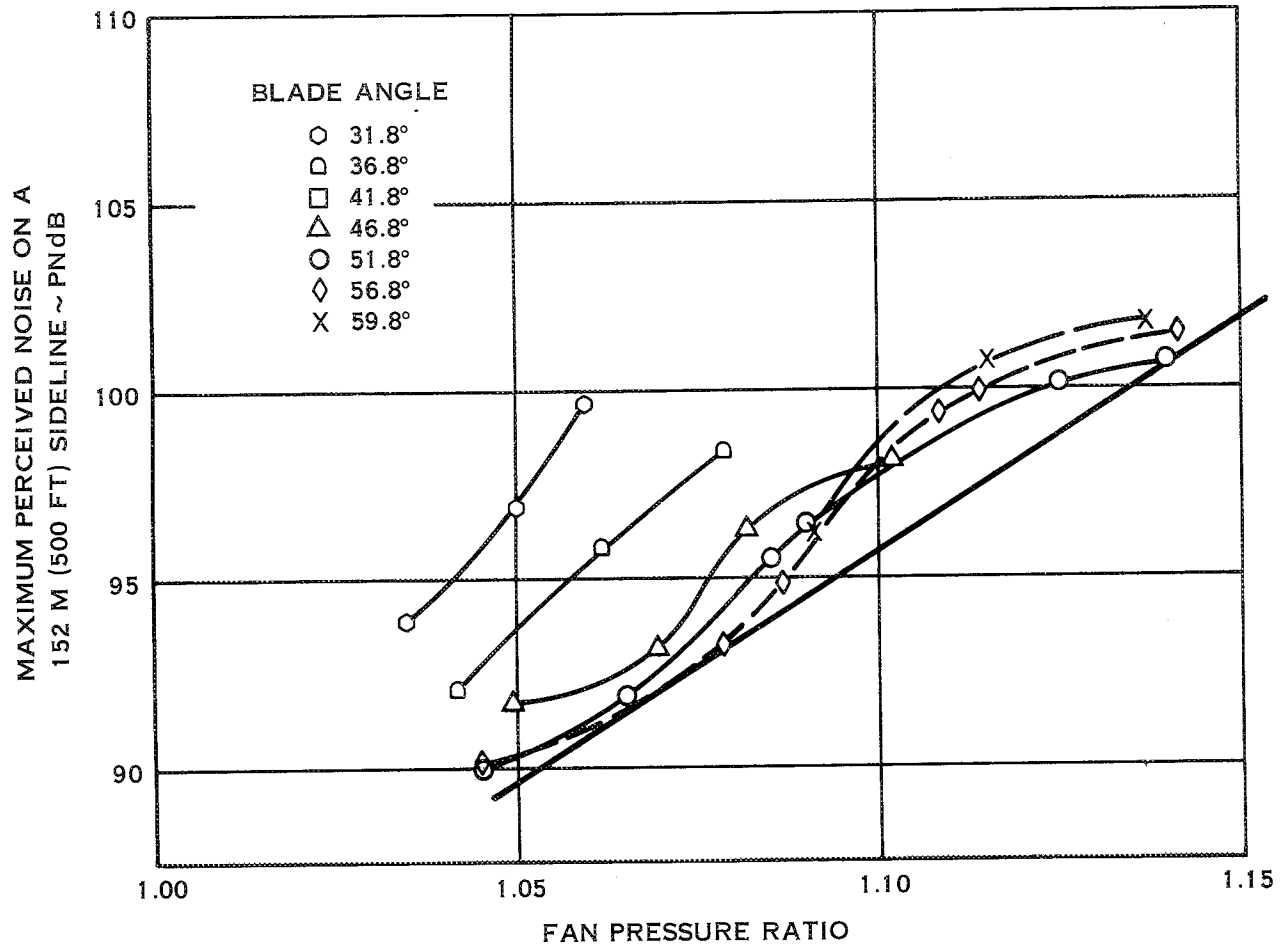


FIGURE 32. 1.402 M (4.6 FT) DIAMETER FAN NOISE SCALED TO 66720N (15000 LB) THRUST

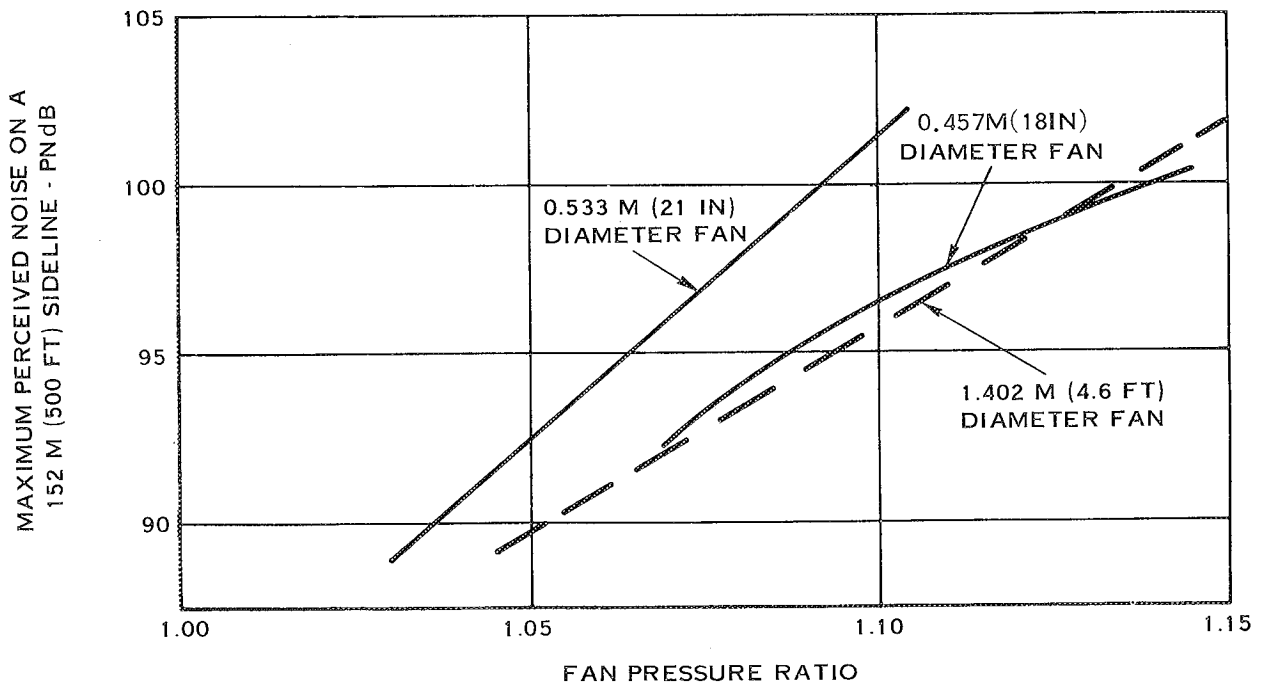


FIGURE 33. COMPARISON OF PNL VERSUS PRESSURE RATIO VARIATION FOR THE THREE FANS

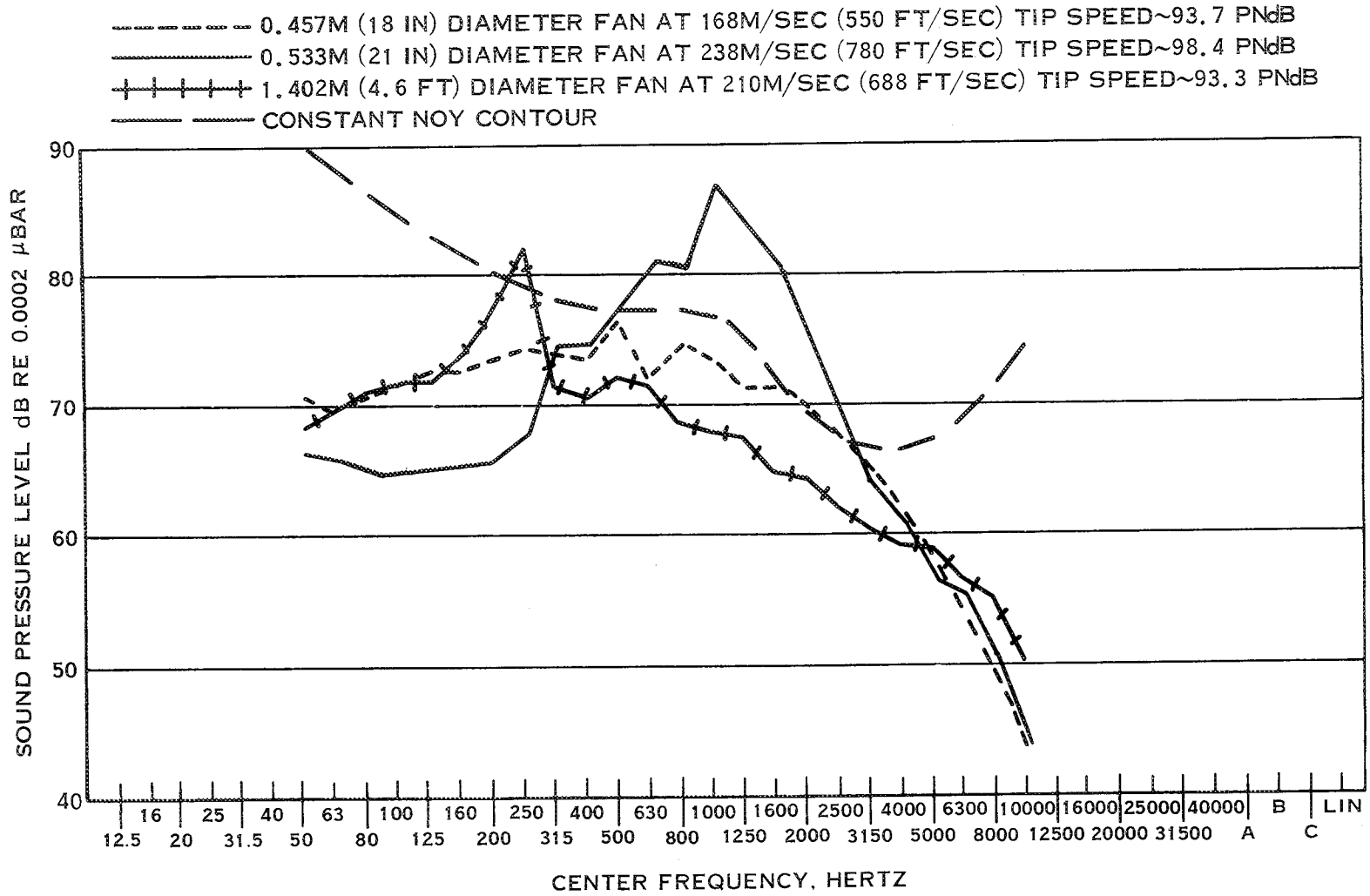


FIGURE 34. COMPARISON OF NOISE SPECTRA AT 1.08 PRESSURE RATIO SCALED TO 66720 N. (15000LB) THRUST

——— MEASURED DATA      92.8 PNdB  
 - - - PREDICTED SPECTRUM    94.6 PNdB  
 212 M/S (697 FT/S) TIP SPEED  
 47.1 DEG BLADE ANGLE

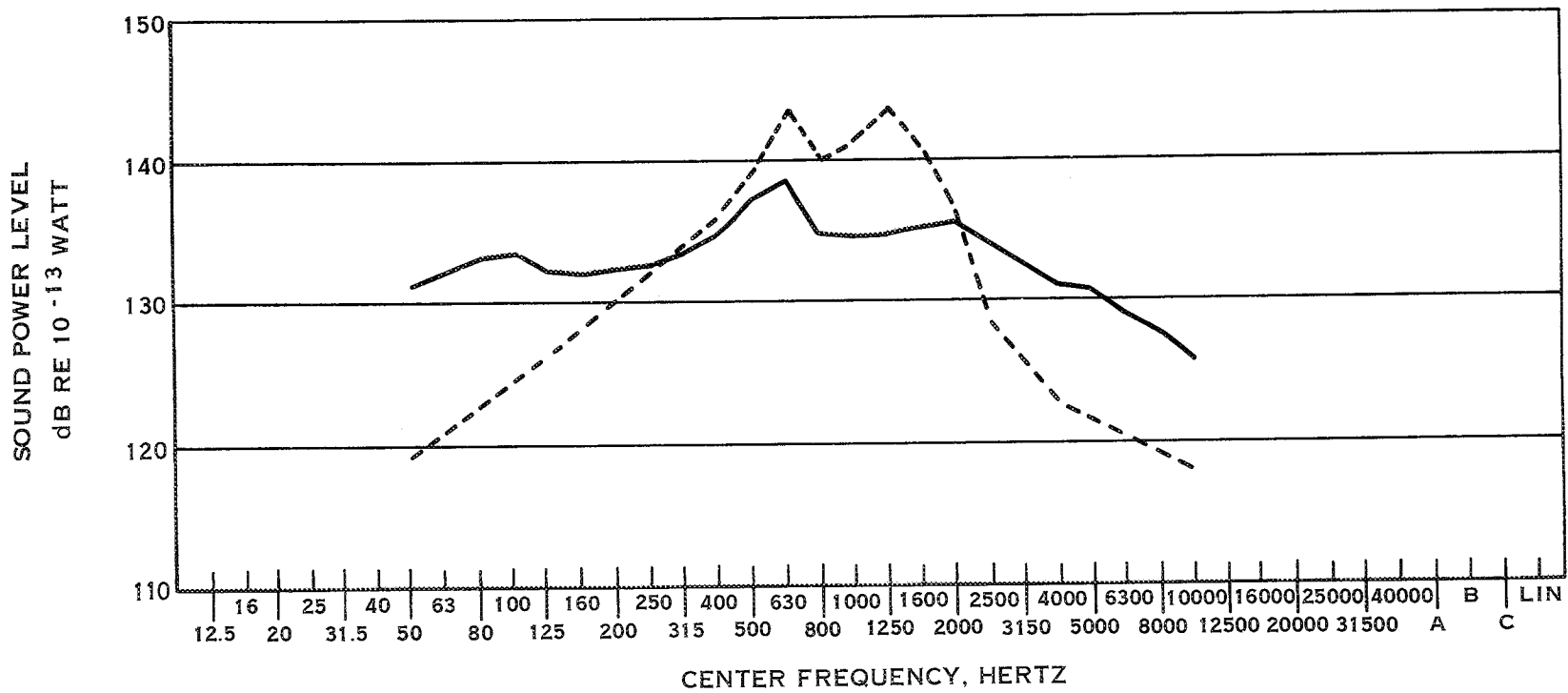


FIGURE 35 COMPARISON OF MEASUREMENTS AND PREDICTIONS - CONDITION #1

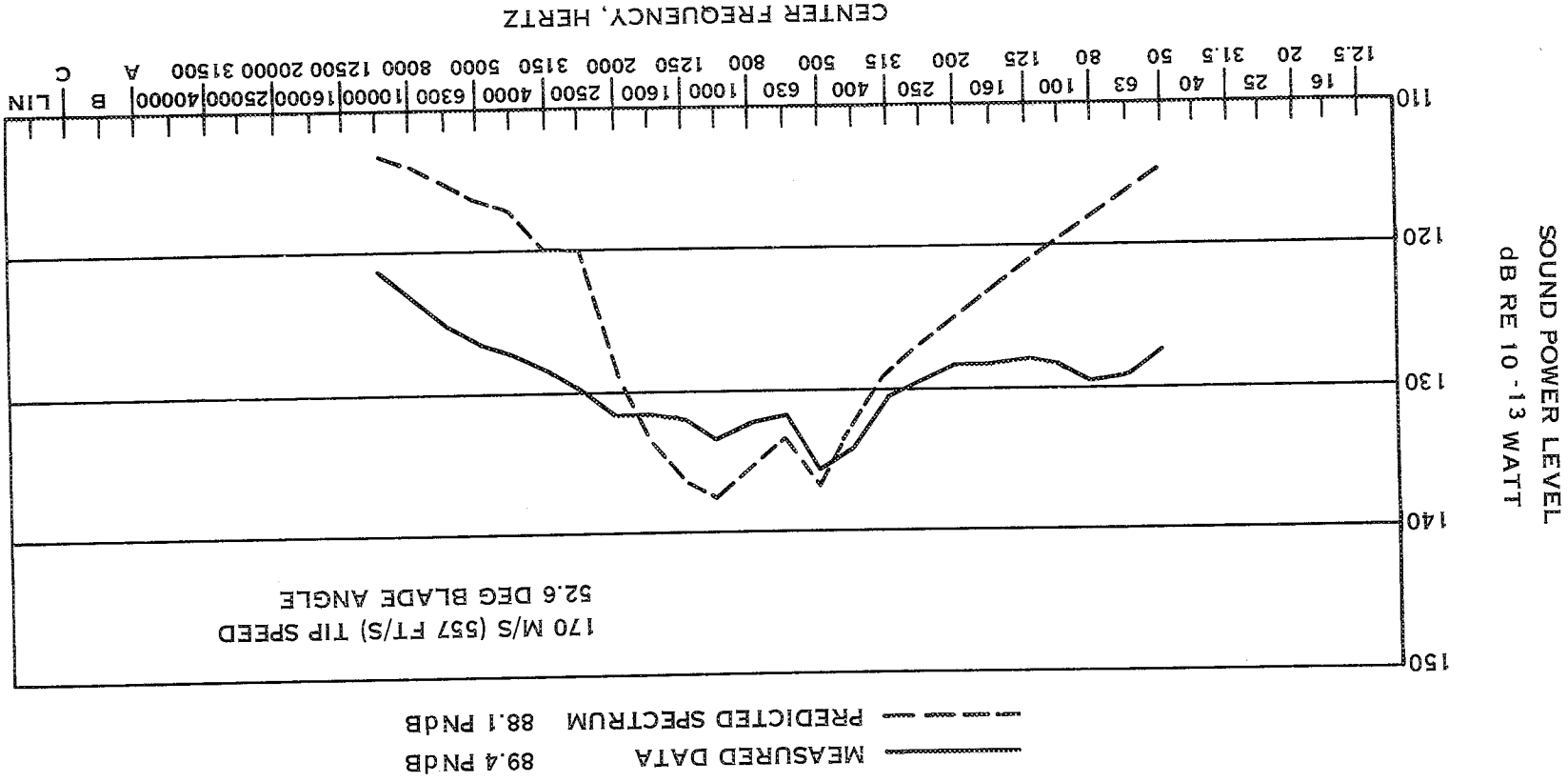


FIGURE 36 COMPARISON OF MEASUREMENTS AND PREDICTIONS - CONDITION #2



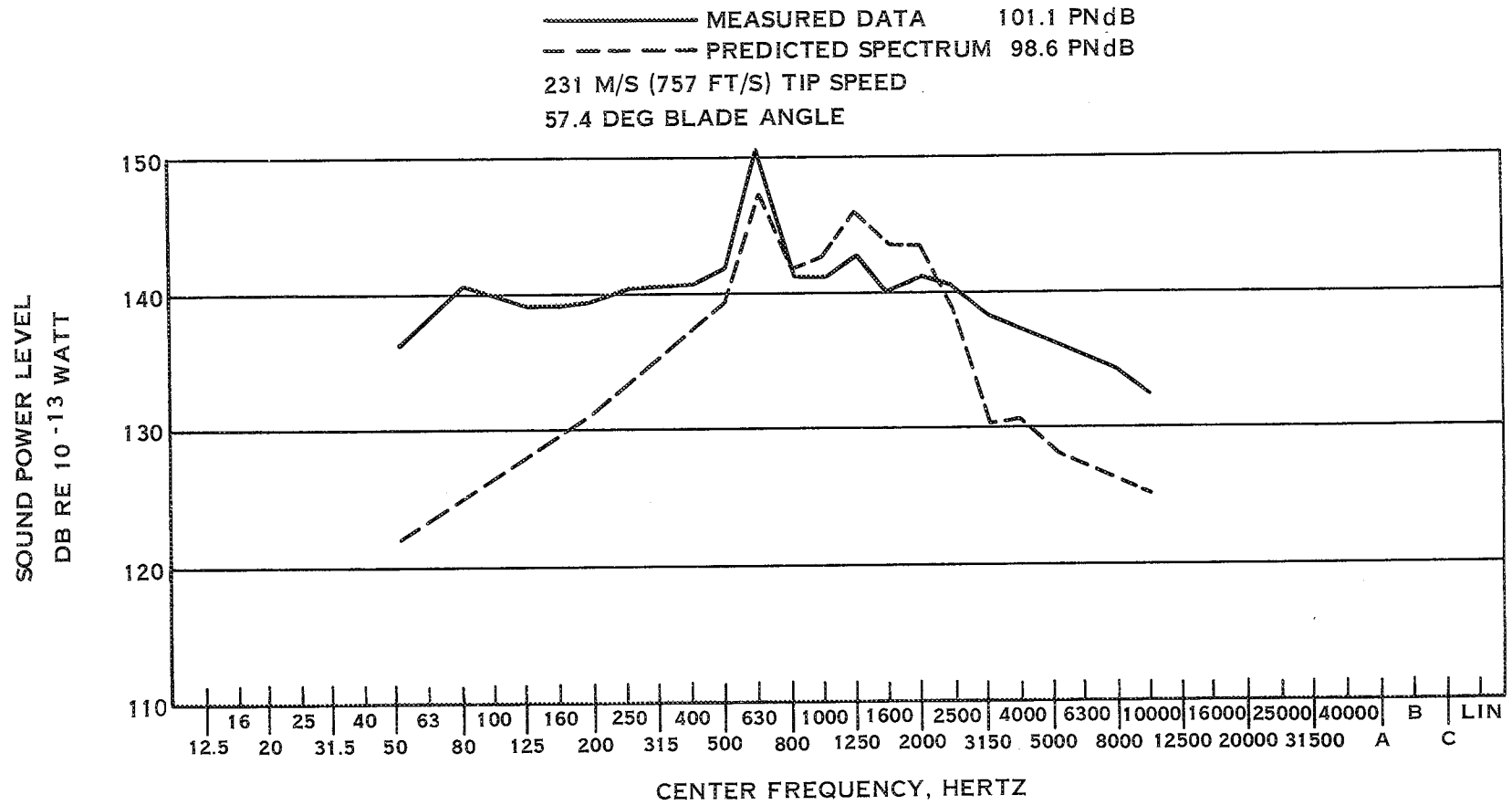


FIGURE 38 - COMPARISON OF MEASUREMENTS AND PREDICTIONS - CONDITION #4

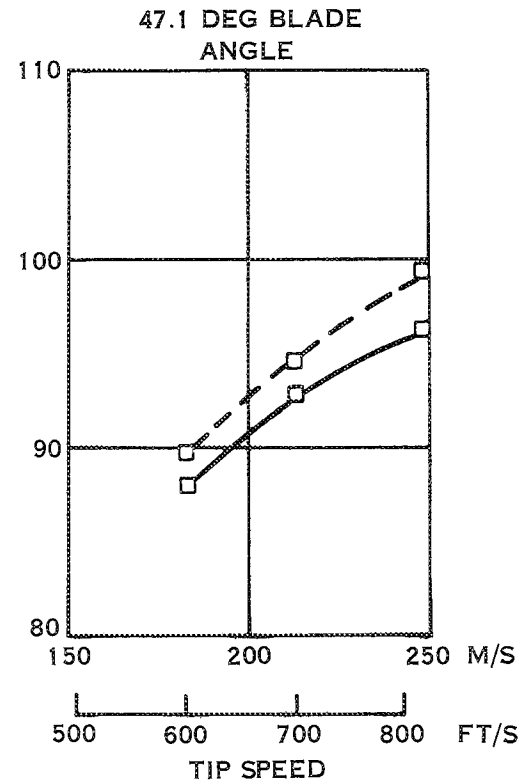
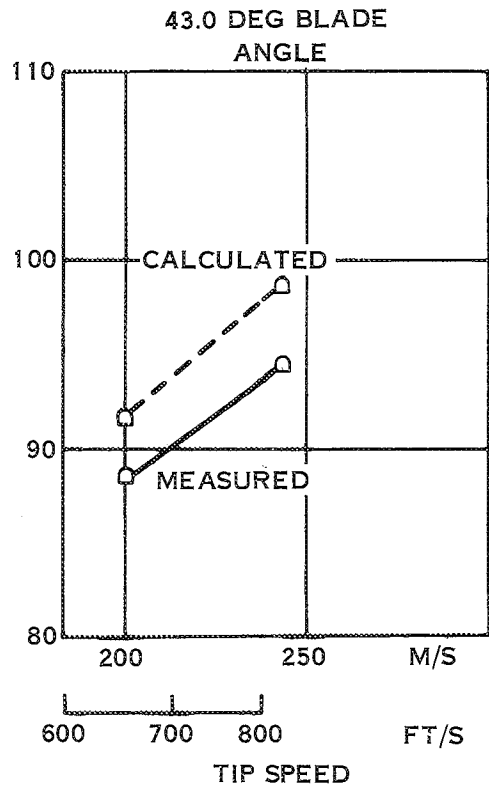
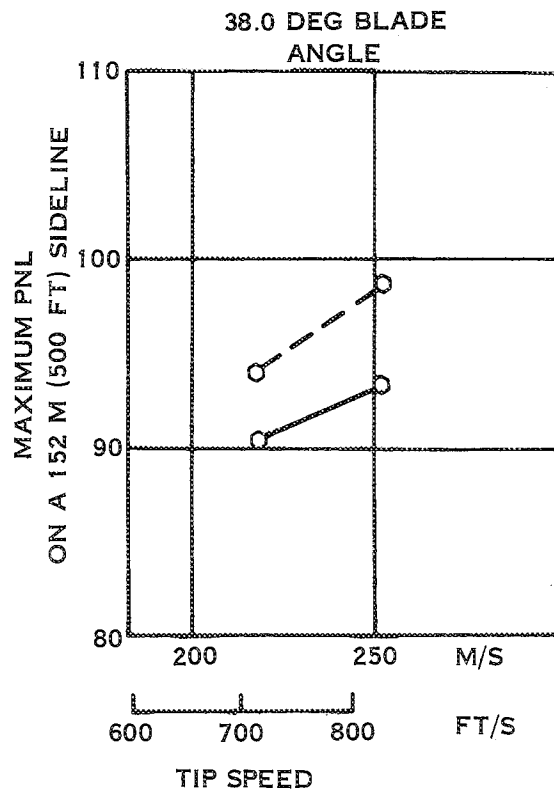


FIGURE 39 COMPARISON OF MEASURED AND CALCULATED NOISE LEVELS SCALED TO A DIAMETER OF 1.402 M (4.6 FT) AT 38.0, 43.0, AND 47.1 DEG BLADE ANGLE

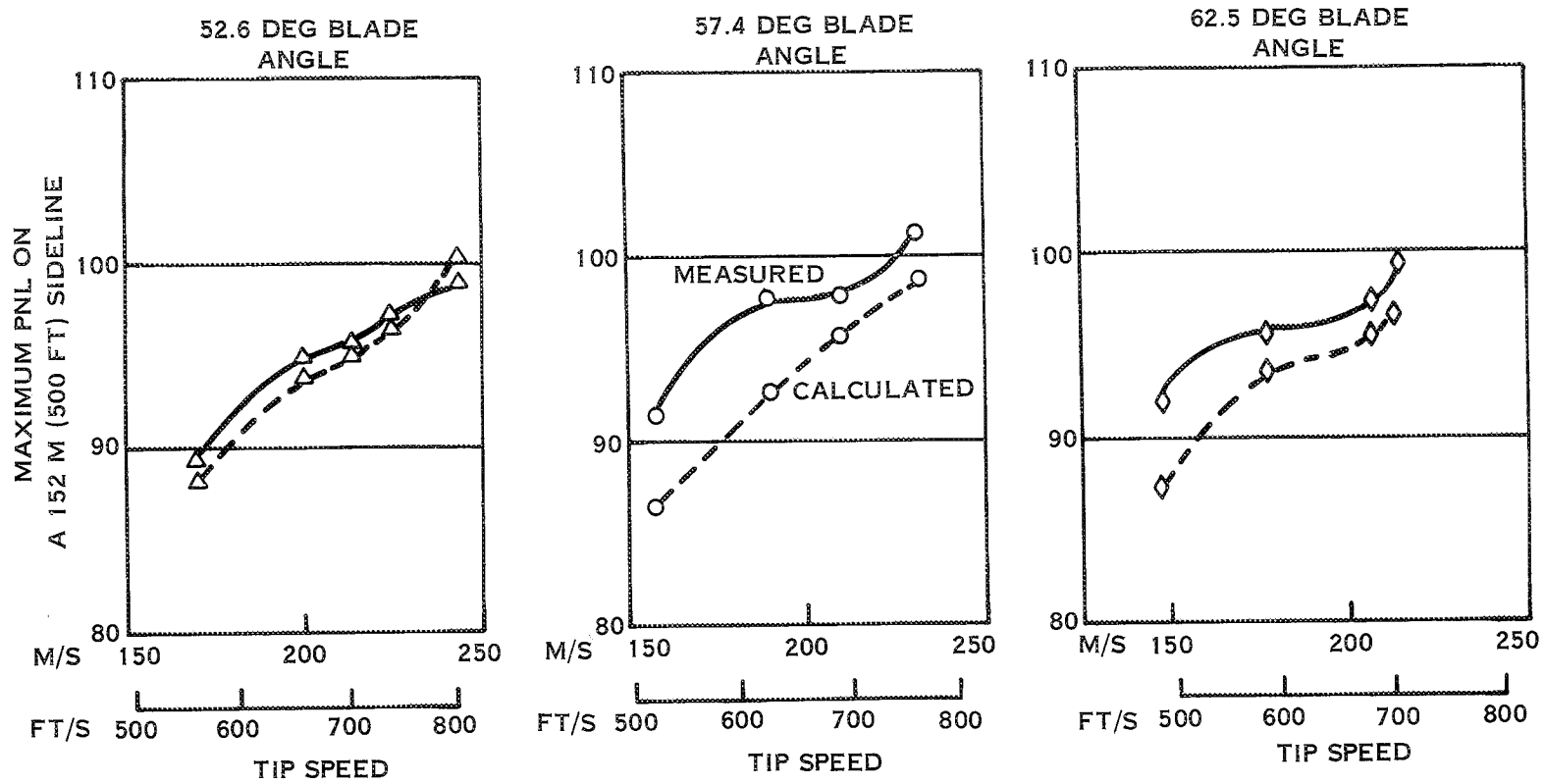


FIGURE 40 COMPARISON OF MEASURED AND CALCULATED NOISE LEVELS SCALED TO A DIAMETER OF 1.402M (4.6 FT) AT 52.6, 57.4 AND 62.5 DEG BLADE ANGLE

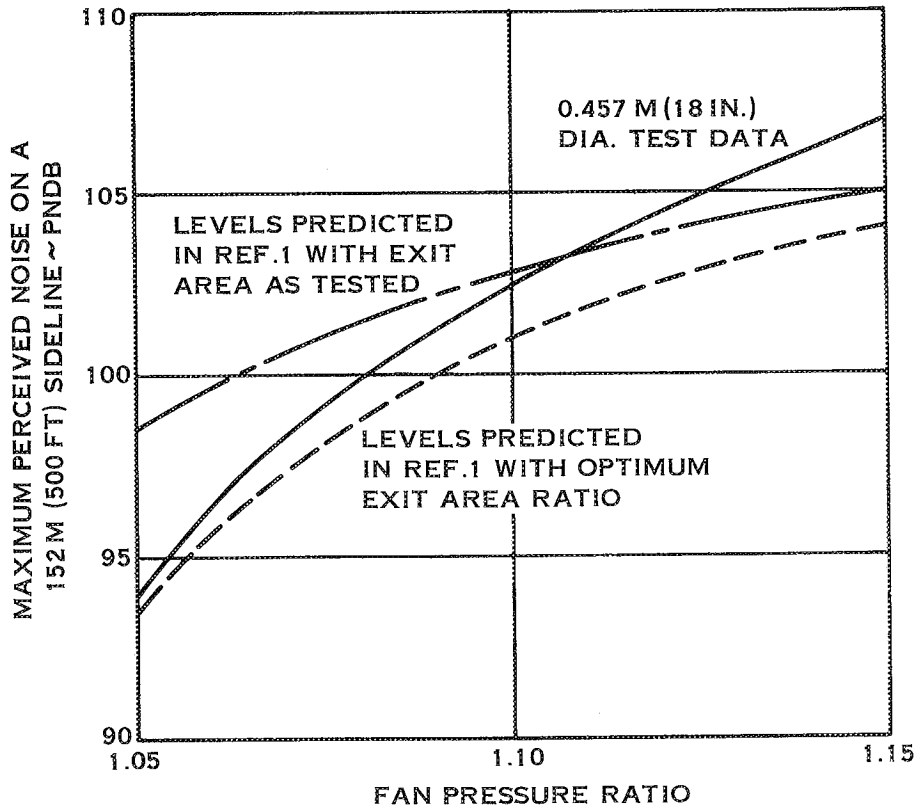
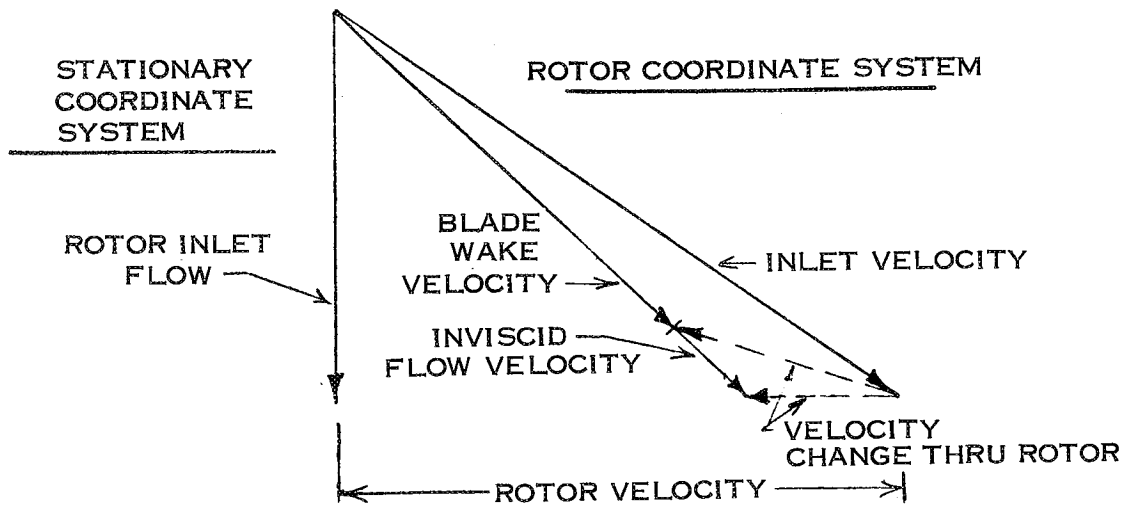


FIGURE 41-COMPARISON OF MEASURED AND CALCULATED PNL VARIATION WITH PRESSURE RATIO FOR A 45360 KG (100,000 LB) AIRCRAFT

WITHOUT ROTOR SPEED



WITH ROTOR SPEED

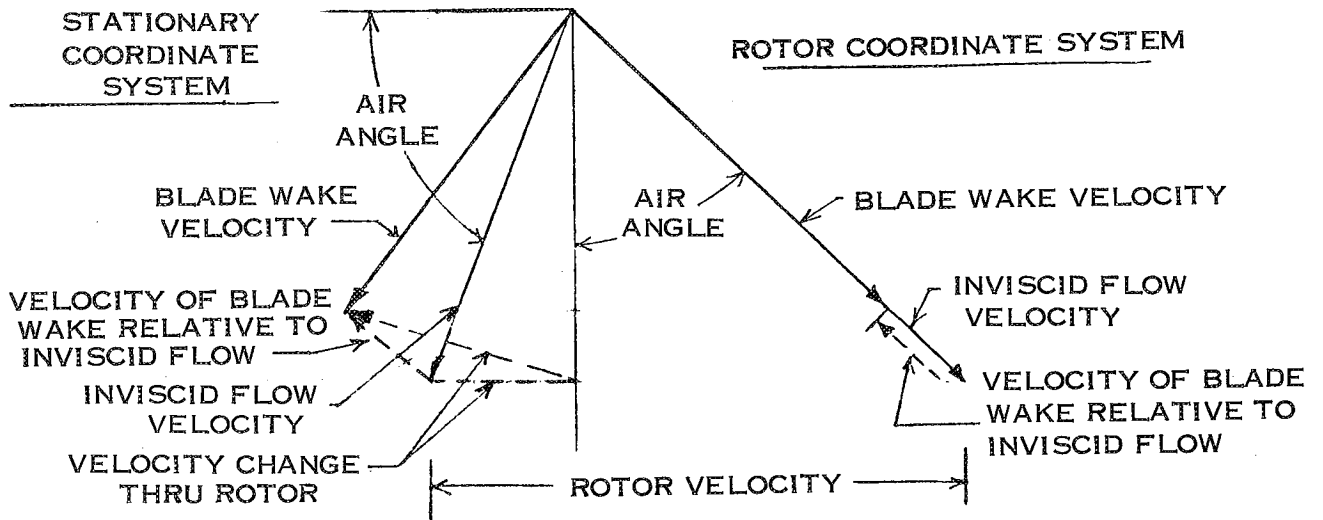


FIGURE 42. SKETCH OF VELOCITY VECTORS

$\tau = 20 \mu\text{SEC}$

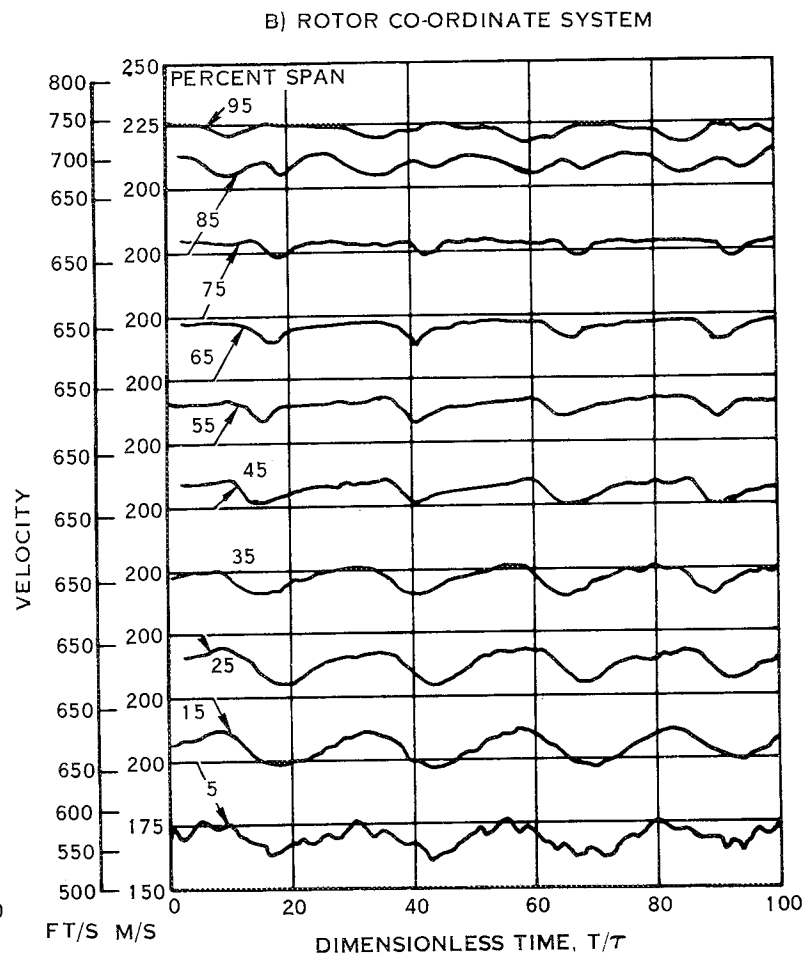
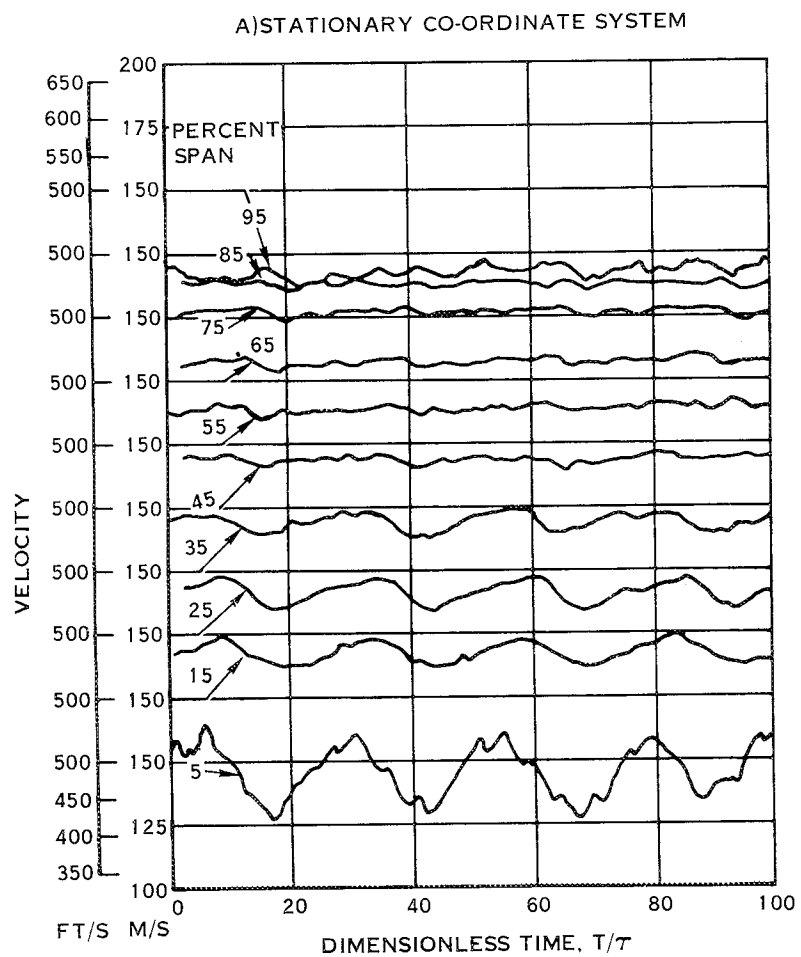


FIGURE 43. COMPARISON OF RESULTANT VELOCITY PROFILES FOR FLOW CONDITION I

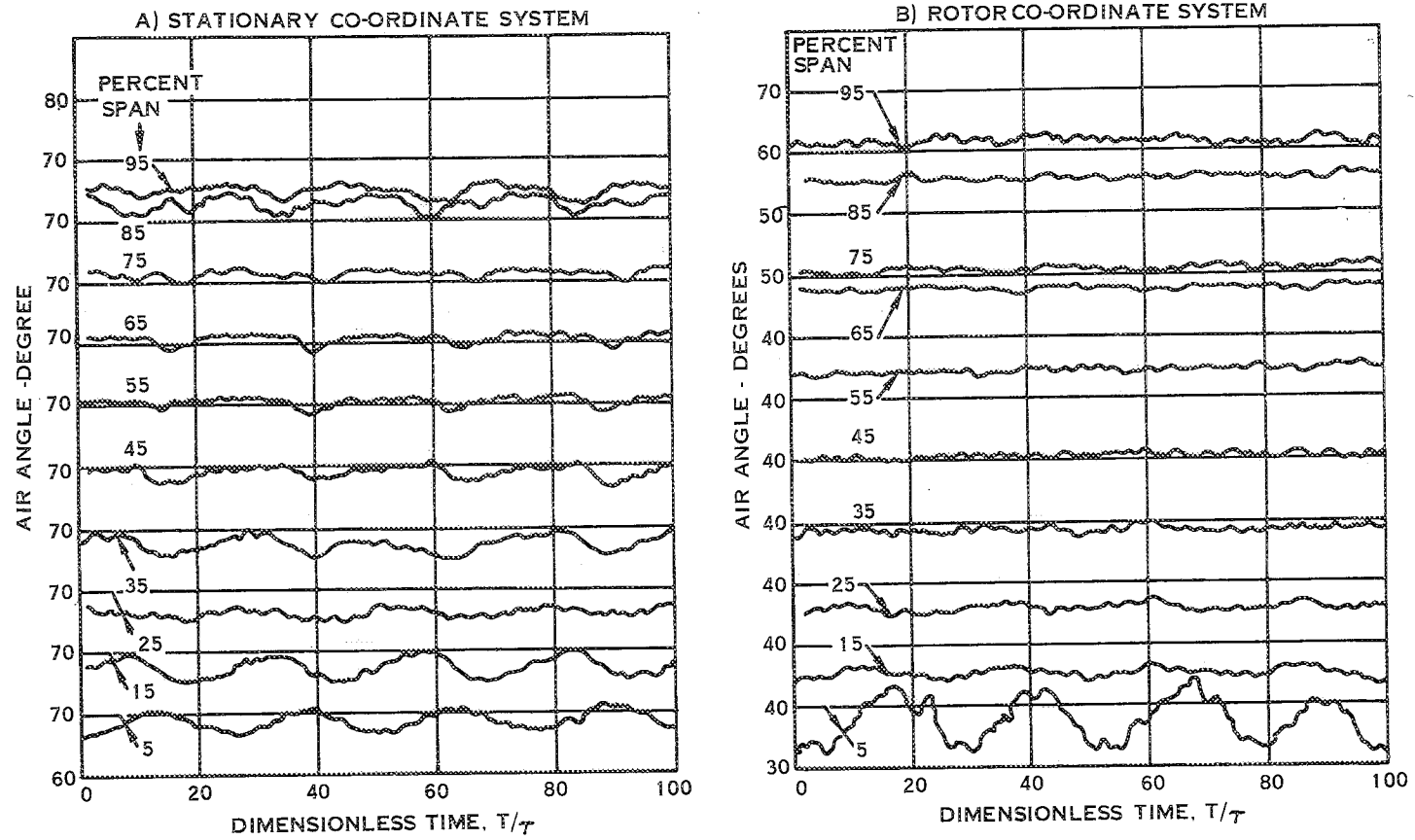
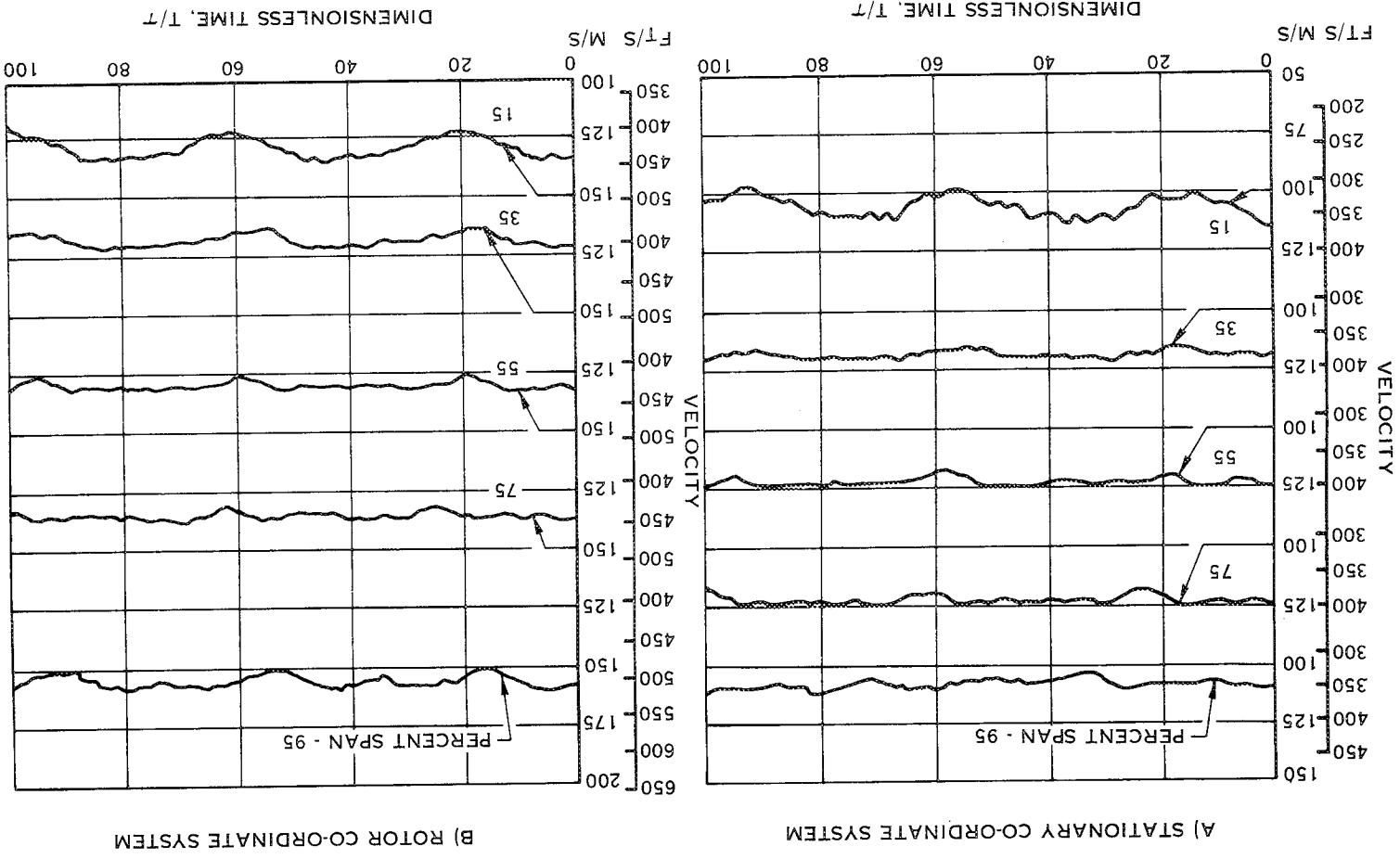
$\tau = 20 \mu\text{SEC}$ 

FIGURE 44. COMPARISON OF AIR ANGLES FOR FLOW CONDITION I

FIGURE 45. COMPARISON OF RESULTANT VELOCITY PROFILES FOR FLOW CONDITION II



$T = 20 \mu \text{ SEC}$

FIGURE 46 COMPARISON OF AIR ANGLES FOR FLOW CONDITION II

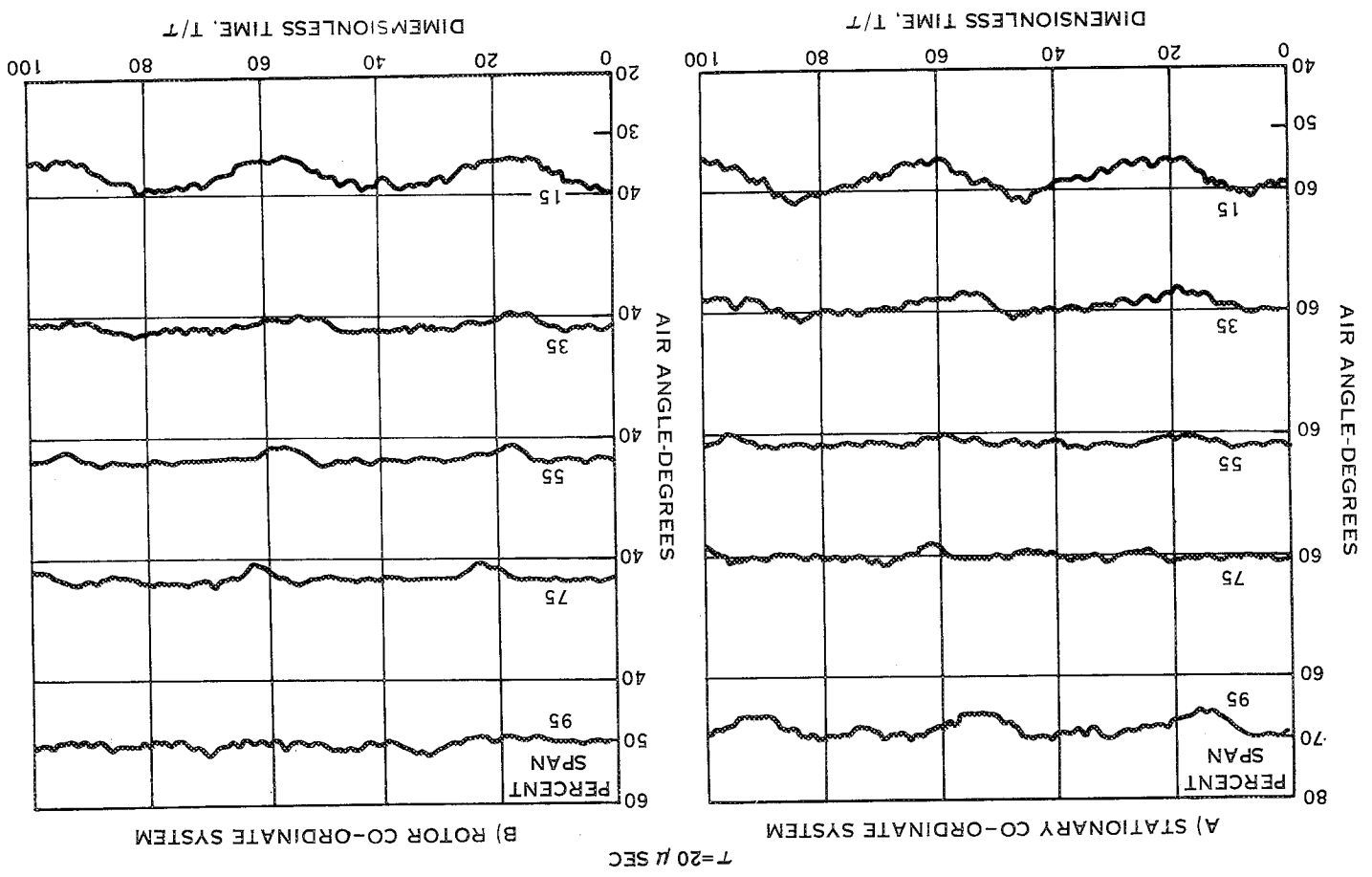
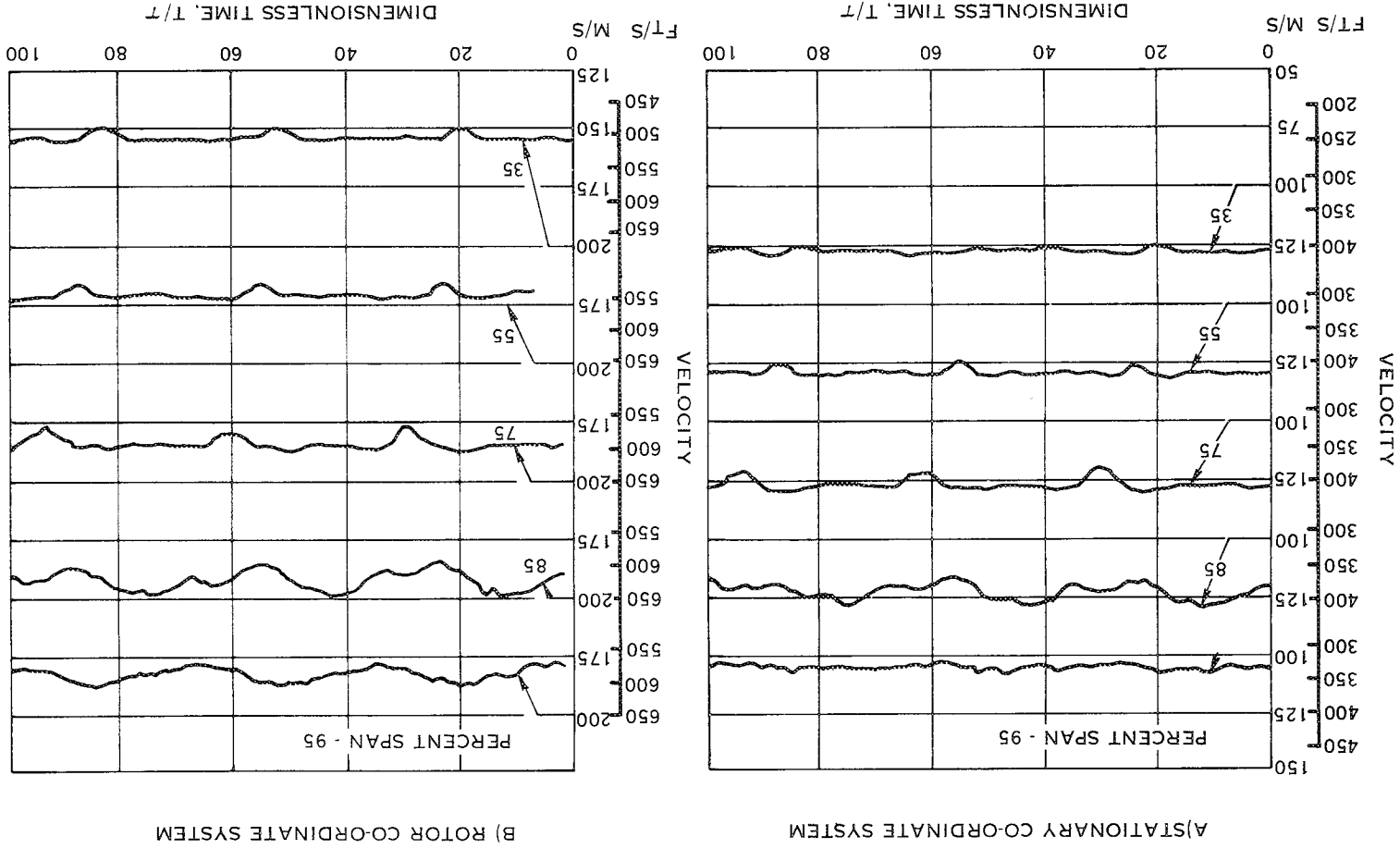


FIGURE 47. COMPARISON OF RESULTANT VELOCITY PROFILES FOR FLOW CONDITION III



T = 20 μ SEC

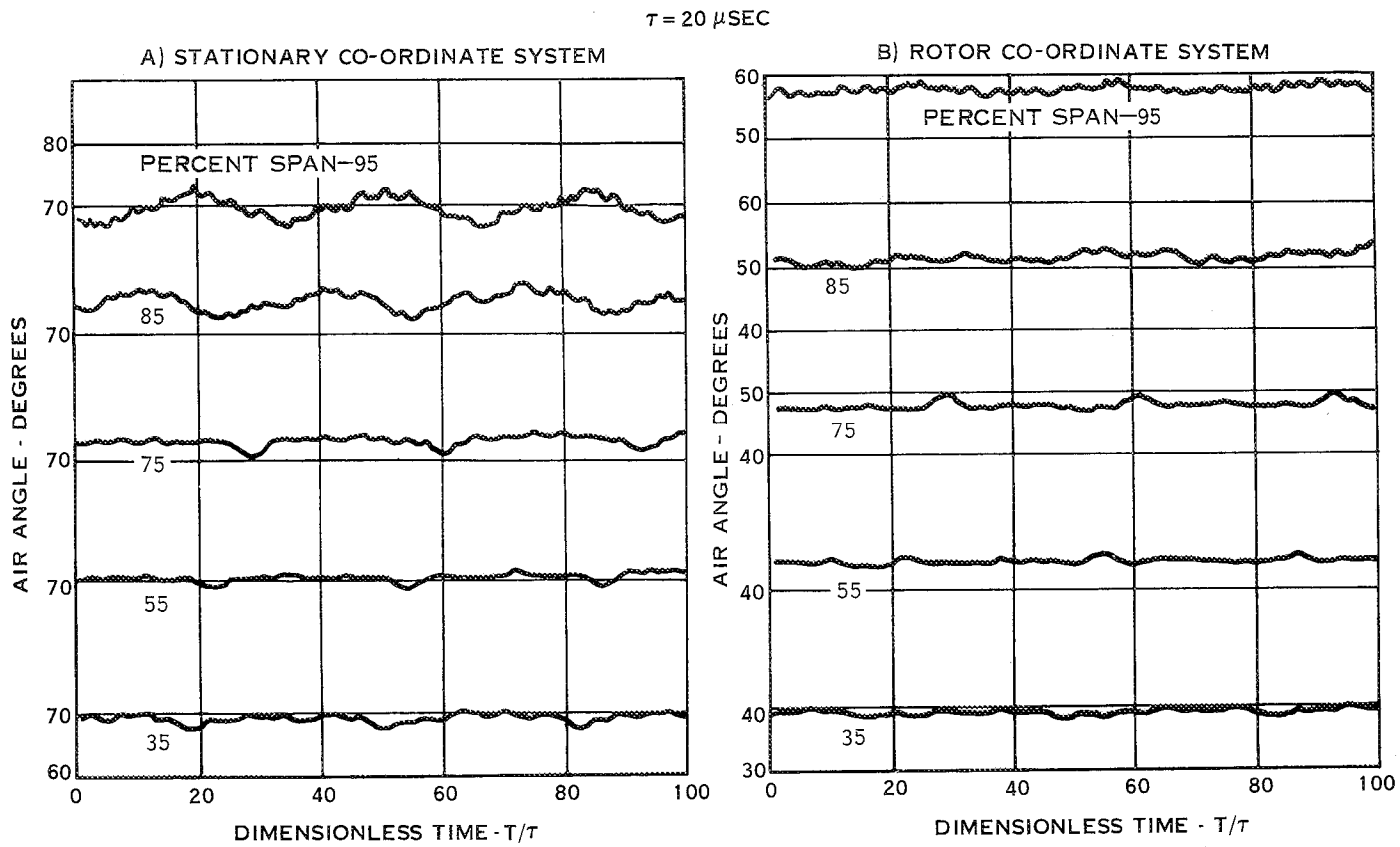


FIGURE 48 COMPARISON OF AIR ANGLES FOR FLOW CONDITION III

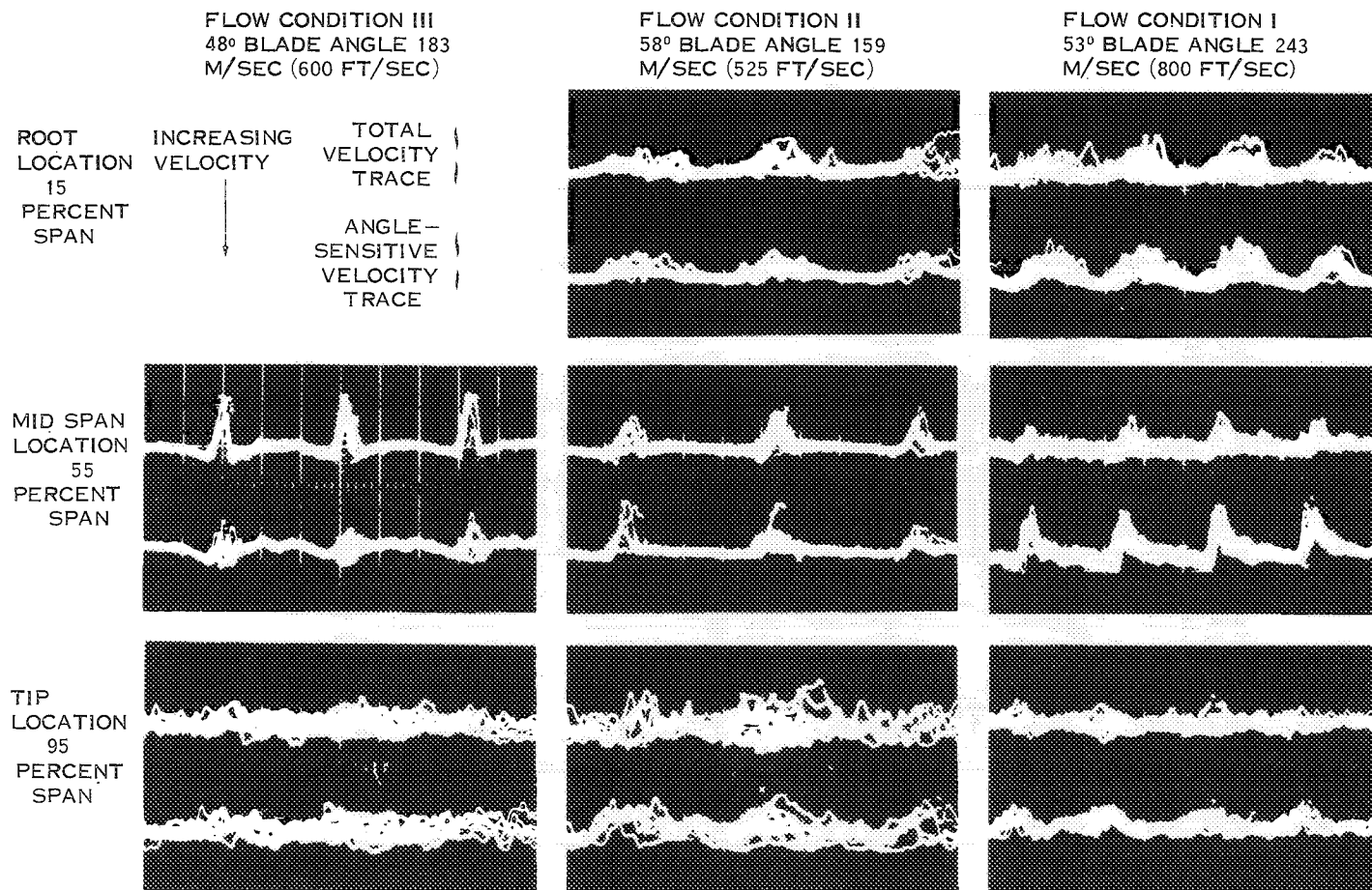


FIGURE 49 HOT WIRE ANMOMETER DATA SHOWING WAKE MODULATION

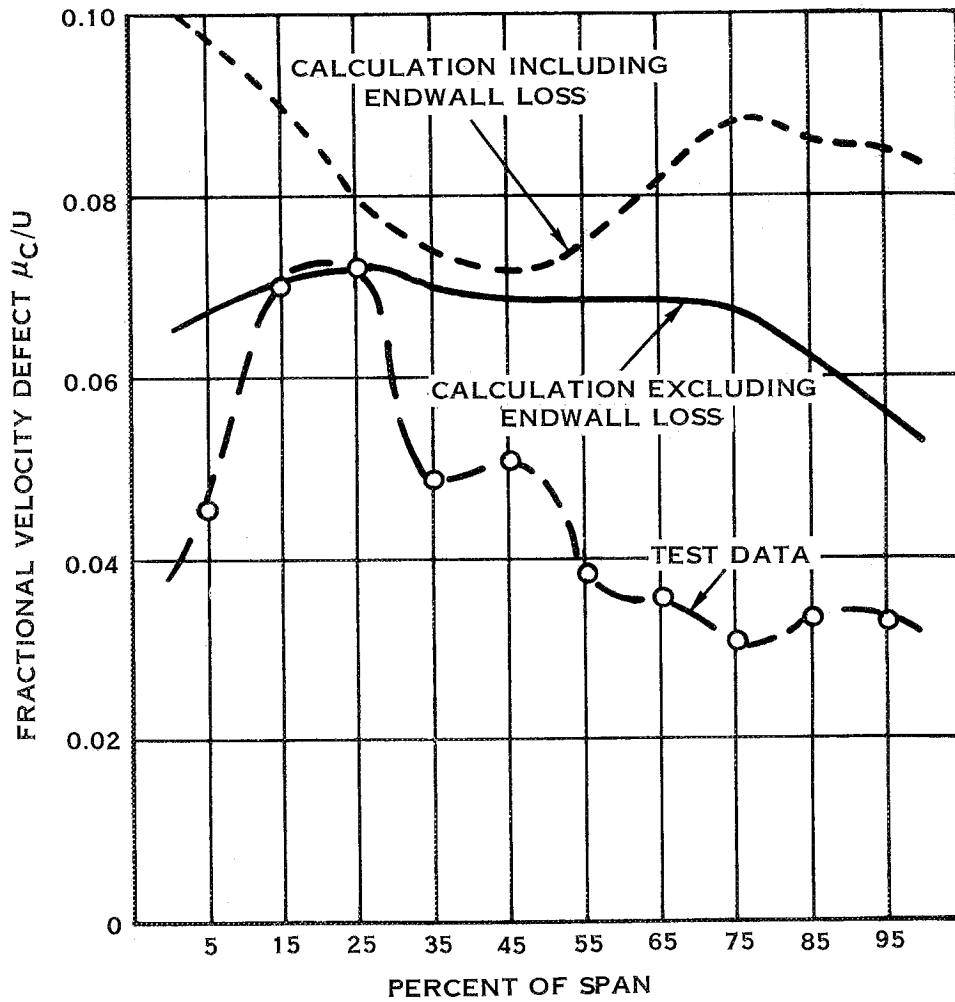


FIGURE 50. FRACTIONAL VELOCITY DEFECT COMPARISONS FOR TEST CONDITION I

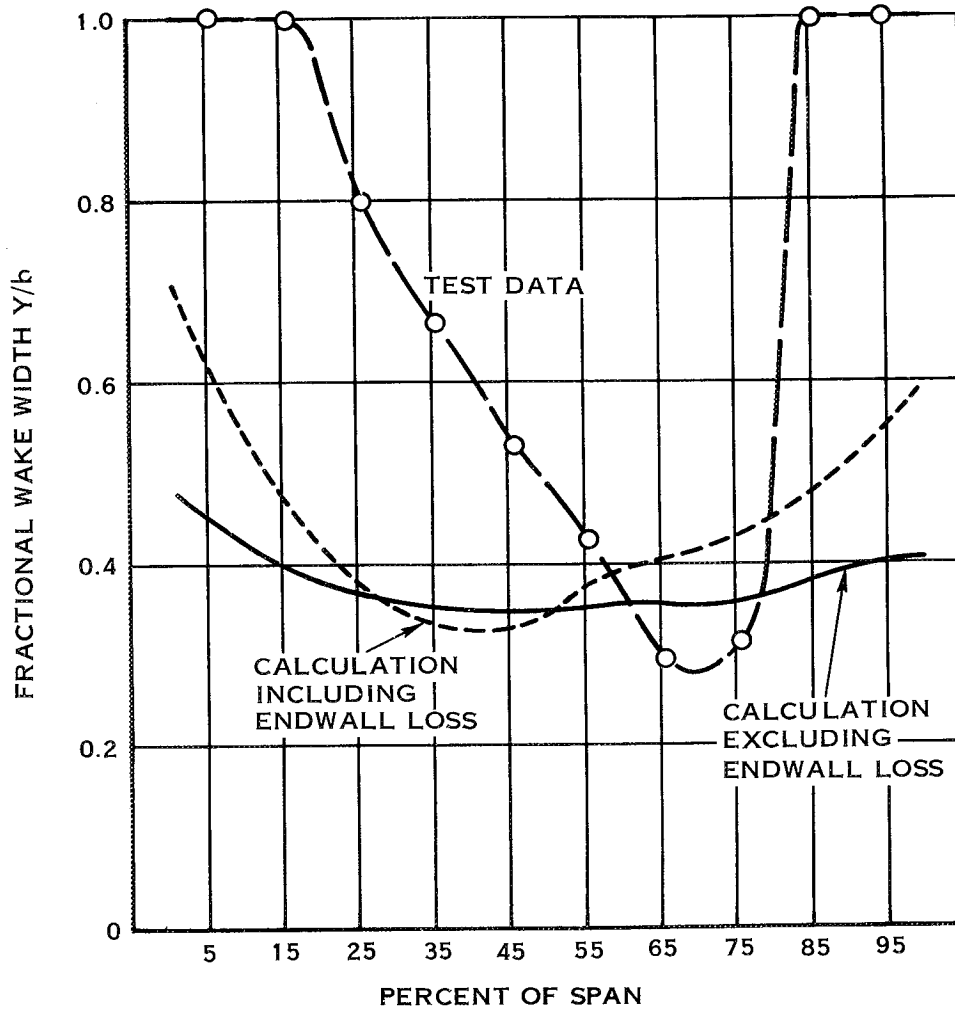


FIGURE 51. FRACTIONAL WAKE WIDTH COMPARISONS FOR TEST CONDITION I

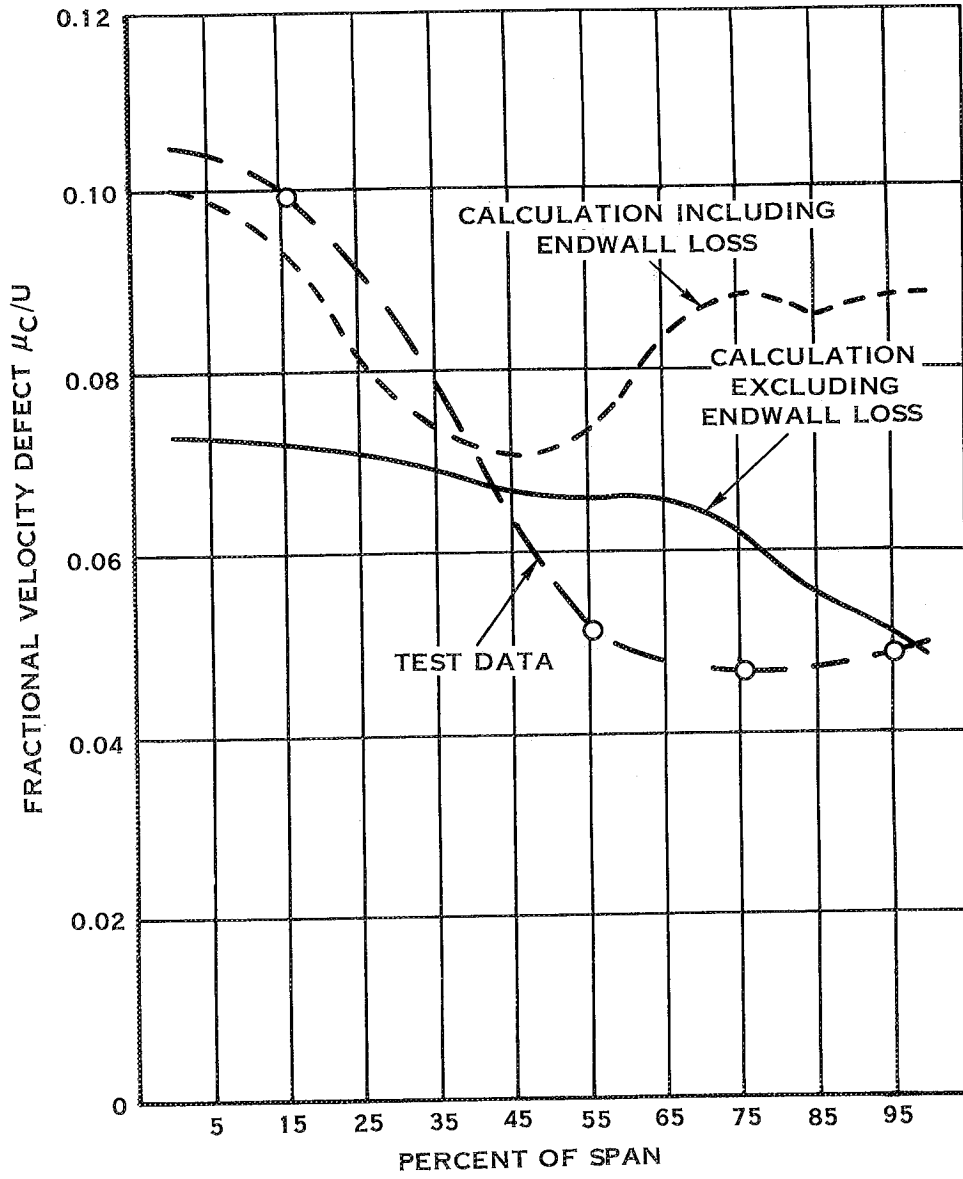


FIGURE 52. FRACTIONAL VELOCITY DEFECT COMPARISONS FOR TEST CONDITION II

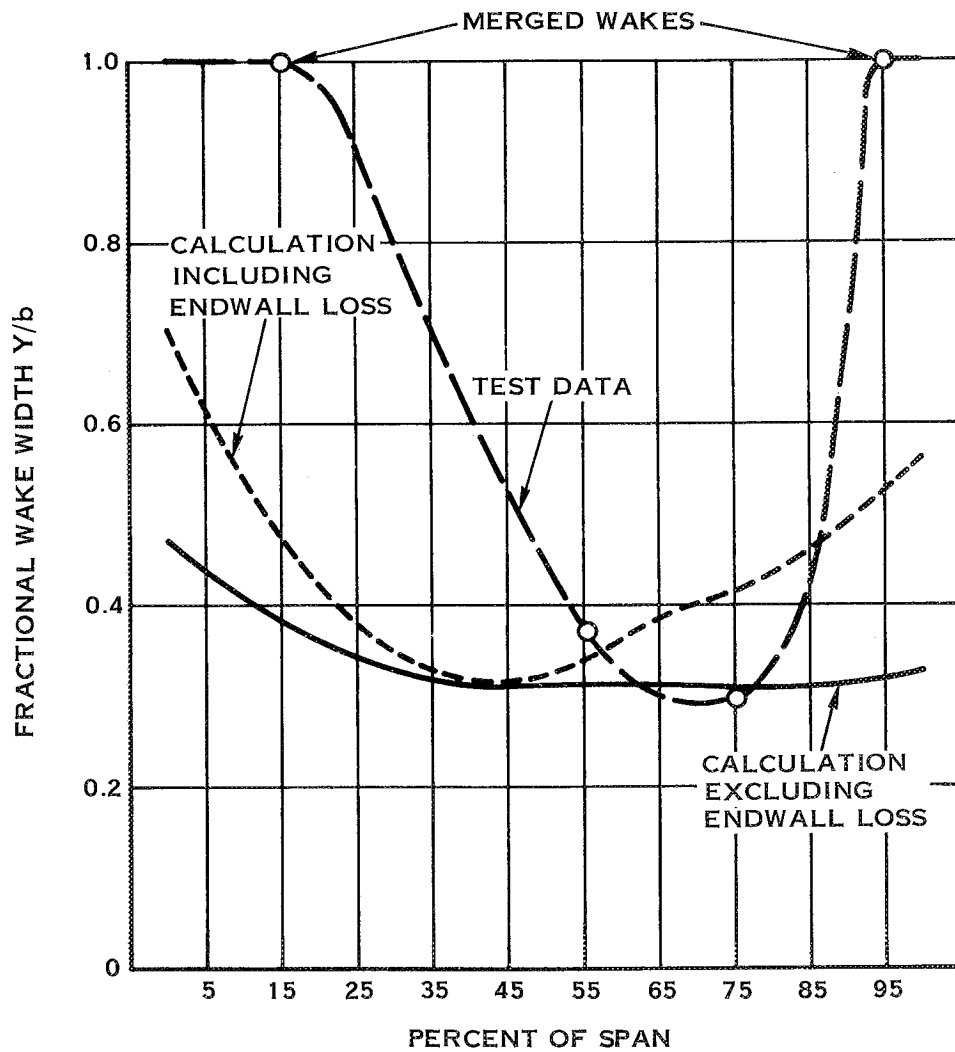


FIGURE 53. FRACTIONAL WAKE WIDTH COMPARISONS FOR TEST CONDITION II

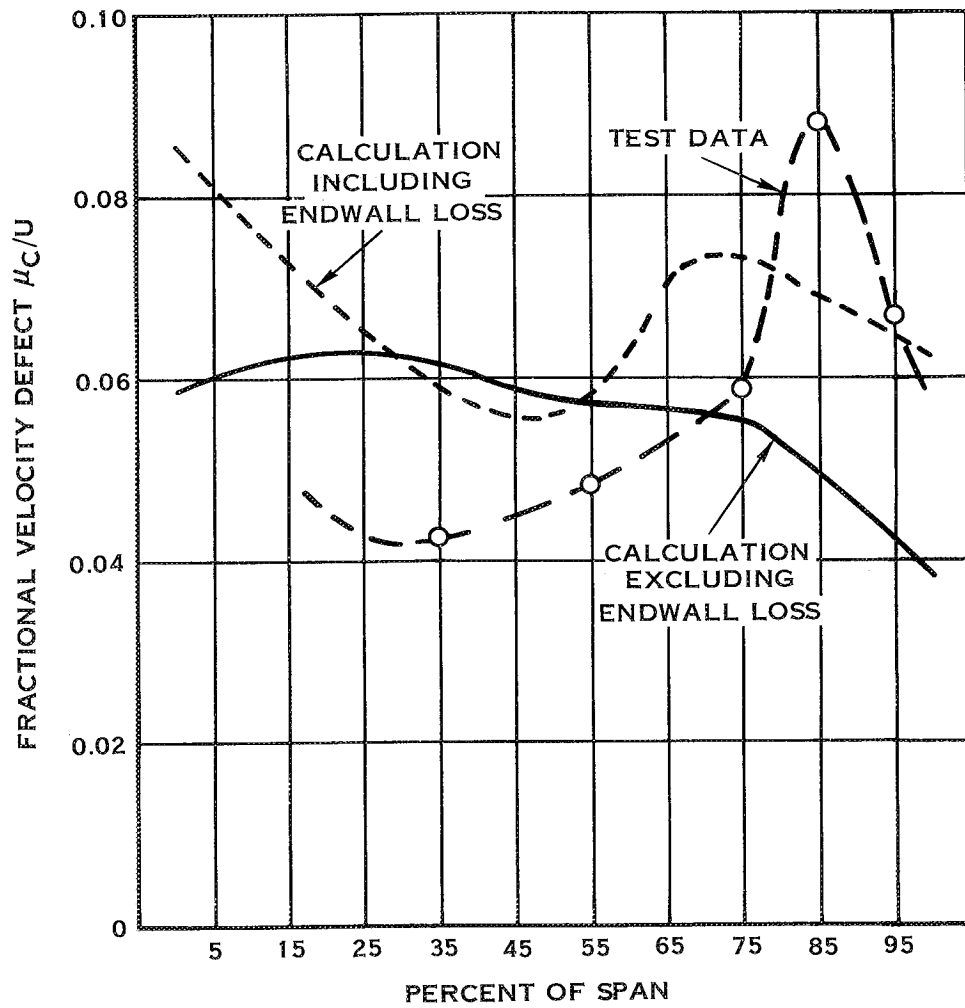


FIGURE 54. FRACTIONAL VELOCITY DEFECT COMPARISONS FOR TEST CONDITION III

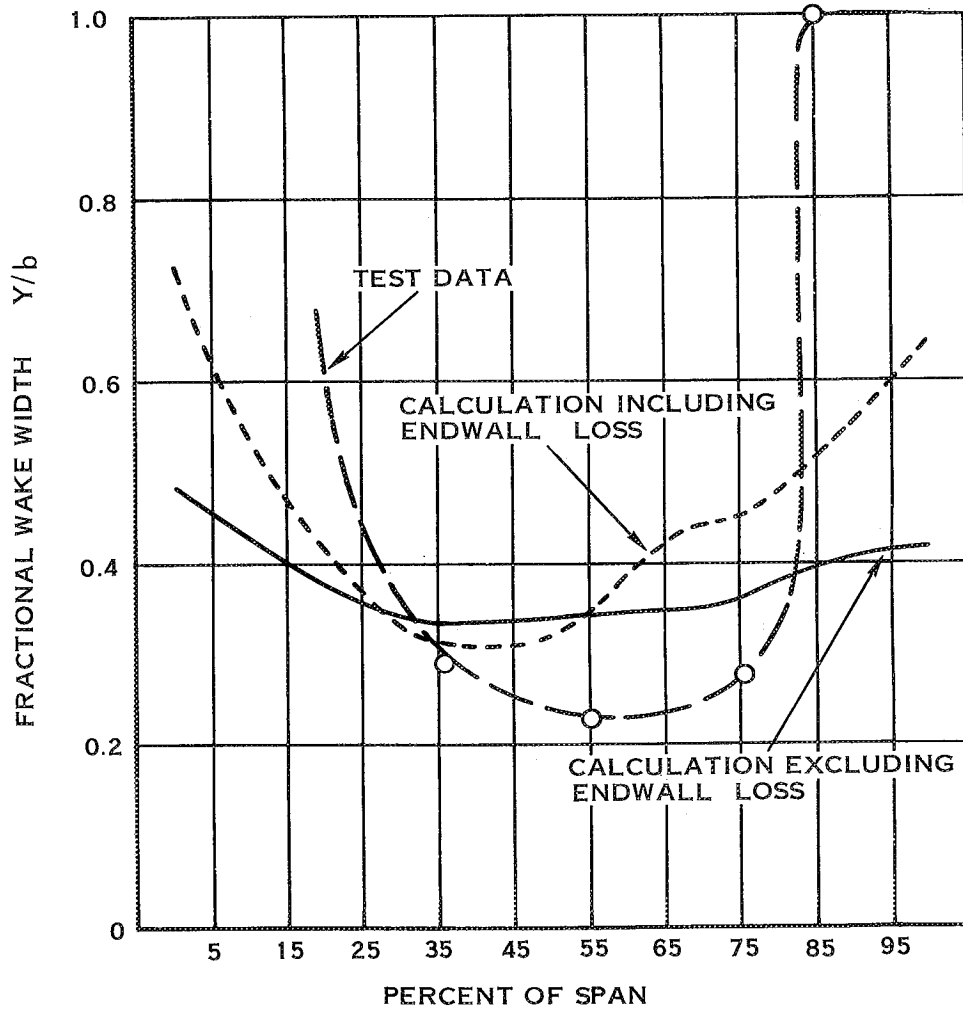


FIGURE 55. FRACTIONAL WAKE WIDTH COMPARISONS FOR TEST CONDITION III

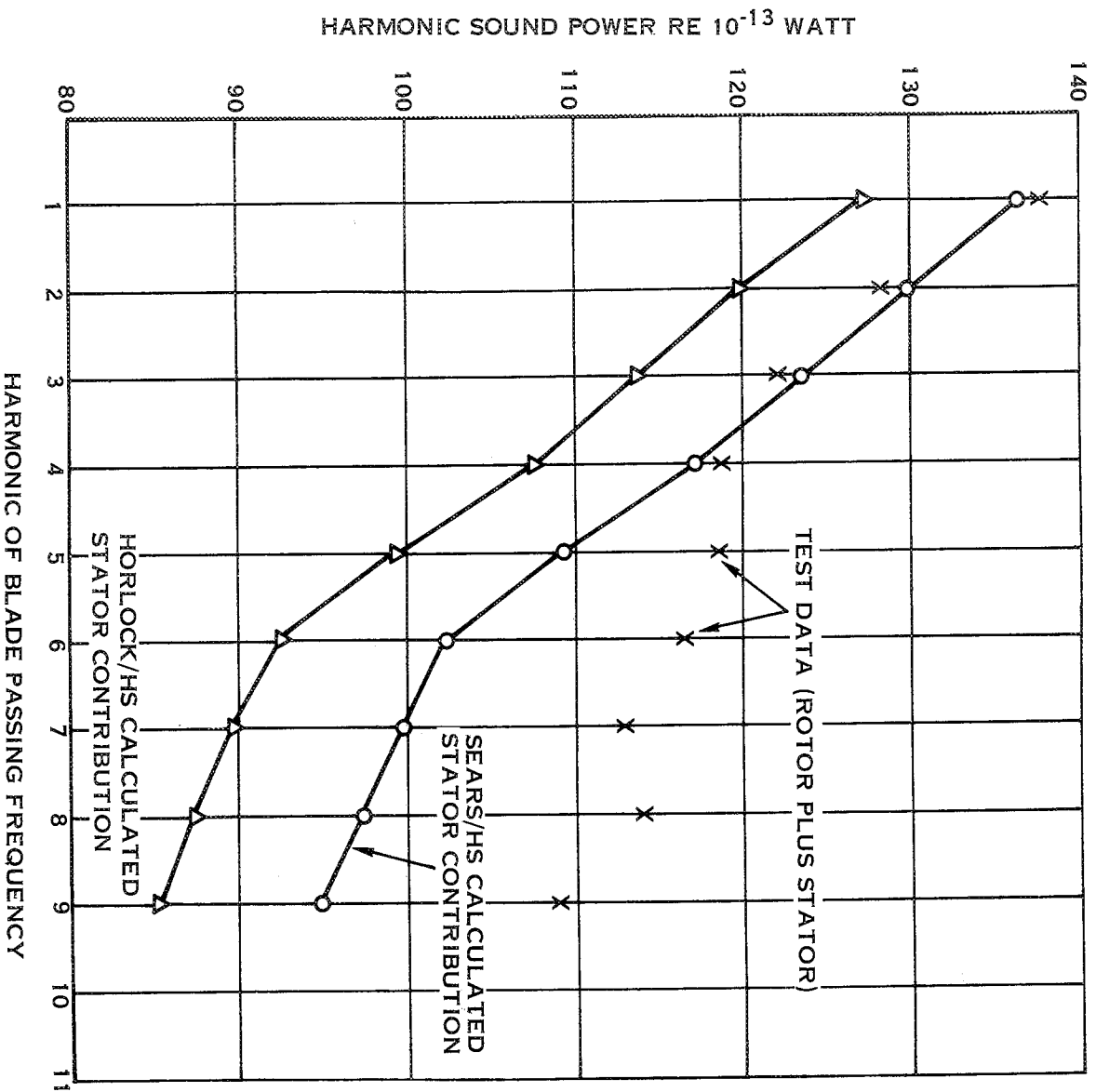


FIGURE 56. CONTRIBUTION OF STATOR TO HARMONIC NOISE AT FLOW CONDITION I

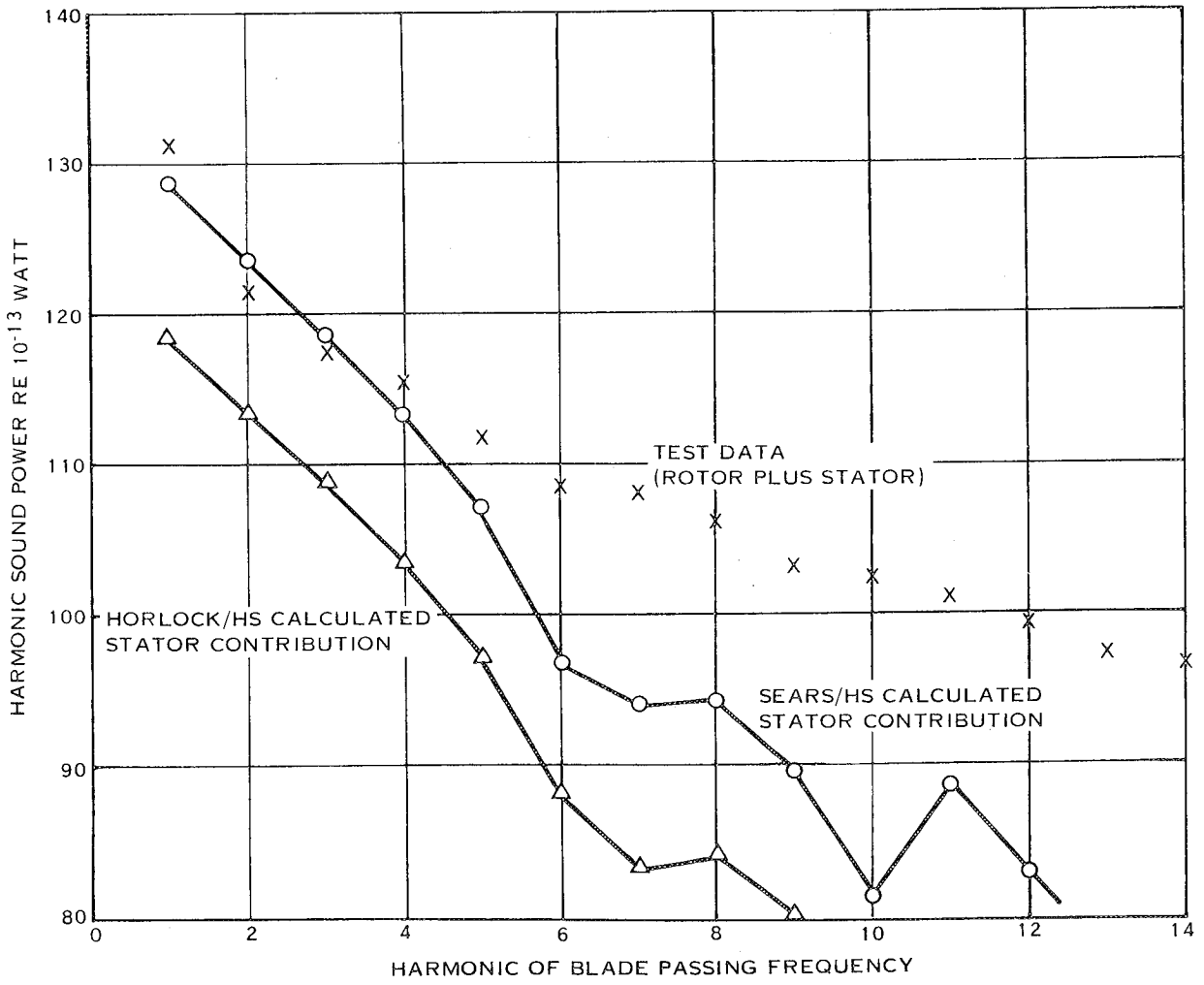


FIGURE 57. CONTRIBUTION OF STATOR TO HARMONIC NOISE AT FLOW CONDITION II

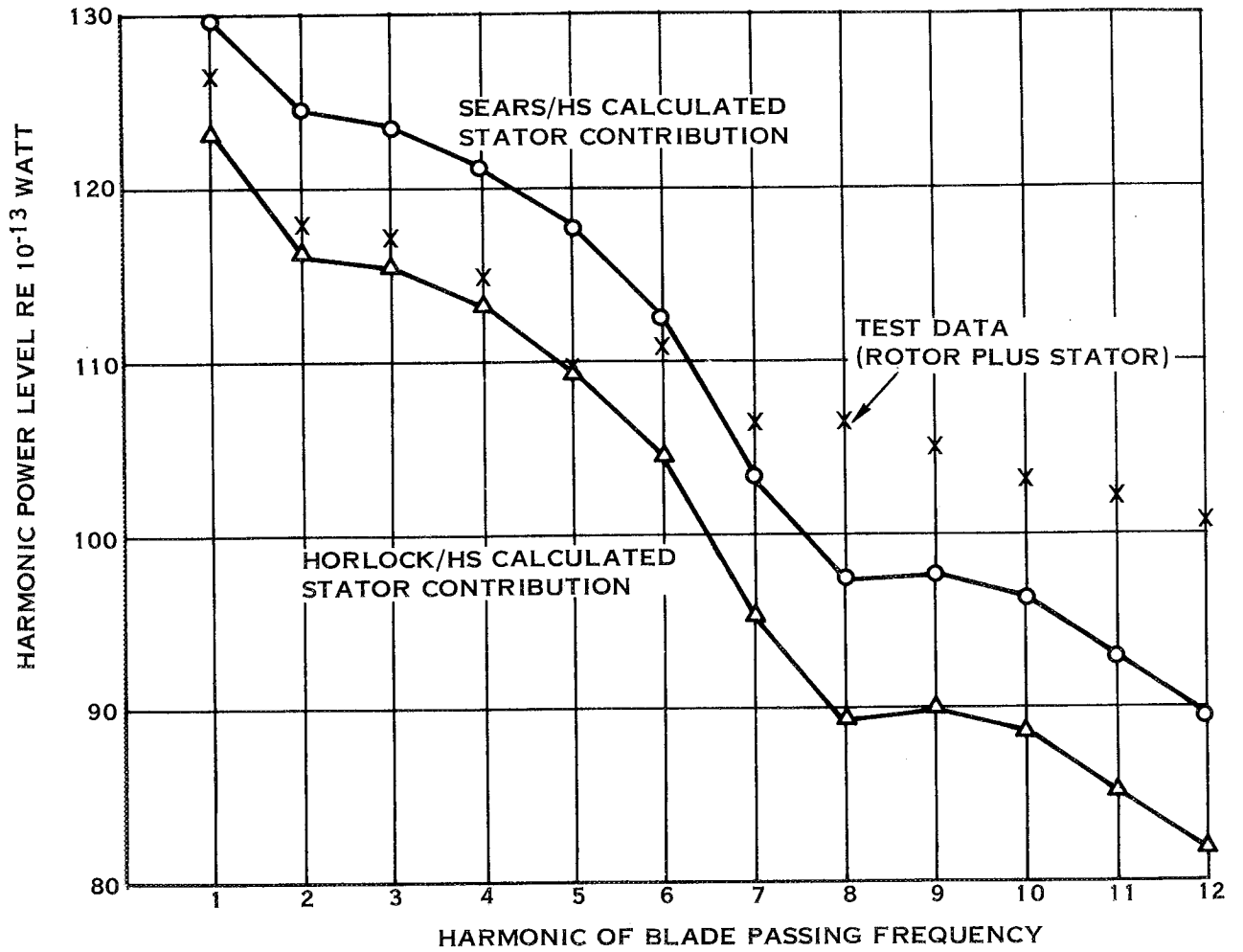


FIGURE 58. CONTRIBUTION OF STATOR TO HARMONIC NOISE AT FLOW CONDITION III